Elements with penalized equilibrium and rotational degrees of freedom in fracture mechanics problems

by
A. de Klerk

A dissertation submitted in partial fulfillment
of the requirements for the degree of

Master of Engineering

in the Department of Mechanical and Aeronautical Engineering,
University of Pretoria

March 2005

Abstract

Title:	Elements with penalized equilibrium and rotational degrees of freedom in fracture mechanics problems
Author:	Antoinette de Klerk
Supervisor:	Prof. A.A. Groenwold
Department:	Department of Mechanical Engineering
Degree:	Master of Engineering
Keywords:	Finite element method, fracture mechanics, path independent integrals, J integral, I^* integral, stress intensity factor, penalized equilibrium, drilling degrees of freedom, isotropic material, orthotropic material.

This thesis deals with the solution of linear elastic fracture mechanics problems. To solve the linear elastic fracture mechanics problems, the finite element method and path independent integrals are employed, namely Rice's J integral and an alternative path independent integral I^*, which is the energy complement to J. Stress intensity factors for typical mode I and mode II fracture mechanics problems in isotropic and orthotropic elastic plates are calculated. The problems considered are a center cracked panel subjected to uniform tension, a single edge cracked panel subjected to uniform tension, a double edge cracked panel subjected to uniform tension, and a center cracked panel subjected to uniform shear.

Firstly, classical displacement based finite elements, elements with penalized equilibrium and elements with drilling degrees of freedom are presented and implemented in a *MATLAB* environment.

Secondly, two different ways to evaluate the stress intensity factor are considered, namely the displacement extrapolation approach, and the path independent integrals J and I^*. The numerical implementation and path independence of the J and I^* integral is demonstrated. It is shown that the J integral can estimate the lower bound of the stress intensity factor when used with displacement based finite elements, while the I^* integral can estimate the upper bound of the stress intensity factor, when used with stress equilibrium elements.

Thirdly, the path independent integrals J and I^* are applied to isotropic fracture mechanics prob-

lems to determine the stress intensity factor at the tip of a crack. Convergence studies are presented to investigate the influence of mesh refinement on the stress intensity factor predicted using the J and I^* integral. The path independence of J and I^* are investigated. Numerical results for typical fracture specimens are presented and discussed.

Finally, the path independent integrals J and I^* are applied to orthotropic fracture mechanics problems to determine the stress intensity factor at the crack tip. Again, convergence studies are done, and the path independence of J and I^* are investigated for orthotropic problems. Numerical results for typical fracture specimens are presented and discussed. The effect of the degree of anisotropy and fiber orientation on the stress intensity factor is also demonstrated.

A novel contribution in this thesis are the results for elements with drilling degrees of freedom in fracture mechanics problems. In addition, the results presented here may serve to clarify published stress intensity factor results for *orthotropic* materials presented in the literature, since many of the results previously presented are contradictory.

Opsomming

Titel:	Elemente met gepenaliseerde ewewig en rotasionele vryheidsgrade in breukmeganika probleme
Outeur:	Antoinette de Klerk
Leier:	Prof. A.A. Groenwold
Departement:	Departement Meganiese Ingenieurswese
Graad:	Meester van Ingenieurswese
Sleutelwoorde:	Eindig element metode, breukmeganika, pad onafhanklike integrale, J integraal, I^* integraal, spanningsintensiteitsfaktor, gepenaliseerde ewewig, rotasionele vryheidsgrade, isotropiese materiaal, orthotropies materiaal.

Hierdie verhandeling is gemoeid met die oplos van linêere elastiese breukmeganika probleme. Om die linêere breukmeganika probleme op te los, word die eindige element metode en pad onafhanklike integrale gebruik, naamlik Rice se J integraal en 'n alternatiewe I^* integraal, wat die energie komplement van J is. Spanningsintensiteitsfaktore vir tipiese mode I en mode II breukmeganika probleme in isotropiese en ortotropiese elastiese plate word bereken. Die volgende probleme word beskou, eerstens 'n sentraal gekraakte paneel onderhewig aan uniform spanning, 'n enkel kant gekraakte paneel onderhewig aan uniforme spanning,'n dubbel kant gekraakte paneel onderhewig aan uniforme spanning en 'n sentraal gekraakte paneel onderhewing aan uniforme skuif.

Eerstens word klassieke verplasings gebaseerde elemente, elemente met gepenaliseerde ewewig, en elemente met rotasionele vryheidsgrade voorgestel en geimplimiteer in 'n *MATLAB* omgewing.

Tweedens word twee verskillende maniere om die spanningsintensiteitsfaktor te bereken beskou, naamlik die verplasingsekstrapolasie metode en die pad onafhanklike J en I^* integrale. Die numeriese implementasie en pad onafhanklikheid van laasgenoemde word gedemonstreer. Dit word aangetoon dat die J integraal die ondergrens tot die spanningintensiteitsfaktor kan voorspel as dit gekombineer word met verplasing gebaseerde elemente, terwyl die I^* integraal die bogrens kan voorspel as dit gekombineer word met spanningsewewig elemente.

Derdens word die pad onafhanklike integrale J en I^* toegepas op isotropiese breukmeganika prob-

leme om die spanningsintensiteitsfaktore te bereken. Konvergensie studies word aangebied om die invloed van maas verfyning op die spanningsintensiteitsfaktor, bereken met die J en I^* integrale, te ondersoek. Die pad onafhanklikheid van die J en I^* integrale word ondersoek. Numeriese resultate vir tipiese breukmeganika probleme word aangebied en bespreek.

Laastens word die pad onafhanklike integrale J en I^* toegepas op ortotropies breukmeganika probleme om die spanningsintensiteitsfaktore te bereken. Konvergensie studies word weereens uitgevoer, en die padonafhanklikheid van J en I^* word ondersoek vir ortotropiese probleme. Numeries resultate vir tipiese breukmeganika probleme word aangebied en bespreek. Die effek van die graad van anisotropie op die spanningsintensiteitsfaktor word ook in berekening gebring.

'n Nuwe bydrae in hierdie studie is die toepassing van elemente met rotasionele vryheidsgrade in breukmeganika probleme. Die resultate wat aangebied word kan verder ook gebruik word om die verwarrende spanningsintensiteitsfaktor waardes in die literatuur vir *ortotropiese* materiale te beoordeel, aangesien talle voorheen gepubliseerde resultate teenstrydig is.

Acknowledgments

I would like to express my sincere gratitude towards the following persons:

- My advisor, Professor A.A. Groenwold for his guidance and support throughout this study.
- To both my parents for their encouragement and unfailing support.
- My fellow students for their assistance.

Financial support granted by Sasol, the National Research Foundation, the CSIR and Kentron is gratefully acknowledged.

Contents

Abstract ii

Opsomming iv

Acknowledgments vi

List of Figures xiii

List of Tables xvi

1 Introduction 1

1.1 Motivation . . . 1
1.2 Objectives . . . 2
1.3 Approach . . . 2
1.4 Thesis overview . . . 3

2 Classical element formulations 5

2.1 Introduction . . . 5
2.2 Classical displacement based formulation in 2-D . . . 5
2.3 Assumed stress formulation in 2-D . . . 7
2.3.1 Finite element implementation . . . 9
2.4 Numerical example . . . 9
2.4.1 Cook's membrane . . . 9

3 Elements with penalized equilibrium formulation 11

3.1 Penalized equilibrium in assumed stress elements . . . 11
3.1.1 Allowable values of α for hybrid elements . . . 12
3.1.2 Cook's membrane . . . 13
3.2 Penalized equilibrium in displacement based elements . . . 13

3.2.1 Element defects . . . 13
3.2.2 Displacement based elements with penalized equilibrium . . . 15
3.2.3 On critical values of α . . . 16
3.2.4 Optimal values of α . . . 18
3.3 Separation of the higher order deformation modes in Q4 . . . 18
3.4 Numerical example . . . 19
3.5 Discussion . . . 19

4 Elements with drilling degrees of freedom 21
4.1 Formulation of elements with drilling degrees of freedom . . . 21
4.2 Variational formulation . . . 21
4.2.1 Finite element interpolation . . . 23
4.3 Membrane locking correction . . . 26
4.4 Assumed stress formulation . . . 28
4.4.1 Finite element discretization . . . 28
4.4.2 Interpolating the assumed stress field . . . 29
4.4.3 Penalty-equilibrated approach . . . 30
4.5 Numerical Results . . . 31
4.5.1 Cook's membrane . . . 31

5 Fracture mechanics: Classical and numerical treatments 32
5.1 Historical overview . . . 32
5.2 Linear elastic fracture mechanics assumptions . . . 33
5.3 Loading modes . . . 33
5.4 Stress intensity factor . . . 34
5.5 Fracture toughness . . . 35
5.6 Finite elements in fracture mechanics . . . 35
5.7 Crack tip singularity modeling . . . 36
5.8 Interpretation of the finite element results . . . 36

6 Fracture mechanics: Displacement extrapolation 38
6.1 Displacement extrapolation basics . . . 38
6.2 Numerical example . . . 40
6.3 Discussion . . . 40

7 Fracture mechanics: J integral 43

7.1 J integral method . . . 43
7.2 J integral definition . . . 43
7.3 Derivation of J . . . 46
7.4 Path independence of J . . . 48
7.5 Lower bound theorem for J . . . 51
7.5.1 Proof of the lower bound theorem for J . . . 52
7.5.2 J integral in FEM . . . 53
7.5.3 Choice of integration path in element . . . 55

8 Fracture mechanics: The I^* integral as the dual form of the J integral 57
8.1 The I^* integral . . . 57
8.2 Derivation of the I^* integral . . . 57
8.3 Path independence of I^* . . . 58
8.4 Upper bound theorem for I^* . . . 59
8.5 Proof of the upper bound theorem . . . 59
8.5.1 Determination of the stress intensity factor K_I using the J and I^* integrals 60

9 Fracture mechanics: Isotropic results 62
9.1 Problem description . . . 62
9.2 Analytical stress intensity factors expressions . . . 64
9.3 Convergence study . . . 65
9.4 Results for different panels . . . 67

10 On the stability of drilling elements 77
10.1 Effect of reduced integration . . . 77
10.1.1 5-Point integration rule . . . 77
10.1.2 Influence of center point weight W_0 . . . 78
10.2 Different values for γ . . . 78

11 Fracture mechanics: Orthotropic materials 84
11.1 Introduction . . . 84
11.2 Anisotropic stress and displacement field near a crack tip . . . 84

12 Fracture mechanics: Orthotropic results 86
12.1 Overview . . . 86
12.2 Convergence study . . . 87
12.3 Selected results demonstrating path independence . . . 89

12.4 The effect of fiber orientation on the stress intensity factor 90
12.5 The effect of the degree of anisotropy on K 94

13 Conclusions **109**
13.1 Recommendations for further studies 110

Bibliography **111**

A Eigenvalues of Q4(α) and 5β **114**
A.1 Square Q4(α) element with side lengths $2a$ 114
A.2 Square 5β element with side lengths $2a$ 115
A.3 Rectangular Q4(α) element with side lengths $2a$, $2b$, $a \geq b$ 115
A.4 Rectangular 5β element with side lengths $2a$, $2b$, $a \geq b$ 115
A.5 Rectangular Q4($\alpha_x \alpha_y$) element with side lengths $2a$, $2b$, $a \geq b$ 116

B Sample input file **117**

C Source code listings **119**
C.1 Element routines: J integral (for a Q4 element) 119
C.2 Element routines: I^* integral (for a PS(α) element) 123
C.3 Element: Element with drilling degrees of freedom (8$\beta\alpha$) for composite material . 128
C.3.1 Element routines: Main program 128
C.3.2 Element routines: Stiffness matrix 131
C.3.3 Element routines: P matrix for 8β 135
C.3.4 Element routines: P matrix for 9β 136
C.3.5 Element routines: Material matrix for composite material 137
C.4 Element: Q4 with penalized equilibrium 137
C.4.1 Element routines: Main program 137
C.4.2 Element routines: Calculate penalized stiffness matrix 140
C.4.3 Element routines: Derivatives of form functions 141

List of Figures

2.1 Cook's membrane 10

3.1 Typical variation of the eigenvalues of a penalized, arbitrary distorted 5β assumed stress element 12
3.2 Deformation mode in bending: (a) A rectangular block of material in pure bending (b) A Q4 element under bending load 14
3.3 Straining modes of a rectangular Q4 element, side lengths $2a$ and $2b$, $a \geq b$ 16
3.4 Slender and short beams in pure bending 19

4.1 Four-node quadrilateral element with drilling degrees of freedom 24
4.2 Spurious higher order mode for a four-node quadrilateral element with drilling degrees of freedom 26

5.1 The three modes of loading : (a) mode I opening mode (b) mode II sliding mode (c) mode III tearing mode 34

6.1 Stress intensity factor evaluation by extrapolation. Example of mesh that can be used 39
6.2 Stress intensity factor evaluation by extrapolation. Plot of stress intensity factor K vs. radial distance r from the crack tip 39
6.3 Single edge cracked plate used for displacement extrapolation: (a) Geometry of the SECP problem (b) A 10×10 mesh for the single edge crack plate (SECP) . . 41
6.4 Normalized K_I vs. radial distance for $\theta = 90^\circ$ 41
6.5 Normalized K_I vs. radial distance for $\theta = 0^\circ$ 42

7.1 Center crack panel 44
7.2 A closed contour Γ used in defining the J integral 44
7.3 A cracked body of unit thickness loaded by a traction T 46
7.4 A closed contour Γ with parameters used in defining the J integral 49
7.5 A closed contour ABCDEF for a cracked body 51
7.6 Contour path for J integral evaluation 53

7.7 Radial finite element mesh around a crack tip 55
7.8 Contour for J evaluation involving paths along both ζ and η directions and "corner" elements 56
7.9 Path through corner elements 56

9.1 Cracked panels: (a) Center cracked panel (CCP) that is subjected to tension (b) Single edge cracked panel (SECP) subjected to uniform tension (c) Double edge cracked panel (DECP) subjected to uniform tension (d) Center cracked panel (CCP) subjected to uniform shear 63
9.2 Finite element mesh and five selected integration contours for one-quarter of the CCP and one half of the SECP and the DECP. (a) Mesh 1 (b) Mesh 3 70
9.3 Convergence study for the CCP with different elements: (a) Q4 (b) Q4X (c) PS, and (d) PS(α) 71
9.4 Convergence study for the CCP with different elements: (a) 8β (b) 8$\beta(\alpha)$ (c) 9β (d) 9$\beta(\alpha)$ 72
9.5 Displacement of cracked panels ($\times$ 0.1): (a) Center cracked panel (CCP) (b) Single edge cracked panel (SECP) (c) Double edge cracked panel (DECP) (d) Center cracked panel (CCP) with uniform shear 73
9.6 Summary of results for cracked isotropic panels with different elements: (a) CCP subjected to uniform tension (b) SECP subjected to uniform tension 74
9.7 Summary of results for cracked isotropic panels with different elements: (a) DECP subjected to uniform tension (b) CCP subjected to uniform shear 75

10.1 5-Point integration scheme 78
10.2 Nodal rotation for a center cracked panel using different integration schemes: (a) 5 point integration, $W_0 = 0.01 \times 8/3$ (b) 5 point integration, $W_0 = 0.1 \times 8/3$ (c) 5 point integration, $W_0 = 8/3$ (d) 9 point integration, (all with $\gamma = G$) 79
10.3 τ_0 vs. γ for a center cracked panel with full integration, for $\gamma = 6.5 \times 10^{-4}$ through $\gamma = 6.5 \times 10^{3}$. The solid line indicates the optimal range for γ 80
10.4 Nodal rotations for a center cracked panel: (a) $\gamma = G/1000$ (b) $\gamma = G$ (c) $\gamma = G \times 1000$ (9-point integration scheme) 81
10.5 τ_0 vs. γ for a center cracked panel and a single edge cracked panel with full integration 82
10.6 Stress intensity factor K_I vs. γ for the 5 different integration paths: (a) Center cracked panel (b) Single edge cracked panel 83

12.1 Definition of the fiber orientation in an orthotropic material 86
12.2 Convergence study of K_I for the orthotropic CCP with different displacement based elements: (a) Q4 (b) Q4X 88
12.3 Convergence study of K_I for the orthotropic CCP with different assumed stress elements: (a) PS(α) (b) 8$\beta(\alpha)$ (c) 9$\beta(\alpha)$ 89

12.4 Summary of results for an orthotropic center cracked panel with $\theta = 0^\circ$ fiber angle: (a) Q4, Q4X and PS(α) elements (b) $8\beta(\alpha)$ and $9\beta(\alpha)$ elements 91

12.5 Summary of results for an orthotropic single edge cracked panel with $\theta = 0^\circ$ fiber angle: (a) SECP with $\theta = 0^\circ$ Q4, Q4X, PS and PS(α) elements (b) SECP with $\theta = 0^\circ$ 8β, $8\beta(\alpha)$, 9β and $9\beta(\alpha)$ elements 93

12.6 Summary of results for an orthotropic double edge cracked panel: (a) fiber angle $\theta = 90^\circ$ (b) fiber angle $\theta = 0^\circ$ 93

12.7 Results for the effect of fiber orientation on a double edge crack plate, $\theta = \pm 0^\circ_s$ through $\theta = \pm 90^\circ_s$ (a) Solution for all elements (b) Solution for Q4X and $9\beta\alpha$ only 95

12.8 The effect of the degree of anisotropy and height to width ratio for the orthotropic CCP with 0° ply arrangement: (a) Height to width ratio $h/w = 1$ (b) Height to width ratio $h/w = 1.5$ 98

12.9 The effect of the degree of anisotropy and height to width ratio for the orthotropic CCP with 0° ply arrangement: Height to width ratio $h/w = 2$ 99

List of Tables

2.1 Mid node displacement for Cook's membrane (plane stress) obtained with displacement based Q4 and assumed stress PS elements 9

3.1 Mid-node displacement for Cook's membrane (plane stress), obtained with unpenalized PS and penalized PS(α) assumed stress elements 13
3.2 Numerical results for the slender beam in pure bending 19
3.3 Numerical results for the short beam in pure bending 20

4.1 Mid-node displacement for Cook's membrane (plane stress), obtained with displacement based and assumed stress elements with drilling degrees of freedom and penalized equilibrium 31

6.1 Stress intensity factor for a SECP determined with displacement extrapolation along the radial line $\theta = 90^\circ$ using different numbers of extrapolation points . . . 42

9.1 Convergence of K_1 for an isotropic CCP subjected to uniform tension with Q4 elements 65
9.2 Convergence of K_1 for an isotropic CCP subjected to uniform tension with Q4X elements 66
9.3 Convergence of K_1 for an isotropic CCP subjected to uniform tension with PS elements 66
9.4 Convergence of K_1 for an isotropic CCP subjected to uniform tension with PS(α) elements 67
9.5 Convergence of K_1, for an isotropic CCP subjected to uniform tension with 8β elements 67
9.6 Convergence of K_1 for an isotropic CCP subjected to uniform tension with $8\beta(\alpha)$ elements 68
9.7 Convergence of K_1 for an isotropic CCP subjected to uniform tension with 9β elements 68
9.8 Convergence of K_1 for an isotropic CCP subjected to uniform tension with $9\beta(\alpha)$ elements 69

9.9 K_1 results for the isotropic CCP subjected to uniform tension (Mesh 3) 69
9.10 K_1 results for the isotropic SECP subjected to uniform tension (Mesh 3) 69
9.11 K_1 results for the isotropic DECP subjected to uniform tension (Mesh 3) 76
9.12 K_1 results for the isotropic CCP subjected to uniform shear (Mesh 2) 76

12.1 Convergence of K_1 for an orthotropic CCP subjected to uniform tension with Q4 elements 88
12.2 Convergence of K_1 for an orthotropic CCP subjected to uniform tension with Q4X elements 90
12.3 Convergence of K_1 for an orthotropic CCP subjected to uniform tension with PS(α) elements 90
12.4 Convergence of K_1 for an orthotropic CCP subjected to uniform tension with $8\beta(\alpha)$ elements 91
12.5 Convergence of K_1 for an orthotropic CCP subjected to uniform tension with $9\beta(\alpha)$ elements 91
12.6 K_1 results for the orthotropic CCP with 0° laminate under uniform tension (mesh 3) 92
12.7 K_1 results for the orthotropic SECP with 0° laminate under uniform tension (mesh 3) 92
12.8 K_1 results for the orthotropic DECP with a 90° laminate under uniform tension (mesh 3) 94
12.9 K_1 results for the orthotropic DECP with a 0° laminate under uniform tension (mesh 3) 94
12.10 K_1 results for the isotropic CCP under uniform tension (mesh 3) 96
12.11 Material constants for cracked rectangular plate 97
12.12 The effect of the degree of anisotropy on K_1 for an orthotropic CCP with 0° ply arrangement and height to width ratio h/w = 1, different crack length to width ratios a/w, using Q4 elements 99
12.13 The effect of the degree of anisotropy on K_1 for an orthotropic CCP with 0° ply arrangement and height to width ratio h/w = 1, different crack length to width ratios a/w, using Q4X elements 100
12.14 The effect of the degree of anisotropy on K_1 for an orthotropic CCP with 0° ply arrangement and height to width ratio h/w = 1, different crack length to width ratios a/w, using PS(α) elements 100
12.15 The effect of the degree of anisotropy on K_1 for an orthotropic CCP with 0° ply arrangement and height to width ratio h/w = 1, different crack length to width ratios a/w, using $8\beta(\alpha)$ elements 101
12.16 The effect of the degree of anisotropy on K_1 for an orthotropic CCP with 0° ply arrangement and height to width ratio h/w = 1, different crack length to width ratios a/w, using $9\beta(\alpha)$ elements 101

12.17 Reference solution for the effect of the degree of anisotropy on K_1 for an orthotropic CCP with 0° ply arrangement and height to width ratio h/w = 1, different crack length to width ratios a/w 102
12.18 The effect of the degree of anisotropy on K_1 for an orthotropic CCP with 0° ply arrangement and height to width ratio h/w = 1.5, different crack length to width ratios a/w, using Q4 elements 102
12.19 The effect of the degree of anisotropy on K_1 for an orthotropic CCP with 0° ply arrangement and height to width ratio h/w = 1.5, different crack length to width ratios a/w, using Q4X elements 103
12.20 The effect of the degree of anisotropy on K_1 for an orthotropic CCP with 0° ply arrangement and height to width ratio h/w = 1.5, different crack length to width ratios a/w, using PS(α) elements 103
12.21 The effect of the degree of anisotropy on K_1 for an orthotropic CCP with 0° ply arrangement and height to width ratio h/w = 1.5, different crack length to width ratios a/w, using 8$\beta(\alpha)$ elements 104
12.22 The effect of the degree of anisotropy on K_1 for an orthotropic CCP with 0° ply arrangement and height to width ratio h/w = 1.5, different crack length to width ratios a/w, using 9$\beta(\alpha)$ elements 104
12.23 Reference solution for the effect of the degree of anisotropy on K_1 for an orthotropic CCP with 0° ply arrangement and height to width ratio h/w = 1.5, different crack length to width ratios a/w 105
12.24 The effect of the degree of anisotropy on K_1 for an orthotropic CCP with 0° ply arrangement and height to width ratio h/w = 2, different crack length to width ratios a/w, using Q4 elements 105
12.25 The effect of the degree of anisotropy on K_1 for an orthotropic CCP with 0° ply arrangement and height to width ratio h/w = 2, different crack length to width ratios a/w, using Q4X elements 106
12.26 The effect of the degree of anisotropy on K_1 for an orthotropic CCP with 0° ply arrangement and height to width ratio h/w = 2, different crack length to width ratios a/w, using PS(α) elements 106
12.27 The effect of the degree of anisotropy on K_1 for an orthotropic CCP with 0° ply arrangement and height to width ratio h/w = 2, different crack length to width ratios a/w, using 8$\beta(\alpha)$ elements 107
12.28 The effect of the degree of anisotropy on K_1 for an orthotropic CCP with 0° ply arrangement and height to width ratio h/w = 2, different crack length to width ratios a/w, using 9$\beta(\alpha)$ elements 107
12.29 Reference solution for the effect of the degree of anisotropy on K_1 for an orthotropic CCP with 0° ply arrangement and height to width ratio h/w = 2, different crack length to width ratios a/w 108

Chapter 1

Introduction

1.1 Motivation

Over the last decade or so, the finite element method has been firmly established as a standard numerical technique for solving fracture mechanics problems. It would have been impossible to solve non-linear fracture problems, without the employment of the finite element method [1].

Rice's path-independent integral J is one of the most significant parameters in linear elastic fracture mechanics [1]. Recently the I^* integral was introduced by Wu *et al* [1], which is the dual form of the J integral. The I^* integral is based on the complementary energy principle of the system where the J integral is based on the strain energy density of the system.

Path independent integrals (J/I^*) should be solved with finite elements that are based on the same energy principle as the path independent integrals to ensure path independence. It is due to this fact that the I^* integral makes the assumed stress element (based on the complementary energy principle) play a powerful role in computational fracture mechanics.

In the penalty-equilibrium approach, stress equilibrium is enforced in individual elements. Thus assumed stress elements with penalized equilibrium are ideal to solve the I^* integral.

In fracture mechanics, upper/lower bound estimation of the stress intensity factor becomes a matter of great significance as it is difficult to obtain the exact value of the stress intensity factor (K), no matter what experimental or numerical method is used due to the complexity of non-linear fracture [1]. It can be proved that the J integral forms an approximate lower bound to K when displacement based elements are used to solve the integral and that the I^* integral forms an approximate upper bound to K when stress equilibrium elements are used.

While assumed stress interpolation increases the accuracy of low order membrane elements, drilling degrees of freedom have an additional advantage in low order membrane elements. Above and beyond enrichment of the displacement field, it increases the accuracy of low order elements. Drilling degrees of freedom also increases the modeling capability of these elements.

In recent years, composite materials have been used increasingly in various engineering disciplines, notably in the fields of aerospace and marine engineering.

The crack tip singularity in orthotropic materials can be completely characterized in the same

manner as in the isotopic case by properly defining anisotropic stress intensity factors [2]. Stress intensity factors are important parameters in the assessment of the fracture strength of anisotropic composite structural components. Within the framework of plane, linear elastic fracture mechanics, a problem of continuing interest is the calculation of the stress intensity factor in cracked orthotropic plates modeling fiber reinforced composites [3].

1.2 Objectives

The primary objective of this study is the numerical evaluation of mode I and mode II stress intensity factors for basic isotropic and orthotropic fracture mechanics problems.

The stress intensity factors are evaluated by using the finite element method, combined with path independent integrals.

A secondary objective is to investigate the capability of different finite elements to evaluate the J and I^* integral. This is done by comparing elements with drilling degrees of freedom and penalized equilibrium with standard displacement based and assumed stress elements.

In particular the application of elements with drilling degrees of freedom and penalized equilibrium in fracture mechanics is of interest.

1.3 Approach

A finite element package was programmed in *MATLA*B [4]. The program employs different elements to evaluate fracture mechanics problems.

The following elements were implemented in *MATLAB*:

- Q4 (A displacement based quadrilateral element)
- PS (The assumed stress quadrilateral element proposed by Pian and Sumihara [5])
- PS(α) (A penalized version of the assumed stress quadrilateral element proposed by Pian and Sumihara [5])
- Q4X (A displacement based quadrilateral element with drilling degrees of freedom)
- 8β (An assumed stress quadrilateral element with drilling degrees of freedom and 8 β parameters)
- 8$\beta(\alpha)$ (A penalized version of the assumed stress quadrilateral element with drilling degrees of freedom and 8 β parameters)
- 9β (An assumed stress quadrilateral element with drilling degrees of freedom and 9β parameters)
- 9$\beta(\alpha)$ (A penalized version of the assumed stress quadrilateral element with drilling degrees of freedom and 9 β parameters)

The package also employs path independent integrals to evaluate the stress intensity factors.

1.4 Thesis overview

The thesis is arranged as follows:

- In Chapter 2 the classic formulations of the standard displacement based bi-linear isoparametric membrane element (Q4) and the assumed stress membrane element proposed by Pian and Sumihara are presented.
- In Chapter 3 the penalized version of the assumed stress element proposed by Pian and Sumihara and the Q4 element are presented and discussed.
- In Chapter 4 the formulation of a displacement based membrane finite element and two assumed stress membrane finite elements with two translational and one rotational degree of freedom per node are presented. Secondly, a penalty-equilibrium approach, in which stress equilibrium is enforced in individual elements, is used for the two assumed stress elements is presented.
- In Chapter 5 a brief overview of fracture mechanics history is given and important fracture mechanics concepts are discussed.
- In Chapter 6 the displacement based extrapolation method for determining the stress intensity factor is discussed and implemented.
- In Chapter 7 the path independent J integral is discussed. The path independence and lower bound theorem are investigated and proved.
- In Chapter 8 the path independent I^* integral is discussed. The derivation, path independence and upper bound theorem for the I^* integral is investigated and proved.
- In Chapter 9 the influence of mesh refinement is considered and results for basic isotropic fracture problems are presented and discussed.
- In Chapter 10 the stability of the element with drilling degrees of freedom in fracture mechanics are considered.
- In Chapter 11, fracture mechanics in orthotropic plates, and stress and displacement distributions around the crack tip in an anisotropic material is considered.
- In Chapter 12, basic orthotropic fracture mechanics problems are considered. The problems are evaluated by using the J and I^* integrals with different displacement based and assumed stress elements. Results are compared with known solutions. A convergence study is done to investigate the effect of mesh refinement on the path independent integrals. The effect of fibre orientation and the degree of anisotropy on the stress intensity factors are also considered.

The Appendices include the following:

- In Appendix A, symbolic eigenvalues for the Q4 and 5β (or PS) elements are given.
- A sample input file is given in Appendix B.
- Appendix C contains representative parts of the source code developed for this study.

Chapter 2

Classical element formulations

In this chapter the classic formulation of the standard displacement based bi-linear isoparametric membrane element (Q4) and the assumed stress membrane quadrilateral element (PS) are presented. The computer implementation of the elements is set out in Appendix C.

2.1 Introduction

In formulating displacement-based finite elements, the principle of virtual displacements (also called the principle of virtual work) is often used. This principle is equivalent to invoking the stationary condition of the total potential energy $\mathbf{\Pi}$ [6], where $\mathbf{\Pi} = U_{\text{int}} - W_{\text{ext}}$. Here, U_{int} and W_{ext} respectively indicate the total internal strain energy of a system, and the total potential of the applied loads. The variational approach provides an elegant and powerful approach for the analysis of continuous systems.

A rudimentary knowledge of functional analysis is required to study these formulations. The reader is referred to Bathe [6] for further details. Clear treatments are also presented in amongst others [7, 8, 9].

2.2 Classical displacement based formulation in 2-D

In the following, we limit ourselves to linear elastostatics, and, for the sake of brevity, we restrict ourselves to the Dirichlet problem. However, more complex boundary conditions may be incorporated in a standard manner, e.g. see [10].

Let Ω be a region occupied by a body. The boundary value problem under consideration is [7]: Given $\boldsymbol{f}$, the body force vector, find $\boldsymbol{u}$ such that

$$\text{div}\,\boldsymbol{\sigma} + \boldsymbol{f} = \mathbf{0} \quad \text{in } \Omega \tag{2.1}$$

$$\boldsymbol{\sigma} = \boldsymbol{C}\boldsymbol{\epsilon} \quad \text{in } \Omega \tag{2.2}$$

$$\boldsymbol{u} = \mathbf{0} \quad \text{on } \Gamma = \partial\Omega_u \tag{2.3}$$

where (2.1) - (2.3) are, respectively, the equilibrium equations, the constitutive equation, and the displacement boundary condition. $\partial\Omega$ represents the boundary of Ω, and $\partial\Omega_u$ represents the part of the boundary on which the displacements u are prescribed. For an isotropic material and plane stress, the constitutive modulus tensor $\boldsymbol{C} = \{C_{ijkl}\}$ has the form

$$C_{ijkl} = \lambda\delta_{ij}\delta_{kl} + \mu\left(\delta_{ik}\delta_{jl} + \delta_{il}\delta_{jk}\right) \quad i,j,k,l \in \{1,2\} \tag{2.4}$$

where

$$\lambda = \frac{\nu E}{(1-\nu^2)}, \tag{2.5}$$

and

$$\mu = \frac{E}{2\,(1+\nu)}. \tag{2.6}$$

E and ν are Young's modulus and Poisson's ratio, respectively. The potential energy functional for *each element*[1] is given by

$$\boldsymbol{\Pi}(\boldsymbol{u}) = \frac{1}{2}\int_\Omega \boldsymbol{\epsilon}^T\boldsymbol{C}\boldsymbol{\epsilon}\;\mathrm{d}\Omega - \int_\Omega \boldsymbol{u}^T\boldsymbol{f}\;\mathrm{d}\Omega, \tag{2.7}$$

with

$$\boldsymbol{\epsilon} = \boldsymbol{\partial}_\epsilon\boldsymbol{u}. \tag{2.8}$$

The stationary condition of the potential energy yields the corresponding variational equation

$$\delta\boldsymbol{\Pi}(\boldsymbol{u}) = 0 = \int_\Omega \delta\boldsymbol{\epsilon}^T\boldsymbol{C}\boldsymbol{\epsilon}\;\mathrm{d}\Omega - \int_\Omega \delta\boldsymbol{u}^T\boldsymbol{f}\;\mathrm{d}\Omega. \tag{2.9}$$

Since we interpolate $\boldsymbol{u}$ as

$$\boldsymbol{u} = \boldsymbol{N}\boldsymbol{q}, \tag{2.10}$$

we obtain

$$\boldsymbol{\epsilon} = \boldsymbol{\partial}_\epsilon\boldsymbol{u} = \boldsymbol{\partial}_\epsilon\boldsymbol{N}\boldsymbol{q} = \boldsymbol{B}\boldsymbol{q}. \tag{2.11}$$

Using matrix notation, the *discrete version* of (2.9) is written as

$$\int_\Omega \delta[\boldsymbol{B}\boldsymbol{q}]^T\boldsymbol{C}\boldsymbol{B}\boldsymbol{q}\;\mathrm{d}\Omega - \int_\Omega \delta(\boldsymbol{N}\boldsymbol{q})^T\boldsymbol{f}\;\mathrm{d}\Omega = 0, \tag{2.12}$$

or

$$\delta\boldsymbol{q}^T\int_\Omega \boldsymbol{B}^T\boldsymbol{C}\boldsymbol{B}\;\mathrm{d}\Omega\;\boldsymbol{q} - \delta\boldsymbol{q}^T\int_\Omega \boldsymbol{N}^T\boldsymbol{f}\;\mathrm{d}\Omega = 0, \tag{2.13}$$

where we note that $\delta\boldsymbol{q}^T$ is arbitrary. Hence,

$$\int_\Omega \boldsymbol{B}^T\boldsymbol{C}\boldsymbol{B}\;\mathrm{d}\Omega\;\boldsymbol{q} = \int_\Omega \boldsymbol{N}^T\boldsymbol{f}\;\mathrm{d}\Omega. \tag{2.14}$$

Denoting

$$\boldsymbol{K} = \int_\Omega \boldsymbol{B}^T\boldsymbol{C}\boldsymbol{B}\;\mathrm{d}\Omega, \tag{2.15}$$

[1] Summation over all the elements is implied when calculating the structural potential.

and

$$\boldsymbol{r} = \int_{\Omega} \boldsymbol{N}^T \boldsymbol{f} \, \mathrm{d}\Omega, \tag{2.16}$$

we rewrite the force-displacement relationship as

$$\boldsymbol{K}\boldsymbol{q} = \boldsymbol{r}, \tag{2.17}$$

which completes the formulation.

The finite element implementation of the element is well known, and therefore not explicitly given here.

2.3 Assumed stress formulation in 2-D

The general formulation of an assumed stress hybrid element[2] is based on *independent interpolations for stresses* $\boldsymbol{\sigma}$ *and displacements* $\boldsymbol{u}$. Hence we obtain strains $\boldsymbol{\epsilon} = \boldsymbol{\partial}_{\epsilon}\boldsymbol{u}$ derived from the displacements $\boldsymbol{u}$, and strains $\hat{\boldsymbol{\epsilon}}$ that satisfy the constitutive equation $\hat{\boldsymbol{\epsilon}} = \boldsymbol{C}^{-1}\boldsymbol{\sigma}$. It is of course required that these two independently obtained strain fields are equivalent, which may be effected by enforcing equivalence in a weak sense. The Hellinger-Reissner 2-field principle:

$$\boldsymbol{\Pi}(\boldsymbol{u}, \boldsymbol{\sigma}) = -\frac{1}{2}\int_{\Omega} \boldsymbol{\sigma}^T \boldsymbol{C}^{-1} \boldsymbol{\sigma} \, \mathrm{d}\Omega + \int_{\Omega} \boldsymbol{\sigma}^T \boldsymbol{\epsilon} \, \mathrm{d}\Omega - \int_{\Omega} \boldsymbol{u}^T \boldsymbol{f} \mathrm{d}\Omega. \tag{2.18}$$

Enforcing the variation of the functional to both the stress parameters and the nodal displacements leads to

$$\delta\boldsymbol{\Pi} = 0 = -\int_{\Omega} \delta\boldsymbol{\sigma}^T \boldsymbol{C}^{-1} \boldsymbol{\sigma} \, \mathrm{d}\Omega + \int_{\Omega} \delta\boldsymbol{\sigma}^T \boldsymbol{\epsilon} \, \mathrm{d}\Omega + \int_{\Omega} \boldsymbol{\sigma}^T \delta\boldsymbol{\epsilon} \, \mathrm{d}\Omega - \int_{\Omega} \delta\boldsymbol{u}^T \boldsymbol{f} \, \mathrm{d}\Omega. \tag{2.19}$$

Performing the variation with respect to the stress $\boldsymbol{\sigma}$ leads to

$$\int_{\Omega} \delta\boldsymbol{\sigma}^T \boldsymbol{\epsilon} \, \mathrm{d}\Omega - \int_{\Omega} \delta\boldsymbol{\sigma}^T \boldsymbol{C}^{-1} \boldsymbol{\sigma} \, \mathrm{d}\Omega = 0, \tag{2.20}$$

and the variation with respect to the displacement $\boldsymbol{u}$

$$\int_{\Omega} \boldsymbol{\sigma}^T \delta\boldsymbol{\epsilon} \mathrm{d}\Omega - \int_{\Omega} \delta\boldsymbol{u}^T \boldsymbol{f} \, \mathrm{d}\Omega = 0. \tag{2.21}$$

In Ω, the stresses $\boldsymbol{\sigma}$ are approximated via the interpolation [11, 12]

$$\boldsymbol{\sigma} = \boldsymbol{P}\boldsymbol{\beta}, \tag{2.22}$$

with $\boldsymbol{P}$ the matrix of the interpolation functions and $\boldsymbol{\beta}$ the vector of stress parameters. The strains, $\boldsymbol{\epsilon}$ are written in terms of the nodal displacements as

$$\boldsymbol{\epsilon} = \boldsymbol{\partial}_{\epsilon}\boldsymbol{u} = \boldsymbol{\partial}_{\epsilon}\boldsymbol{N}\boldsymbol{q} = \boldsymbol{B}\boldsymbol{q}, \tag{2.23}$$

[2]For the sake of simplicity, we consider equilibrium on the element level, as opposed to structural equilibrium. Again, summation over all elements is implied when calculating the structural potential.

where the displacements are as usual interpolated in the standard way, and $\boldsymbol{N}$ represents the displacement interpolation functions. (As usual, $\boldsymbol{u} = \boldsymbol{N}\boldsymbol{q}$.) By substituting the above interpolations into (2.20) and (2.21), we now write (2.20) as

$$\int_\Omega \delta\boldsymbol{\beta}^T \boldsymbol{P}^T \boldsymbol{B}\, \boldsymbol{q}\, \mathrm{d}\Omega - \int_\Omega \delta\boldsymbol{\beta}^T \boldsymbol{P}^T \boldsymbol{C}^{-1} \boldsymbol{P}\, \boldsymbol{\beta}\, \mathrm{d}\Omega = 0, \tag{2.24}$$

and (2.21) as

$$\int_\Omega \boldsymbol{\beta}^T \boldsymbol{P}^T \boldsymbol{B}\, \delta\boldsymbol{q}\, \mathrm{d}\Omega - \int_\Omega \delta\boldsymbol{q}^T \boldsymbol{N}^T \boldsymbol{f}\, \mathrm{d}\Omega = 0. \tag{2.25}$$

Defining $\boldsymbol{G}$ and $\boldsymbol{H}$ as

$$\boldsymbol{G} = \int_\Omega \boldsymbol{P}^T \boldsymbol{B}\, \mathrm{d}\Omega, \tag{2.26}$$

$$\boldsymbol{H} = \int_\Omega \boldsymbol{P}^T \boldsymbol{C}^{-1} \boldsymbol{P}\, \mathrm{d}\Omega, \tag{2.27}$$

(2.24) can be written as

$$\delta\boldsymbol{\beta}^T \boldsymbol{G}\, \boldsymbol{q} - \delta\boldsymbol{\beta}^T \boldsymbol{H}\, \boldsymbol{\beta} = 0, \tag{2.28}$$

and (2.25) as

$$\boldsymbol{\beta}^T \boldsymbol{G}\, \delta\boldsymbol{q} = \delta\boldsymbol{q}^T \boldsymbol{r} = \delta\boldsymbol{q}^T \boldsymbol{G}^T \boldsymbol{\beta}, \tag{2.29}$$

(2.28) and (2.29) can now be rewritten in matrix notation

$$\begin{bmatrix} \boldsymbol{0} & \boldsymbol{G}^T \\ \boldsymbol{G} & -\boldsymbol{H} \end{bmatrix} \begin{bmatrix} \boldsymbol{q} \\ \boldsymbol{\beta} \end{bmatrix} = \begin{bmatrix} \boldsymbol{r} \\ \boldsymbol{0} \end{bmatrix}.$$

From (2.28) $\boldsymbol{\beta}$ can be written as

$$\boldsymbol{\beta} = \boldsymbol{H}^{-1} \boldsymbol{G}\, \boldsymbol{q}. \tag{2.30}$$

By substituting (2.30) into (2.29) we obtain

$$\boldsymbol{G}^T \boldsymbol{H}^{-1} \boldsymbol{G}\, \boldsymbol{q} = \boldsymbol{r}. \tag{2.31}$$

The force-displacement relationship is defined by

$$\boldsymbol{K}\boldsymbol{q} = \boldsymbol{r}. \tag{2.32}$$

From (2.31) and (2.32) the stiffness matrix can then be written as

$$\boldsymbol{K} = \boldsymbol{G}^T \boldsymbol{H}^{-1} \boldsymbol{G}, \tag{2.33}$$

which completes the formulation.

2.3.1 Finite element implementation

For a 2-D 4-node quadrilateral membrane element, the displacements $\boldsymbol{u}$ are typically interpolated as

$$\boldsymbol{u} = \boldsymbol{N}\boldsymbol{q}, \tag{2.34}$$

with $\boldsymbol{N}$ the bi-linear Lagrangian interpolation functions, and $\boldsymbol{q}$ the (unknown) element nodal displacements. The stresses $\boldsymbol{\sigma}$ are interpolated as

$$\boldsymbol{\sigma} = \boldsymbol{T}\boldsymbol{P}\boldsymbol{\beta}, \tag{2.35}$$

with $\boldsymbol{P}$ the stress interpolation matrix, $\boldsymbol{T}$ an optional transformation or constraint matrix, and $\boldsymbol{\beta}$ the (unknown) elemental stress parameters. Selecting $\boldsymbol{T}$ and $\boldsymbol{P}$ is not straight forward; there are no unique optimal formulations. $\boldsymbol{P}$ depends on issues like completeness in the Cartesian coordinate system, which may compete with the limiting principle of Fraeijs de Veubeke [13]. Nevertheless, for the 4-node quadrilateral element at least, previous experience has shown that a number of formulations are accurate and robust. Typically, 5 β parameters are used, with

$$\boldsymbol{P} = \begin{bmatrix} 1 & 0 & 0 & \eta & 0 \\ 0 & 1 & 0 & 0 & \xi \\ 0 & 0 & 1 & 0 & 0 \end{bmatrix}, \tag{2.36}$$

and ξ and η the natural coordinates. For $\boldsymbol{T}$, the simplest formulation is probably the rational approach proposed by Pian and Sumihara [5].

2.4 Numerical example

2.4.1 Cook's membrane

The swept and tapered cantilever beam proposed by Cook (Fig 2.1), has been used by many authors. The center displacement u_{2c} for the various elements studied is tabulated in Table 2.1. The results are compared with the best known solution of $u_{2c} = 23.94$.

Table 2.1 clearly illustrates the vastly superior performance of the PS element over the Q4 element.

Element	1×1	2×2	4×4	8×8
Q4	5.9677	11.8451	18.2993	22.0790
PS	16.7223	21.1284	23.0215	23.6887
Best known		23.94		

Table 2.1: Mid node displacement for Cook's membrane (plane stress) obtained with displacement based Q4 and assumed stress PS elements

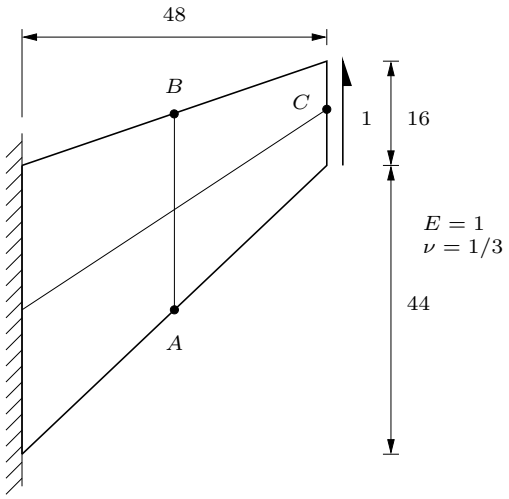

Figure 2.1: Cook's membrane

Chapter 3

Elements with penalized equilibrium formulation

In this chapter, the penalized equilibrium formulation of membrane elements is outlined. The computer implementation of the theory is reflected in Appendix C.

3.1 Penalized equilibrium in assumed stress elements

As indicated in Chapter 2, assumed stress hybrid elements are renowned for their accurate stress solutions, due to the fact that the stress and displacement trial functions are selected independently.

Accurate stress solutions in the sense of the energy norm do not necessarily imply pointwise accurate stress predictions within elements [14]. Indeed, most hybrid elements only yield accurate stress predictions at the element centroid, while stress predictions at element edges and in particular element nodes, can be highly inaccurate.

To improve the accuracy of point wise predictions in hybrid elements, a number of formulations have been proposed. This includes pre- and post-treatment [14], with the latter simpler and superior. Post treatment via penalized equilibrium is outlined as follows: While distributed body forces may induce important loads on a structure, they can usually be ignored on the element level in stress calculations [15]. Hence element equilibrium is written as

$$\boldsymbol{\partial\sigma} = \boldsymbol{D}^T\boldsymbol{\sigma} = \mathbf{0} \text{ in } \Omega \tag{3.1}$$

with $\boldsymbol{D}$ the 2-D differential operator; Ω indicates the elemental domain.

Enforcement of (3.1) in the variational formulation (2.20) yields a functional $\boldsymbol{\Pi}^*$ of the form

$$\boldsymbol{\Pi}^*(\boldsymbol{u},\boldsymbol{\sigma}) \;=\; \boldsymbol{\Pi}(\boldsymbol{u},\boldsymbol{\sigma}) - \alpha\int(\boldsymbol{\partial\sigma})^T(\boldsymbol{\partial\sigma})d\Omega, \;\; \alpha \gg 0, \tag{3.2}$$

where $\boldsymbol{\Pi}(\boldsymbol{u},\boldsymbol{\sigma})$ represents the potential of the Hellinger-Reissner principle (2.20). Using matrix notation, and for the sake of convenience setting $\alpha \leftarrow \alpha/2E$, the potential of the assumed stress elements becomes

$$\boldsymbol{\Pi}^*(\boldsymbol{u},\boldsymbol{\sigma}) \;=\; \boldsymbol{\beta}^T\boldsymbol{G}\boldsymbol{q} - \frac{1}{2}\boldsymbol{\beta}^T\left(\boldsymbol{H} + \frac{\alpha}{E}\boldsymbol{H}_p\right)\boldsymbol{\beta} - \boldsymbol{q}^T\boldsymbol{r} \tag{3.3}$$

with

$$\boldsymbol{G} = \int_{\Omega} \boldsymbol{P}^T \boldsymbol{B}\, d\Omega, \tag{3.4}$$

$$\boldsymbol{H} = \int_{\Omega} \boldsymbol{P}^T \boldsymbol{C}^{-1} \boldsymbol{P}\, d\Omega, \tag{3.5}$$

$$\boldsymbol{r} = \int_{\Omega} \boldsymbol{N}^T \boldsymbol{f}\, d\Omega, \tag{3.6}$$

and

$$\boldsymbol{H}_p = \int_{\Omega} (\boldsymbol{\partial P})^T (\boldsymbol{\partial P}) d\Omega, \tag{3.7}$$

where $\boldsymbol{P}$ is now understood to represent the matrix product $\boldsymbol{TP}$.

The force-displacement relationship is obtained as

$$\boldsymbol{G}^T \left(\boldsymbol{H} + \frac{\alpha}{E} \boldsymbol{H}_p \right)^{-1} \boldsymbol{G}\, \boldsymbol{q} = \boldsymbol{r}, \tag{3.8}$$

or

$$\boldsymbol{K}\boldsymbol{q} = \boldsymbol{r}. \tag{3.9}$$

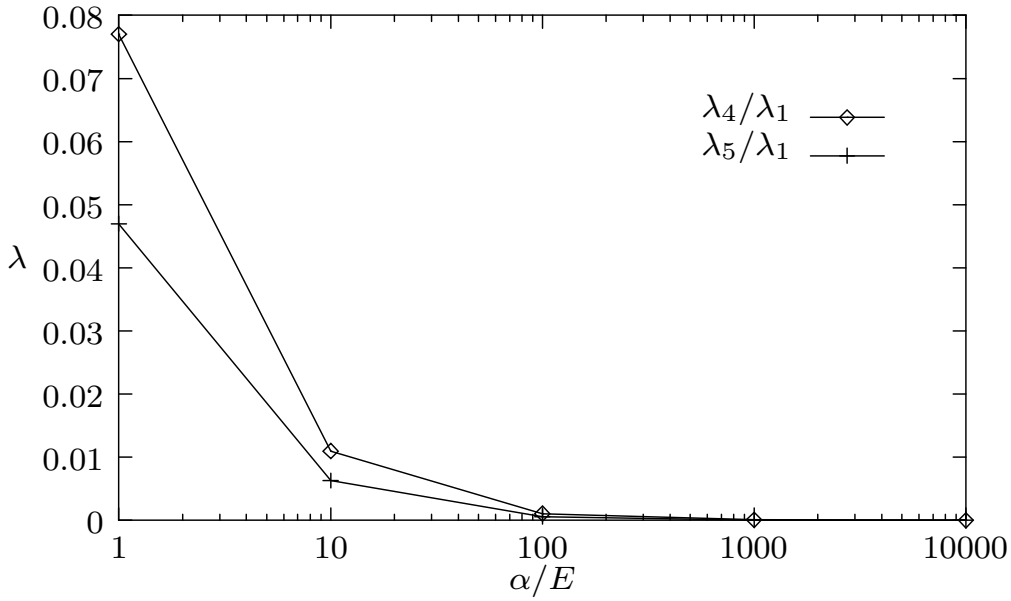

Figure 3.1: Typical variation of the eigenvalues of a penalized, arbitrary distorted 5β assumed stress element

3.1.1 Allowable values of α for hybrid elements

In the penalty formulation, we note that $\alpha \gg 0$ is required. Wu and Cheung merely report that results converge for $\alpha/E \geq 10000$, but they present no comments on element accuracy in the limit

of enforcing $\alpha \gg 0$. They then suggest that the equality represented in this relationship be used for practical implementations.

For elements of regular geometry, penalized equilibrium has no influence. (A 'regular' geometry is understood to be square or rectangular.) However, for elements of irregular geometry, the stiffness associated with the higher order deformation modes completely vanishes as $\alpha \to \infty$ (e.g. see Fig 3.1).

In an assembly of elements, even very high values of α are normally adequate to prevent communicable mechanisms (spurious modes); in addition, the higher order modes of course have no influence in passing the patch test. Hence connected elements are unconditionally convergent. Nevertheless, for single elements (or a very small number of elements), the higher order modes may vanish for all practical purposes, resulting in very low stiffness, and therefore significant over-displacement, in bending dominated problems.

3.1.2 Cook's membrane

We again study Cook's membrane (see Section 2.4.1), to compare the penalized and unpenalized assumed stress elements.

The penalized assumed stress element converges from above to the best known result, while the unpenalized assumed stress element converges from below. Typically, penalized elements are more accurate than their unpenalized counterparts, although very coarse meshes can results in displacements that are too large.

Element	1×1	2×2	4×4	8×8
PS	16.7223	21.1284	23.0215	23.6887
PS(α)	46.7567	25.9153	24.0925	23.9639
Best known		23.94		

Table 3.1: Mid-node displacement for Cook's membrane (plane stress), obtained with unpenalized PS and penalized PS(α) assumed stress elements

.

3.2 Penalized equilibrium in displacement based elements

3.2.1 Element defects

While the finite element method is an established method for solving complicated structural problems, the quest for elements of ever increasing accuracy and robustness continues.

A typical example is the formulation of elements that perform well in bending. The standard displacement based bi-linear isoparametric membrane element (Q4) is notorious for its low accuracy

under bending dominated conditions. Distortion of the element geometry further aggravates the already bad performance, which is an indication of the lack of robustness of this element.

When the standard displacement based Q4 element is used in bending it develops shear strains as well as the expected bending strains. The Q4 element cannot exhibit pure bending, since the parasitic shear strains absorb strain energy. Hence, when a given bending deformation is prescribed, the bending moment needed to produce it is larger than the correct value. In other words, the Q4 element exhibits shear locking behavior [15].

Strain energy U in a linearly elastic body of volume V, without initial stress or strain, can be evaluated from the expression

$$U = \frac{1}{2}\int \boldsymbol{\epsilon}^T \boldsymbol{D}\boldsymbol{\epsilon} dV \tag{3.10}$$

where, for the 2D case $\boldsymbol{\epsilon} = [\epsilon_x \epsilon_y \gamma_{xy}]^T$

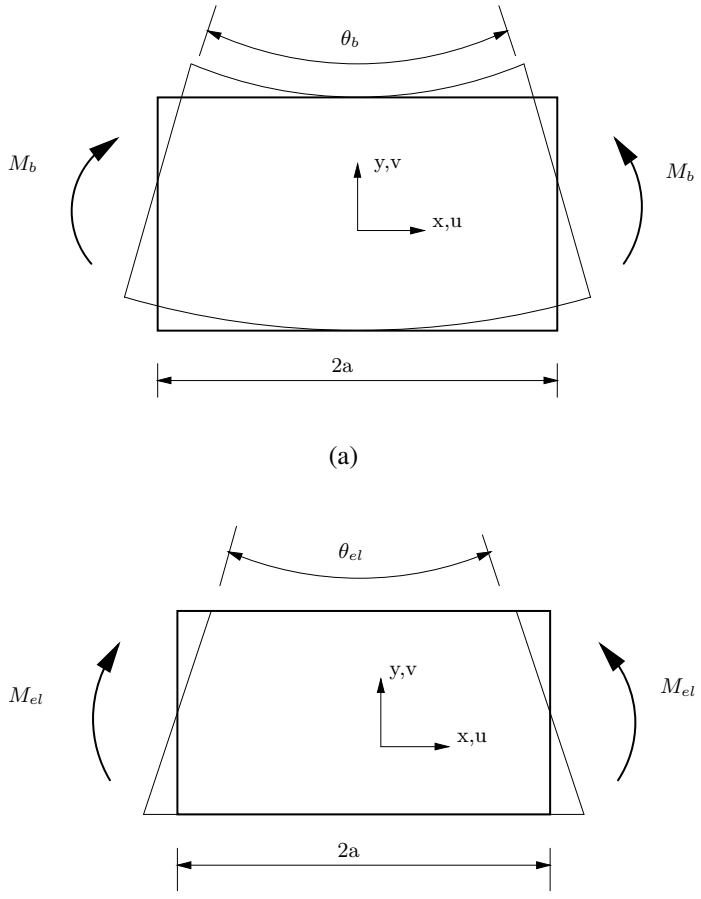

Figure 3.2: Deformation mode in bending: (a) A rectangular block of material in pure bending (b) A Q4 element under bending load

and, for a plane element of thickness t, the volume increment is $dV = tdxdy$. In pure bending, as

shown in Fig 3.2(a) a block of material experiences the strains

$$\epsilon_x = -\frac{\theta_b y}{2a} \quad \epsilon_y = \nu\frac{\theta_b y}{2a} \quad \gamma_{xy} = 0. \tag{3.11}$$

When a Q4 element is bent, as shown in Fig 3.2(b), its top and bottom sides remain straight, and each node has only horizontal displacement of magnitude $\theta_{el}b/2$. Hence, from the strain-displacement relation $\boldsymbol{\epsilon} = \boldsymbol{Bd}$, the element strains are

$$\epsilon_x = -\frac{\theta_{el} y}{2a} \quad \epsilon_y = 0 \quad \gamma_{xy} = -\frac{\theta_{el} x}{2a}. \tag{3.12}$$

Thus ϵ_x in the element is exact and ϵ_y is approximate (but exact if $\nu = 0$). Of the greatest concern is the nonzero shear strain γ_{xy} which should be zero in bending.

3.2.2 Displacement based elements with penalized equilibrium

Various methodologies have been proposed to overcome the bending deficiency of the standard displacement based element. Amongst others, proposed remedies include reduced integration with stabilization modes, the introduction of incompatible modes [16], assumed stress interpolations [17, 18], enhanced strain modes [19], and the inclusion of in-plane drilling degrees of freedom [20, 21, 22].

In this chapter, we study some of the fundamental reasons for the poor performance of the Q4 element using a penalty formulation; it is not the intention to present yet another 4 node element formulation. Nevertheless, in the following sections it is demonstrated that the accuracy of the undistorted Q4 element may be raised to the linear strain capability, albeit at the introduction of elemental parameters. The elemental parameters are selected such that spurious zero energy modes are not introduced, for which an investigation of the characteristic equations of the elemental stiffness matrix may be used. For the Q4 element with bi-linear interpolation, enforcement of $\boldsymbol{\partial\sigma} = \mathbf{0}$ in Ω seems difficult, if not impossible. However, it may be attempted to soften the higher order deformation modes via the introduction of elemental parameters, expressed in terms of the element equilibrium equations.

The straining or deformation modes of a typical rectangular Q4 element are depicted in Fig 3.3. The (very stiff) higher order modes are to be blamed for the poor performance of this element in bending. For the element, the stresses are obtained from

$$\boldsymbol{\sigma} = \boldsymbol{C\epsilon}, \tag{3.13}$$

viz.

$$\boldsymbol{\sigma} = \boldsymbol{CBq}. \tag{3.14}$$

Hence

$$\boldsymbol{\partial\sigma} = \boldsymbol{\partial(CBq)} = \boldsymbol{C(\partial B)q} = \boldsymbol{\bar{B}q} \tag{3.15}$$

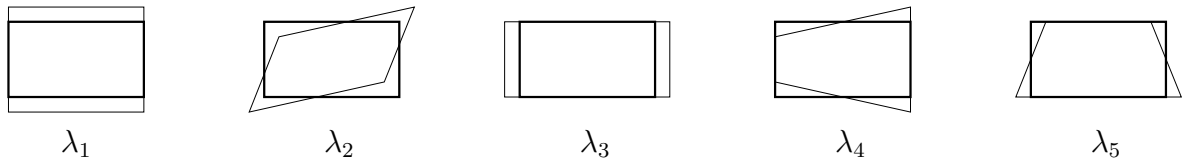

Figure 3.3: Straining modes of a rectangular Q4 element, side lengths $2a$ and $2b$, $a \geq b$

The potential energy functional is then written as:

$$\boldsymbol{\Pi}^*(\boldsymbol{u}) = \frac{1}{2}\int_\Omega \boldsymbol{\epsilon}^T \boldsymbol{C}\boldsymbol{\epsilon}\, d\Omega - \alpha \int_\Omega (\boldsymbol{C}\boldsymbol{\epsilon})^T(\boldsymbol{C}\boldsymbol{\epsilon})\, d\Omega$$

$$- \int_\Omega \boldsymbol{u}^T \boldsymbol{f}\, d\Omega \tag{3.16}$$

with

$$\boldsymbol{\epsilon} = \boldsymbol{\partial}\boldsymbol{u}. \tag{3.17}$$

Interpolating for $\boldsymbol{u}$ as

$$\boldsymbol{u} = \boldsymbol{N}\boldsymbol{q}, \tag{3.18}$$

(3.16) becomes

$$\boldsymbol{\Pi}^*(\boldsymbol{u}) = \frac{1}{2}\boldsymbol{q}^T \int_\Omega \boldsymbol{B}^T\boldsymbol{C}\boldsymbol{B}\, d\Omega\, \boldsymbol{q} -$$

$$\alpha \boldsymbol{q}^T \int_\Omega \bar{\boldsymbol{B}}^T \bar{\boldsymbol{B}}\, d\Omega\, \boldsymbol{q} - \boldsymbol{q}^T\boldsymbol{r}. \tag{3.19}$$

Substituting $\alpha \leftarrow \alpha E/2$, the stationary condition yields

$$(\boldsymbol{K} - \alpha E \bar{\boldsymbol{K}})\boldsymbol{q} = \boldsymbol{r} \tag{3.20}$$

with

$$\boldsymbol{K} = \int_\Omega \boldsymbol{B}^T\boldsymbol{C}\boldsymbol{B}\, d\Omega, \tag{3.21}$$

$$\bar{\boldsymbol{K}} = \int_\Omega \bar{\boldsymbol{B}}^T \bar{\boldsymbol{B}}\, d\Omega, \tag{3.22}$$

and

$$\boldsymbol{r} = \int_\Omega \boldsymbol{N}^T \boldsymbol{f}\, d\Omega \tag{3.23}$$

3.2.3 On critical values of α

The parameter α must be selected such that spurious zero energy modes are not introduced, for which an investigation of the characteristic equations of the modified stiffness matrix suffices. In general in 2-D, α must be selected such that

$$\left(\boldsymbol{K} - \alpha E \bar{\boldsymbol{K}}\right) \tag{3.24}$$

is positive semi-definite, with rank $(n-3)$, where $n = \dim(\boldsymbol{K})$. For Q4, $n = 8$. The critical (maximum) value of α is that value that results in the introduction of a spurious zero energy mode. α_{crit} may directly be obtained from the characteristic polynomial of (3.24). We will now symbolically determine critical values of α for square and rectangular geometries. In doing so, we will denote the eigenvalues of (3.24) λ_1 through λ_8, with $\lambda_1 > \lambda_2 > \cdots > \lambda_8$.

Square element, side length $2a$

For a square element of unit thickness and side length $2a$, an investigation of the characteristic polynomial of (3.24) results in the following *linear* relationship between the critical eigenvalue λ_5 and α:

$$\lambda_5 = \frac{E}{12a^2}(2a^2\nu^2 - 8\nu a^2 - 3\nu\alpha - 3\alpha + 6a^2) \times (\nu^3 - \nu^2 - \nu + 1). \tag{3.25}$$

Since $E \neq 0$ and $(\nu^3 - \nu^2 - \nu + 1) \neq 0$ for $0 \leq \nu \leq 0.5$, the critical value of α may be obtained through the equality

$$(2a^2\nu^2 - 8\nu a^2 - 3\nu\alpha - 3\alpha + 6a^2) = 0, \tag{3.26}$$

which directly yields

$$\alpha_{crit} = \frac{2a^2(\nu^2 - 4\nu + 3)}{3(\nu + 1)E^2}. \tag{3.27}$$

Rectangular element, side lengths $2a$ and $2b$, $a \geq b$

For a rectangular element of unit thickness and side lengths $2a$ and $2b$, $a \geq b$, the critical eigenvalue is obtained as

$$\lambda_5 = \frac{-Ea}{12b}(3\nu\alpha + 3\alpha - 2a^2 + 4a^2\nu - 2a^2\nu^2 - 4b^2 + 4b^2\nu)(\nu^3 - \nu^2 - \nu + 1). \tag{3.28}$$

Hence

$$\alpha_{crit} = \frac{2a^2(\nu^2 - 2\nu + 1) + 4b^2(1 - \nu)}{3(\nu + 1)E^2}. \tag{3.29}$$

It is noted that only the higher order modes (associated with λ_4, λ_5) are a function of α.

Irregular geometries

In the foregoing, we have considered only regular geometries; a treatment for irregular (generally distorted geometries) is awaiting. This can probably be done using

1. analytical or symbolic techniques to find the characteristic polynomial, or
2. through approximate relationships derived from the mapping to a 'regular' parent element.

Nevertheless, it is easy to use mathematical programming techniques to determine α_{crit} for arbitrary distorted elements. Enforcement of $\lambda_5 > \epsilon$, ϵ positive and prescribed, will always guarantee convergence, since the resultant element is rank sufficient, and passes the patch test.

3.2.4 Optimal values of α

While any value of $\alpha < \alpha_{crit}$ will prevent spurious modes, values close to α_{crit} are not necessarily optimal. Although 'optimality' is subjective, it seems sensible to make the Q4 element 'bending-exact', which can, at least for square elements, be done by making the element stiffness matrix equivalent to that of the assumed stress element.

For a square element, this is simple. Equating (A.4) and (A.9) (or (A.5) and (A.10)) in the Appendix results in

$$\alpha = 2/3\,\frac{a^2\,(1-\nu)\,(2\,\nu^2-\nu+1)}{(\nu+1)E^2}. \tag{3.30}$$

For a rectangular element, two sets of equations are to be equated, which are for the sake of brevity not presented here. This results in two expressions, namely

$$\alpha_1 = 2/3\,\frac{(1-\nu)\,(2\,a^2\nu^2-b^2\nu+b^2)}{(\nu+1)E^2}, \tag{3.31}$$

and

$$\alpha_2 = 2/3\,\frac{(1-\nu)\,(2\,\nu^2 b^2-a^2\nu+a^2)}{(\nu+1)E^2}, \tag{3.32}$$

with $\alpha_1 \neq \alpha_2$; it is impossible to satisfy both expressions at the same time.

3.3 Separation of the higher order deformation modes in Q4

To overcome the implications of $\alpha_1 \neq \alpha_2$, it is proposed to separate the expressions for the orthogonal higher order modes

$$\boldsymbol{\partial\sigma}_x \text{ in } \Omega, \quad \text{and} \tag{3.33}$$

$$\boldsymbol{\partial\sigma}_y \text{ in } \Omega. \tag{3.34}$$

where Ω again refers to the elemental domain. This results in an elemental formulation of the form

$$\boldsymbol{\Pi}^*(\boldsymbol{u}) = \boldsymbol{\Pi}(\boldsymbol{u}) - \alpha_x \int (\boldsymbol{\partial}_x\boldsymbol{\sigma})^T(\boldsymbol{\partial}_x\boldsymbol{\sigma})d\Omega$$

$$-\alpha_y \int (\boldsymbol{\partial}_y\boldsymbol{\sigma})^T(\boldsymbol{\partial}_y\boldsymbol{\sigma})d\Omega, \tag{3.35}$$

with $\boldsymbol{\sigma}$ derived from the displacement $\boldsymbol{u}$ as $\boldsymbol{\sigma} = \boldsymbol{DBq}$. We will denote this formulation Q4($\hat{\alpha}$).

In formulating this (bending-exact) element, the following two equations must be solved simultaneously:

$$4\,b^2v^4 - 2\,a^2v^3 + \left(3\,E^2\alpha_x + 2\,a^2 - 4\,b^2 + 12\,E^2\alpha_y\right)v^2 + \left(2\,a^2 - 6\,E^2\alpha_x\right)v - 2\,a^2 + 3\,E^2\alpha_x = 0, \tag{3.36}$$

and

$$4\,a^2v^4 - 2\,b^2v^3 + \left(3\,E^2\alpha_y + 2\,b^2 - 4\,a^2 + 12\,E^2\alpha_x\right)v^2 + \left(2\,b^2 - 6\,E^2\alpha_y\right)v - 2\,b^2 + 3\,E^2\alpha_y = 0. \tag{3.37}$$

This may be done analytically during assembly of element stiffness matrices; no inversion of submatrices in the element stiffness matrix is required.

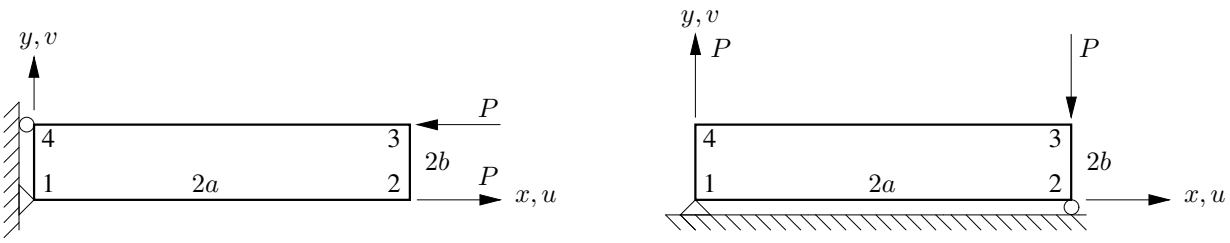

$E = 1500, \nu = 0.25, 2a = 10, 2b = 2, P = 1000$

Figure 3.4: Slender and short beams in pure bending

3.4 Numerical example

Consider the slender and short beams in pure bending depicted in Fig 3.4. Numerical results are presented in Tables 3.2 and 3.3 for the slender and the short beam respectively. In the tables, α_{crit} results from (3.29), α_1 and α_2 represent values that enforce (3.31) and (3.32) respectively, while $\alpha_{ave} = (\alpha_1 + \alpha_2)/2$. $|\sigma_b|$ represents the bending stress at an elemental centroid for a 2×2 mesh discretization.

The tables reveal that $\alpha \rightarrow \alpha_{crit}$ results in severe over-displacement, while $\alpha = \alpha_2$ or $\alpha = \alpha_{ave}$ does not overcome the locking behavior of the element. Q4$(\hat{\alpha})$ on the other hand, is bending-exact in terms of nodal displacements; even the bending stresses at the reduced integration points are exact.

Element	u_2	v_2	σ_b
5β	20.0	100.0	1500
Q4	1.81	9.02	426
Q4(α), $\alpha = \alpha_1$	20.0	100.0	1500
Q4(α), $\alpha = \alpha_2$	2.22	11.11	500
Q4(α), $\alpha = \alpha_{ave}$	4.0	20.0	750
Q4(α), $\alpha \rightarrow \alpha_{crit}$	180.0	963.0	2000
Q4$(\hat{\alpha})$	20.0	100.0	1500
Theory	20.0	100.0	1500

Table 3.2: Numerical results for the slender beam in pure bending

3.5 Discussion

Firstly, it is noted that the post treatment of assumed stress membrane finite elements through penalized equilibrium, in theory, results in complete loss of stiffness associated with higher order deformation modes. While this can be circumvented by prescribing an upper limit on α, significant over-displacement can occur for course meshes.

Element	u_4	v_4	σ_b
5β	0.80	0.160	300
Q4	0.78	0.157	294
Q4(α), $\alpha = \alpha_1$	0.87	0.174	326
Q4(α), $\alpha = \alpha_2$	0.80	0.160	300
Q4(α), $\alpha = \alpha_{ave}$	0.83	0.160	313
Q4($\hat{\alpha}$)	0.80	0.160	300
Theory	0.80	0.160	300

Table 3.3: Numerical results for the short beam in pure bending

Secondly, we note that the introduction of elemental parameters into the displacement based Q4 element soften the higher order deformation modes, appropriate choices render the element exact in bending.

Chapter 4

Elements with drilling degrees of freedom

In this chapter, the formulation of membrane finite elements with drilling degrees of freedom is outlined. The computer implementation of the theory is given in Appendix C.

4.1 Formulation of elements with drilling degrees of freedom

In membrane analysis, displacements (and hence strains and stresses) are uniquely defined by two in-plane translations. Strictly speaking, this makes additional in-plane rotational degrees of freedom seem superfluous. However, because of enrichment of the displacement field, the in-plane behavior of low order elements is vastly improved when rotational degrees of freedom are included in the element formulation. In addition, drilling degrees of freedom allow for beam-slab connections and provide the needed 6^{th} d.o.f in shell analysis.

4.2 Variational formulation

The condensed treatment of Ibrahimbegovic *et al* [22] presented by [23] is followed closely without further proof or motivation. The formulation is limited to linear elastic problems and discussion of boundary conditions is omitted. Boundary conditions may be incorporated in a standard manner.

Let Ω be a region occupied by a body. The boundary value problem under consideration is: For all $\mathbf{x} \in \Omega$

$$\text{div } \boldsymbol{\sigma} + \boldsymbol{f} = \mathbf{0} \tag{4.1}$$

$$\text{skew } \boldsymbol{\sigma} = \mathbf{0} \tag{4.2}$$

$$\boldsymbol{\psi} = \text{skew } \bigtriangledown \boldsymbol{u} \tag{4.3}$$

$$\text{symm } \boldsymbol{\sigma} = \boldsymbol{C} \cdot \text{symm } \bigtriangledown \boldsymbol{u} \tag{4.4}$$

where (4.1) to (4.4) are, respectively, the equilibrium equations, the symmetry conditions for stress, the definition of rotation in terms of displacement gradient and the constitutive equations. In (4.1) to (4.4) the Euclidean decomposition of second-rank tensors are employed, e.g

$$\boldsymbol{\sigma} = \text{symm } \boldsymbol{\sigma} + \text{skew } \boldsymbol{\sigma} \tag{4.5}$$

where

$$\text{symm } \boldsymbol{\sigma} = \frac{1}{2}(\boldsymbol{\sigma} + \boldsymbol{\sigma}^T), \tag{4.6}$$

$$\text{skew } \boldsymbol{\sigma} = \frac{1}{2}(\boldsymbol{\sigma} - \boldsymbol{\sigma}^T). \tag{4.7}$$

For an isotropic material and plane stress, the constitutive modulus tensor $\mathbf{C} = \{C_{ijkl}\}$ has the form

$$C_{ijkl} = \lambda\delta_{ij}\delta_{kl} + \mu(\delta_{ik}\delta_{jl} + \delta_{il}\delta_{jk}) \tag{4.8}$$

where

$$\lambda = \frac{\upsilon E}{(1-\upsilon^2)}, \tag{4.9}$$

$$\mu = \frac{E}{2(1+\upsilon)}, \tag{4.10}$$

where E and υ are Young's modulus and Poisson's ratio, respectively. Reissner [24] presented a variational formulation for the boundary value problem reflected in (4.1) to (4.4). The problems of the formulation presented by Reissner are not discussed here, but the reader is referred to [21] instead. The variational problem of Reissner was modified by Hughes and Brezzi [21] in order to preserve the stability of the discrete problem. This modification preserves (4.1) to (4.4) as the Euler-Lagrange equations. In addition, the symmetrical components of stress are eliminated using the constitutive equation (4.4) to give:

Problem(M)

$$\begin{aligned}\boldsymbol{\Pi}_\gamma(\boldsymbol{v}, \boldsymbol{\omega}, \text{skew } \boldsymbol{\tau}) \;=\; & \frac{1}{2}\int_\Omega \text{symm } (\bigtriangledown \boldsymbol{v}) \cdot \boldsymbol{C} \cdot (\text{symm } \bigtriangledown \boldsymbol{v}) d\Omega + \int_\Omega \text{skew } \boldsymbol{\tau}^T \cdot (\text{skew } \bigtriangledown \boldsymbol{v} - \boldsymbol{\omega}) d\Omega \\ & -\frac{1}{2}\gamma^{-1}\int_\Omega |\text{skew } \boldsymbol{\tau}|^2 d\Omega - \int_\Omega \boldsymbol{v} \cdot \boldsymbol{f} d\Omega,\end{aligned} \tag{4.11}$$

where $\boldsymbol{v} \in \boldsymbol{V}$, $\boldsymbol{\omega} \in \boldsymbol{W}$, $\boldsymbol{\tau} \in \boldsymbol{T}$ are spaces of trial displacements, rotations and stresses. This variational formulation requires that the rotations $\boldsymbol{\omega}$ and stresses $\boldsymbol{\tau}$, together with the displacement generalized derivatives $\bigtriangledown \boldsymbol{v}$, belong to the space of square-integrable functions over the region Ω. The variational equation which results from variations on (4.11) is

$$\begin{aligned}0 = \boldsymbol{D}\boldsymbol{\Pi}_\gamma(\boldsymbol{u}, \boldsymbol{\psi}, \text{skew } \boldsymbol{\sigma}) \cdot (\boldsymbol{v}, \boldsymbol{\omega}, \text{skew } \boldsymbol{\tau}) = & \int_\Omega (\text{symm } \bigtriangledown \boldsymbol{v}) \cdot \boldsymbol{C} \cdot (\text{symm } \bigtriangledown \boldsymbol{u}) d\Omega \\ & + \int_\Omega \text{skew } \boldsymbol{\tau}^T \cdot (\text{skew } \bigtriangledown \boldsymbol{u} - \boldsymbol{\psi}) d\Omega + \int_\Omega (\text{skew } \bigtriangledown \boldsymbol{v}^T \cdot \text{skew } \boldsymbol{\sigma} - \boldsymbol{\omega}^T \cdot \text{skew } \boldsymbol{\sigma}) d\Omega \\ & -\gamma^{-1}\int_\Omega \text{skew } \boldsymbol{\tau}^T \cdot \text{skew } \boldsymbol{\sigma} d\Omega - \int_\Omega \boldsymbol{v} \cdot \boldsymbol{f} d\Omega.\end{aligned} \tag{4.12}$$

It is possible to eliminate the skew-symmetric part of the stress tensor (see [21]) by substituting

$$\gamma^{-1}\text{skew } \boldsymbol{\sigma} = \text{skew } \bigtriangledown \boldsymbol{u} - \boldsymbol{\psi} \tag{4.13}$$

into Problem (M) to obtain Problem (D)

$$\begin{aligned}\tilde{\Pi}_\gamma(\boldsymbol{v},\boldsymbol{\omega}) &= \frac{1}{2}\int_\Omega \text{symm}\,(\bigtriangledown \boldsymbol{v})\cdot\boldsymbol{C}\cdot(\text{symm}\,\bigtriangledown\boldsymbol{v})d\Omega \\ &\quad +\frac{1}{2}\gamma\int_\Omega |\text{skew}\;\bigtriangledown\boldsymbol{v}-\boldsymbol{w}\,|^2 d\Omega - \int_\Omega \boldsymbol{v}\cdot\boldsymbol{f}d\Omega. \end{aligned} \tag{4.14}$$

The corresponding variational equation now is

$$\begin{aligned} 0 = \boldsymbol{D}\tilde{\Pi}_\gamma(\boldsymbol{u},\boldsymbol{\psi})\cdot(\boldsymbol{v},\boldsymbol{\omega}) &= \int_\Omega (\text{symm}\,\bigtriangledown\boldsymbol{u})\cdot\boldsymbol{C}\cdot(\text{symm}\,\bigtriangledown\boldsymbol{v})d\Omega \\ &\quad +\gamma\int_\Omega (\text{skew}\,\bigtriangledown\boldsymbol{v}-\boldsymbol{\omega})^T\cdot(\text{skew}\,\bigtriangledown\boldsymbol{u}-\boldsymbol{\psi})d\Omega - \int_\Omega \boldsymbol{v}\cdot\boldsymbol{f}d\Omega. \end{aligned} \tag{4.15}$$

The variational equation (4.15) is taken as the basis for constructing the displacement-type discrete formulation which is presented in the next section. The parameter γ in the foregoing formulation is problem dependent [21].

4.2.1 Finite element interpolation

As with the foregoing, the treatment of Ibrahimbegovic et al. [22] is followed closely and the same notation is used. However, only the displacement-penalty approach is presented here. The mixed-type variational approach may be found in [22]. The particular choice for finite dimensional spaces $\mathbf{V}^h$,$\mathbf{W}^h$,$\mathbf{T}^h$ is presented along with the resulting discrete formulations. First the discrete version of Problem(D) is considered:

Problem $(D)^h$

$$\begin{aligned} 0 &= \int_{\Omega^h} (\text{symm}\,\bigtriangledown\boldsymbol{v}^h)^T\cdot\boldsymbol{C}\cdot(\text{symm}\,\bigtriangledown\boldsymbol{u}^h)d\Omega \\ &\quad +\gamma\int_{\Omega^h} (\text{skew}\;\bigtriangledown\boldsymbol{v}^h-\omega^h)^T\cdot(\text{skew}\;\bigtriangledown\boldsymbol{u}^h-\psi^h)d\Omega - \int_\Omega \boldsymbol{v}^{hT}\cdot\boldsymbol{f}d\Omega. \end{aligned} \tag{4.16}$$

Consider a 4-node quadrilateral element with degrees of freedom as depicted in Fig 4.1. The reference surface of the element is defined by

$$\boldsymbol{x} = \sum_{I=1}^{4} N_I^e(\zeta,\eta)\boldsymbol{x}_I, \tag{4.17}$$

where x represents co-oordinates (x_1, x_2) of a point on the reference surface and $N_I(\zeta,\eta)$ are the isoparametric shape functions [25]

$$N_I^e(\zeta,\eta) = \frac{1}{4}(1+\zeta_I\zeta)(1+\eta_I\eta)\;;\text{I = 1,2,3,4.} \tag{4.18}$$

The independent rotation field is interpolated as a standard bilinear field over each element:

$$u_3 = \psi^h = \sum_e\sum_{I=1}^{4} N_I^e(\zeta,\eta)\psi_i. \tag{4.19}$$

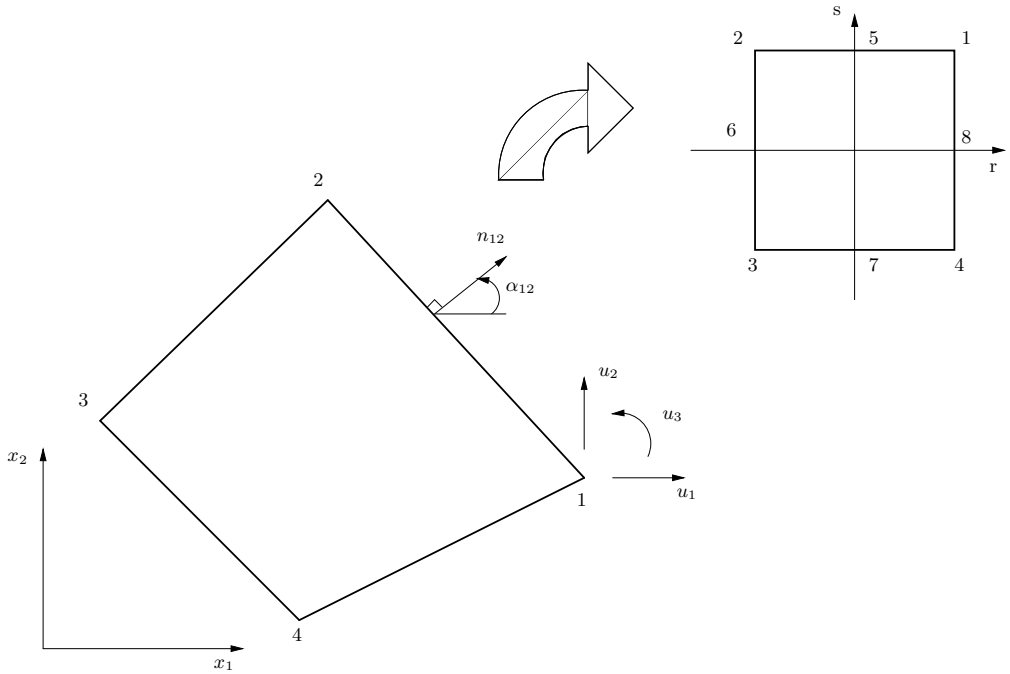

Figure 4.1: Four-node quadrilateral element with drilling degrees of freedom

The in-plane displacement approximation is taken as an Allman-type interpolation

$$\begin{pmatrix} u_1 \\ u_2 \end{pmatrix} = \boldsymbol{u}^h = \sum_e \sum_{I=1}^{4} N_I^e(\zeta,\eta)\boldsymbol{u_I} + \sum_e \sum_{I=5}^{8} NS_I^e(\zeta,\eta)\frac{l_{JK}}{8}(\psi_K - \psi_J)\boldsymbol{n}_{JK} + \sum_e NB_9^e(\zeta,\eta) \triangle \boldsymbol{u}_9, \tag{4.20}$$

where l_{JK} and $\mathbf{n}_{JK}$ are the length and outward unit normal vector on the element side associated with the corner nodes J and K, i.e.

$$\boldsymbol{n}_{JK} = \begin{pmatrix} n_1 \\ n_2 \end{pmatrix} = \begin{pmatrix} \cos\alpha_{JK} \\ \sin\alpha_{JK} \end{pmatrix}, \tag{4.21}$$

and

$$l_{JK} = \left((x_{K1} - x_{J1})^2 + (x_{K2} - x_{J2})^2\right)^{\frac{1}{2}}. \tag{4.22}$$

In the above, a FORTRAN-like definition of adjacent corner nodes are employed:

$$J = I - 4; \text{ K = mod(I,4) + 1.} \tag{4.23}$$

In (4.20) the serendipity shape functions are defined by

$$NS_I^e(\zeta,\eta) = \frac{1}{2}(1-\zeta^2)(1+\eta_I\eta); \text{ I = 5,7,} \tag{4.24}$$

$$NS_I^e(\zeta,\eta) = \frac{1}{2}(1+\zeta_I\zeta)(1-\eta^2); \text{ I = 6,8.} \tag{4.25}$$

To illustrate the superior performance of the 9-node Lagrangian element over that of the 8-node serendipity element, a hierarchical bubble interpolation function is added in (4.20) where

$$NB_9^e(\zeta,\eta) = \frac{1}{2}(1-\zeta^2)(1-\eta^2). \tag{4.26}$$

The terms in the element stiffness matrix arising from this interpolation may be eliminated at the element level by static condensation (see Wilson [26]). Employing matrix notation and defining

$$\text{symm } \bigtriangledown \boldsymbol{u}^e = \boldsymbol{B}_I^e \boldsymbol{u}_I + \boldsymbol{G}_I^e \boldsymbol{\psi}_I, \tag{4.27}$$

where $\boldsymbol{u}_i$ and $\boldsymbol{\psi}_I$ are nodal values of the displacement and the rotation fields, respectively. The $\boldsymbol{B}_I^e$ matrix in (4.27) has the standard form

$$\boldsymbol{B}_I^e = \begin{bmatrix} N_{I,1}^e & 0 \\ 0 & N_{I,2}^e \\ N_{I,2}^e & N_{I,1}^e \end{bmatrix} \text{ ; I = 1,2,3,4,} \tag{4.28}$$

where $N_{I,1} = \dfrac{\partial N_I}{\partial x_1}$. The part of the displacement interpolation associated with the rotation defines

$$\boldsymbol{G}_I^e = \frac{1}{8}\begin{bmatrix} (l_{IJ}\cos\alpha_{IJ} NS_{L,1}^e - l_{IK}\cos\alpha_{IK} NS_{M,1}^e) \\ (l_{IJ}\sin\alpha_{IJ} NS_{L,2}^e - l_{IK}\sin\alpha_{IK} NS_{M,2}^e) \\ \left(\begin{array}{c} (l_{IJ}\cos\alpha_{IJ} NS_{L,2}^e - l_{IK}\cos\alpha_{IK} NS_{M,2}^e) \\ + \\ (l_{IJ}\sin\alpha_{IJ} NS_{L,1}^e - l_{IK}\sin\alpha_{IK} NS_{M,1}^e) \end{array} \right) \end{bmatrix}, \tag{4.29}$$

where

$$\begin{gathered} \text{I = 1,2,3,4; M = I + 4; L = M - 1 + 4int(1/I);} \\ K = \text{mod}(M,4) + 1\text{; J = L - 4,} \end{gathered} \tag{4.30}$$

and

$$NS_{L,i} = \frac{\partial NS_L}{\partial x_i}.$$

The above expressions enter into the element stiffness matrix as

$$\boldsymbol{K}^e = \int_{\Omega^e} [\boldsymbol{B}^e \boldsymbol{G}^e]^T \boldsymbol{C} [\boldsymbol{B}^e \boldsymbol{G}^e] d\Omega, \tag{4.31}$$

where $\boldsymbol{K}^e$ is a 12 x 12 matrix. This is, in fact, the QC9 or QC9(8) element (depending on the integration scheme employed to integrate the element area Ω^e. This rank deficient element was reported by Stander and Wilson [27] further to the work of Taylor and Simo [28]. The rank deficiency is associated with the spurious higher order mode shown in Fig 4.2.

It is now required to remove the rank deficiency. Denoting

$$\text{skew } \bigtriangledown \boldsymbol{u}^e - \psi^e = \boldsymbol{b}_I^e \boldsymbol{u}_I + g_I^e \psi_I \tag{4.32}$$

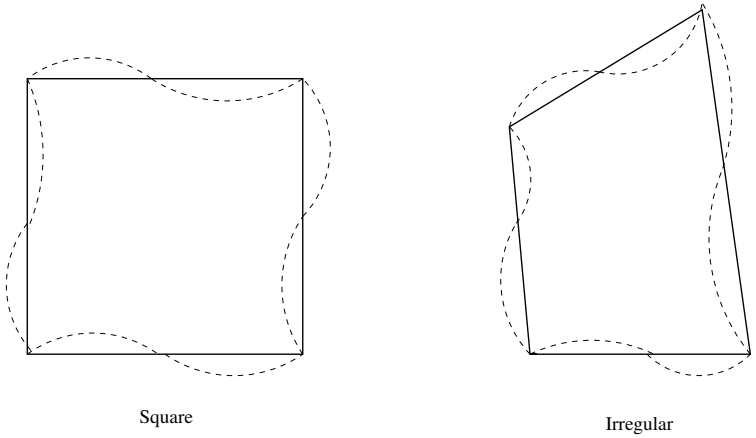

Figure 4.2: Spurious higher order mode for a four-node quadrilateral element with drilling degrees of freedom

where

$$\boldsymbol{b}_I^e =< -\frac{1}{2}N_{I,2}^e \ \frac{1}{2}N_{I,1}^e > \ ; \text{I = 1,2,3,4,} \tag{4.33}$$

and

$$\begin{aligned} g_I^e = [&-\frac{1}{16}(l_{IJ}\cos\alpha_{IJ}NS_{L,2}^e l_{IK}\cos\alpha_{IK}NS_{M,2}^e)] \\ &+\frac{1}{16}(l_{IJ}\cos\alpha_{IJ}NS_{L,1}^e l_{IK}\cos\alpha_{IK}NS_{M,1}^e) - N_I^e]; \text{ I = 1,2,3,4,} \end{aligned} \tag{4.34}$$

with induces J,K,L,M again defined by (4.30) Employing the interpolations for displacement (4.20) and rotations (4.19) and combining with (4.32) directly leads to

$$\boldsymbol{P}^e = \gamma \int_{\Omega_e} \begin{pmatrix} \boldsymbol{b}^e \\ \boldsymbol{g}^e \end{pmatrix} [\boldsymbol{b}^e \ \boldsymbol{g}^e] d\Omega, \tag{4.35}$$

for the second term in Problem $(D)^h$. Hence the element stiffness matrix becomes

$$[\boldsymbol{K}^e + \boldsymbol{P}^e]\boldsymbol{a} = \boldsymbol{f}; \ \boldsymbol{a} = \begin{pmatrix} \boldsymbol{u} \\ \boldsymbol{\psi} \end{pmatrix}, \tag{4.36}$$

$\boldsymbol{P}^e$ is integrated by a single point Gaussian quadrature in (4.36) above. By fully integrating $\boldsymbol{K}^e$ and combining with $\boldsymbol{P}^e$, spurious zero energy modes are prevented [22]. No additional devices are needed (e.g. see [29]). The same holds if a modified 8-point quadrature rule is employed to integrate $\boldsymbol{K}^e$ [22]. In this study a 5-point quadrature rule for which the above holds true is implemented.

The finite element based on (4.36) will be denoted Q4X.

4.3 Membrane locking correction

Flat shell elements assembled from membrane elements with in-plane drilling degrees of freedom suffer from undesirable membrane-bending interactions associated with the drilling degrees of

freedom [30]

Mechanistically, the locking phenomena may be described as follows: Flat quadrilateral shell elements approximate curved shell geometries with the possibilities of kinks between adjacent elements. In this situation the continuity of the three rotation parameters for the shell result in a situation where a non-zero drilling degree of freedom in one element leads to non-zero bending degrees of freedom in an adjacent element (and *vice versa*). Accordingly, the element will exhibit a membrane-bending locking performance, unless the drilling degree of freedom part of the membrane strains may assume a zero value over the element [30].

For the assumed displacement field of the drilling element (4.20), zero strains are not possible for non-zero rotations [30]. (An exception is the special case of identical rotations at opposite nodes.)

Taylor [30] presented a correction which alleviates the membrane bending locking. The correction, which is based on a three field (displacement, strain and stress) formulation, is repeated here, albeit with a slightly different notation.

From (4.27) the membrane strains of the element with drilling degrees of freedom are written as:

$$\boldsymbol{\epsilon} = \boldsymbol{B}_I^e \boldsymbol{u}_I + \boldsymbol{G}_I^e \psi_I \text{ I = 1,2,3,4} \tag{4.37}$$

where $\boldsymbol{u}_I$ and γ_I are nodal values of displacement and rotation respectively and summation is implied. The strain associated with displacements may assume arbitrary values, including zero, as conventional interpolation is employed. Except for constant values of γ_I, the strains associated with rotations cannot be constant or zero. The membrane strains are hence modified as

$$\bar{\boldsymbol{\epsilon}} = \boldsymbol{B}_I^e \boldsymbol{u}_I + \boldsymbol{G}_I^e \psi_I + \bar{\epsilon_0}. \tag{4.38}$$

These modified strain relations are now required to satisfy a requirement that the drilling parameter part can be inextensible. Accordingly, it is desired that

$$\boldsymbol{G}_i^e \psi_I + \bar{\boldsymbol{\epsilon}}_0 = \boldsymbol{0} \tag{4.39}$$

for rotational fields which are inextensible. Unless the drilling degrees of freedom are eliminated completely it is only possible to satisfy (4.39) in a weak sense. A suitable weak form may be constructed by augmenting the usual potential energy functional of each element for a shell by the term

$$\int_{\Omega_e} \bar{\boldsymbol{\sigma}}^T (\boldsymbol{G}_I^e \psi_I + \bar{\boldsymbol{\epsilon}}_0) d\Omega = 0, \tag{4.40}$$

where Ω^e is the surface region of the shell. Both $\bar{\boldsymbol{\sigma}}$ and $\bar{\boldsymbol{\epsilon}}_0$ are assumed constant over each element. Performing the variation with respect to $\bar{\boldsymbol{\sigma}}$ leads to

$$\bar{\boldsymbol{\epsilon}}_0 = -\frac{1}{\Omega^e} \int_{\Omega^e} \boldsymbol{G}_i^e \psi_I d\Omega \tag{4.41}$$

and, hence, the modified strain relationship

$$\bar{\boldsymbol{\epsilon}} = \boldsymbol{B}_I^e \boldsymbol{u}_I + \left(\boldsymbol{G}_I^e - \frac{1}{\Omega^e} \int_{\Omega^e} \boldsymbol{G}_I^e d\Omega \right) \psi_I \tag{4.42}$$

which is the final result presented by Taylor [30].

4.4 Assumed stress formulation

Elements with drilling degrees of freedom and elements with assumed stress interpolations have the potential to improve the modeling capabilities of, in particular, low-order quadrilateral finite elements. Hence, it seems desirable to formulate low-order elements with both an assumed stress interpolation field and drilling degrees of freedom, on condition that the elements are rank sufficient and invariant. The treatment of Geyer and Groenwold [11] is followed closely without further proof or motivation.

The variational formulation of the boundary value problem is given as:

Formulation (D_c)

$$\begin{aligned}\boldsymbol{\Pi}_\gamma(\boldsymbol{u},\boldsymbol{\psi},\boldsymbol{\sigma}) \;=\; & \int_\Omega \text{symm}\,\boldsymbol{\sigma}\cdot\text{symm}\;\bigtriangledown\boldsymbol{u}\,d\Omega - \frac{1}{2}\int_\Omega \text{symm}\,\boldsymbol{\sigma}\cdot\boldsymbol{C}^{-1}\cdot\text{symm}\,\boldsymbol{\sigma}d\Omega \\ & +\frac{1}{2}\gamma\int_\Omega[\text{skew}\,\bigtriangledown\boldsymbol{u}-\boldsymbol{\psi}]^2 d\Omega - \int_\Omega \boldsymbol{u}\cdot\boldsymbol{f}\,d\Omega. \end{aligned} \tag{4.43}$$

This variational formulation also requires that the rotations $\boldsymbol{\psi}$ and the stresses $\boldsymbol{\sigma}$, together with the displacement generalized derivatives $\bigtriangledown\boldsymbol{u}$, belong to the space of square-integrable functions over the region Ω.

4.4.1 Finite element discretization

For a typical element it is required that the three independent interpolation fields arising from the translations, rotations and the assumed stress are constructed. Again, the independent rotation field is interpolated as:

$$\psi^e = \sum_{i=1}^{4} N_i^e(\zeta,\eta)\psi_i, \tag{4.44}$$

with N_i^e the standard bi-linear shape functions. The in-plane displacement approximation is still taken as an Allman-type interpolation field:

$$\begin{pmatrix} u_1 \\ u_2 \end{pmatrix} = \boldsymbol{u}^e = \sum_e\sum_{I=1}^{4} N_I^e(\zeta,\eta)\boldsymbol{u}_i + \frac{l_{jk}}{8}\sum_{I=5}^{8} NS_i^e(\zeta,\eta)(\psi_K-\psi_J)\boldsymbol{n}_{JK}, \tag{4.45}$$

with NS_i^e the serendipity shape functions. l_{jk} and n_{jk} respectively represent the length and outward normal of side i, located between nodes j and k.

Using matrix notation, symm $\bigtriangledown\boldsymbol{u}^e$ is obtained as

$$\text{symm}\,\bigtriangledown\boldsymbol{u}^e = \boldsymbol{B}_i^e\boldsymbol{u}_i + \boldsymbol{G}_{\psi i}^e\boldsymbol{\psi}_i. \tag{4.46}$$

To satisfy the requirement that the drilling parameter part can be inextensible (4.46) is modified to become

$$\text{symm}\,\bigtriangledown\boldsymbol{u}^e = \boldsymbol{B}_i^e\boldsymbol{u}_i + \left(\boldsymbol{G}_{\psi i}^e - \frac{1}{\Omega}\int_\Omega \boldsymbol{G}_{\psi i}^e d\Omega\right)\boldsymbol{\psi}_i. \tag{4.47}$$

Skew $\bigtriangledown \boldsymbol{u}^e$ is given by

$$\text{skew} \bigtriangledown \boldsymbol{u}^e = \boldsymbol{b}_i^e \boldsymbol{u}_i + \boldsymbol{g}_i^e \boldsymbol{\psi}_i. \tag{4.48}$$

For assumed stress field, the global stresses are directly interpolated by the stress parameters β_i

$$\text{symm } \boldsymbol{\sigma}^e = \boldsymbol{P}^e \boldsymbol{\beta}^e, \tag{4.49}$$

where $\boldsymbol{P}^e$ is the interpolation matrix in terms of the local coordinates and $\boldsymbol{\beta}^e$ is the stress parameter vector.

The body force vector is given by

$$\boldsymbol{r} = \int_\Omega \boldsymbol{N}^T \boldsymbol{f} d\Omega. \tag{4.50}$$

In matrix notation, the stationary conditions are

$$\begin{bmatrix} \boldsymbol{G}^{eT} & \boldsymbol{P}_\gamma^e \\ -\boldsymbol{H}^e & \boldsymbol{G}^e \end{bmatrix} \begin{bmatrix} \boldsymbol{\beta} \\ \boldsymbol{q} \end{bmatrix} = \begin{bmatrix} \boldsymbol{f} \\ 0 \end{bmatrix}, \tag{4.51}$$

which leads to

$$[\boldsymbol{K}^e + \boldsymbol{P}_\gamma^e] \boldsymbol{q} = \boldsymbol{r}, \tag{4.52}$$

with $\boldsymbol{q} = [u_{1i}\ u_{2i}\ \psi_i]^T$, i = 1,2,3,4 and

$$\boldsymbol{P}_\gamma^e = \gamma \int_\Omega \begin{bmatrix} \boldsymbol{b}^{eT} \\ \boldsymbol{g}^{eT} \end{bmatrix} \begin{bmatrix} \boldsymbol{b}^e & \boldsymbol{g}^e \end{bmatrix} d\Omega, \tag{4.53}$$

and

$$\boldsymbol{K}^e = \boldsymbol{G}^{eT} \boldsymbol{H}^{e-1} \boldsymbol{G}^e, \tag{4.54}$$

with

$$\boldsymbol{G}^e = \int_\Omega \boldsymbol{P}^{eT} \cdot [\boldsymbol{B}^e \boldsymbol{G}_\psi^e] d\Omega, \tag{4.55}$$

and

$$\boldsymbol{H}^e = \int_\Omega \boldsymbol{P}^{eT} \cdot \boldsymbol{C}^{-1} \cdot \boldsymbol{P}^e d\Omega, \tag{4.56}$$

where $\boldsymbol{C}^{-1}$ denotes the elastic compliance matrix. Finally, stress recovery is obtained through

$$\boldsymbol{\beta} = \boldsymbol{H}^{e-1} \boldsymbol{G}^e \boldsymbol{q}. \tag{4.57}$$

The parameter γ in the foregoing is problem dependent, since it is part of a penalty term.

4.4.2 Interpolating the assumed stress field

The stress field assumed in (4.49) is, without loss of generality, expressed as [11]

$$\text{symm } \boldsymbol{\sigma}^e = \boldsymbol{P}\boldsymbol{\beta} = \text{symm } \boldsymbol{\sigma}_c^e + \text{symm } \boldsymbol{\sigma}_h^e = \begin{bmatrix} \boldsymbol{I}_c & \boldsymbol{P}_h \end{bmatrix} \begin{bmatrix} \boldsymbol{\beta}_c \\ \boldsymbol{\beta}_h \end{bmatrix}, \tag{4.58}$$

where the superscript e is dropped on P for reasons of clarity and brevity. $\boldsymbol{I}_c$ allows for the accommodation of constant stress states, and the higher order stress field is given by symm $\boldsymbol{\sigma}_h^e =$

$\boldsymbol{P}_h\boldsymbol{\beta}_h$. The lowest number of parameters that prevents mechanisms is 8, for which the higher order interpolation matrix $\boldsymbol{P}_h$ becomes

$$\boldsymbol{P}_{h8} = \begin{bmatrix} \eta & 0 & \zeta & 0 & \eta^2 \\ 0 & \zeta & 0 & \eta & -\zeta^2 \\ 0 & 0 & -\eta & -\zeta & 0 \end{bmatrix}. \tag{4.59}$$

Since 8 *beta* parameters are present, the element is denoted the 8β element. With 9 $beta$ parameters, the 9β element is given as:

$$\boldsymbol{P}_{h9} = \begin{bmatrix} \eta & 0 & \zeta & 0 & \eta^2 & 0 \\ 0 & \zeta & 0 & \eta & 0 & -\zeta^2 \\ 0 & 0 & -\eta & -\zeta & 0 & 0 \end{bmatrix} \tag{4.60}$$

The presented stress interpolation matrices represent unconstrained interpolation fields, which are not necessarily optimal. Constraints may be enforced by a suitable transformation matrix. The rational approach of Pian and Sumihara [5] is chosen, i.e.

$$\text{symm}\,\boldsymbol{\sigma}_h^e \leftarrow \boldsymbol{T}_0\boldsymbol{P}_h\boldsymbol{\beta}_h, \tag{4.61}$$

with

$$\boldsymbol{T}_0 = \begin{bmatrix} a_1^2 & a_3^2 & 2a_1a_3 \\ b_1^2 & b_3^2 & 2b_1b_3 \\ a_1b_1 & a_3b_3 & a_1b_3 + a_3b_1 \end{bmatrix}, \tag{4.62}$$

and

$$\begin{bmatrix} a_1 & b_1 \\ a_2 & b_2 \\ a_3 & b_3 \\ a_4 & b_4 \end{bmatrix} = \frac{1}{4}\begin{bmatrix} -1 & 1 & 1 & -1 \\ 1 & -1 & 1 & -1 \\ -1 & -1 & 1 & 1 \\ 1 & 1 & 1 & 1 \end{bmatrix}\begin{bmatrix} x_1 & y_1 \\ x_2 & y_2 \\ x_3 & y_3 \\ x_4 & y_4 \end{bmatrix}. \tag{4.63}$$

4.4.3 Penalty-equilibrated approach

As mentioned previously, while distributed body forces may induce important loads on structures, they can usually be ignored on the element level in stress calculations. Hence element equilibrium is written as [31]

$$\boldsymbol{\partial}(\text{symm}\,\boldsymbol{\sigma}) = \boldsymbol{D}^T(\text{symm}\,\boldsymbol{\sigma}) = \mathbf{0} \text{ in } \Omega, \tag{4.64}$$

with $\boldsymbol{D}$ the 2-D differential operator. This yields a functional $\boldsymbol{\Pi}_\gamma^*$ of the form

$$\boldsymbol{\Pi}_\gamma^*(\boldsymbol{u},\boldsymbol{\psi},\boldsymbol{\sigma}) \;=\; \boldsymbol{\Pi}_\gamma(\boldsymbol{u},\boldsymbol{\psi},\boldsymbol{\sigma}) - \alpha\int(\boldsymbol{\partial}\text{symm}\,\boldsymbol{\sigma})^T(\boldsymbol{\partial}\text{symm}\,\boldsymbol{\sigma})d\Omega, \;\; \alpha \gg 0, \tag{4.65}$$

with $\alpha \gg 0$ is a large number. Using matrix notation, and for the sake of convenience setting $\alpha \leftarrow \dfrac{\alpha}{2E}$, the internal potential of the 8β and 9β families becomes

$$\Pi^*_\gamma(\boldsymbol{u},\boldsymbol{\psi},\boldsymbol{\sigma}) \;=\; \boldsymbol{\beta}^T\boldsymbol{G}\boldsymbol{q} - \frac{1}{2}\boldsymbol{\beta}^T\left(\boldsymbol{H}+\frac{\alpha}{E}\boldsymbol{H}_p\right)\boldsymbol{\beta} - \boldsymbol{q}^T\boldsymbol{P}_\gamma\boldsymbol{q}, \tag{4.66}$$

with $\boldsymbol{\sigma} = \boldsymbol{P}\boldsymbol{\beta}$ and

$$\boldsymbol{H}_p = \int_\Omega (\boldsymbol{\partial P})^T(\boldsymbol{\partial P})d\Omega, \tag{4.67}$$

where $\boldsymbol{P}_\gamma$ is given by (4.53). For 8β, $\boldsymbol{\partial P}$ may be shown to be

$$\boldsymbol{\partial P} = \begin{bmatrix} 0 & 0 & 0 & \eta_{,x} & 0 & \zeta_{,x} & -\eta_{,y} & -\zeta_{,y} & 2\eta\cdot\eta_{,x} \\ 0 & 0 & 0 & 0 & \zeta_{,y} & -\eta_{,x} & \eta_{,y} & -\zeta_{,x} & -2\zeta\cdot\zeta_{,y} \end{bmatrix} \tag{4.68}$$

where

$$\zeta_{,x} = \frac{\partial\zeta}{\partial x}, \text{ etc.} \tag{4.69}$$

The penalty formulation $9\beta(\alpha)$ is obtained in a similar fashion to $8\beta(\alpha)$. For this element, $\boldsymbol{\partial P}$ is given by

$$\boldsymbol{\partial P} = \begin{bmatrix} 0 & 0 & 0 & \eta_{,x} & 0 & \zeta_{,x} & -\eta_{,y} & -\zeta_{,y} & 2\eta\cdot\eta_{,x} & 0 \\ 0 & 0 & 0 & 0 & \zeta_{,y} & -\eta_{,x} & \eta_{,y} & -\zeta_{,x} & 0 & -2\zeta\cdot\zeta_{,y} \end{bmatrix}. \tag{4.70}$$

Upon comparing $8\beta(\alpha)$ and $9\beta(\alpha)$ under pure bending, locking-like behavior is observed for $8\beta(\alpha)$. This deficiency is however not taken into account in this study.

4.5 Numerical Results

4.5.1 Cook's membrane

We again study the swept and tapered cantilever beam proposed by Cook (Fig 2.1). The center displacement u_{2c} for the various elements studied is tabulated in Table 4.1. Although the drilling element Q4X is quite accurate, it is outperformed by the assumed stress elements.

Element	1×1	2×2	4×4	8×8
Q4X	13.7526	19.8808	22.4157	23.2404
8β	14.6522	20.3114	22.7116	23.3517
$8\beta(\alpha)$	34.0329	25.5869	24.7800	23.9012
9β	14.6466	20.3066	22.7121	23.3498
$9\beta(\alpha)$	17.0532	21.4060	23.0398	23.4387
Best known		23.94		

Table 4.1: Mid-node displacement for Cook's membrane (plane stress), obtained with displacement based and assumed stress elements with drilling degrees of freedom and penalized equilibrium

Chapter 5

Fracture mechanics: Classical and numerical treatments

In this chapter a brief overview of the history of fracture mechanics is given and important fracture mechanics concepts are discussed.

5.1 Historical overview

Fracture mechanics is concerned with fracture-dominate failure where the fracture mechanism is the growth of cracks or crack-like defects. The earliest recorded investigation into the phenomenon of fracture would appear to be Leornardo da Vinci's [32] study of the variation of failure strength in different lengths of wire of the same diameter. The first attempt at a mathematical approach to fracture mechanics was by Inglis [33] in 1913. The first successful analysis of a fracture-dominant problem was that of Griffith in 1920, who considered the propagation of brittle cracks in glass [34]. Griffith formulated the now well-known concept that an existing crack will propagate if thereby the total energy of the system is lowered, and he assumed that there is a simple energy balance, consisting of a decrease in elastic strain energy within the stressed body as the crack extends, counteracted by the energy needed to create the new crack surfaces. His theory allows the estimation of the theoretical strength of brittle solids and also gives the correct relationship between fracture strength and defect size [35].

The Griffith concept was first related to the brittle fracture of metallic materials by Zener and Hollomon in 1944. Soon after, Irwin pointed out that the Griffith-type energy balance must be between

- the stored strain energy, and
- the surface energy plus the work done during plastic deformation.

Irwin also recognized that for relatively ductile materials the energy required to form new crack surfaces is generally insignificant compared to the work done in plastic deformation, and he defined a material property G as the total energy absorbed during cracking per unit increase in crack length and per unit thickness. G is called the *energy release rate* or *crack driving force* [35].

In the middle 1950s Irwin contributed another major advance by showing that the local stresses near the crack tip are of the general form:

$$\sigma_{ij} = \frac{K}{\sqrt{(2\pi r)}} f_{ij}(\theta) + ... \tag{5.1}$$

where r and θ are polar coordinates of a point with respect to the crack tip and K is the stress intensity factor. The stress intensity factor K describes the magnitude of the elastic crack tip stress field. He further showed that the energy approach is equivalent to a stress intensity approach, according to which fracture occurs when a critical stress distribution ahead of the crack tip is reached. The material property governing fracture may therefore be stated as a critical stress intensity, K_c, or in terms of energy as a critical value G_c. Demonstration of the equivalence of G and K provided the basis for development of the discipline of Linear Elastic Fracture Mechanics (LEFM). This is because the form of the stress distribution around and close to the crack tip is always the same. Thus tests on suitably shaped and loaded specimens to determine K_c make it possible to determine which flaws are tolerable in an actual structure under given conditions. Furthermore, materials can be evaluated for their fitness for purpose in situations where fracture is possible. It has also been found that the sensitivity of structures to sub critical cracking such as fatigue crack growth and stress corrosion can, to some extent, be predicted on the basis of tests, using the stress intensity approach [35].

5.2 Linear elastic fracture mechanics assumptions

Linear elastic fracture mechanics (LEFM) principles are used to relate the stress magnitude and distribution near the crack tip to [36]

- remote stresses applied to the cracked component,
- the crack size, shape, the geometry of the cracked component, and
- the material properties of the cracked component.

LEFM is based on the application of the theory of elasticity to bodies containing cracks or defects. The assumptions used in elasticity are also inherent in the theory of LEFM: namely, small displacements and general linearity between stresses and strains. The general form of the LEFM equations given in (5.1) illustrates that a singularity exists such that as r, the distance from the crack tip, tends towards zero, the stresses go to infinity. Since materials plastically deform as the yield stress is exceeded, a plastic zone will form near the crack tip. The basis of LEFM remains valid, though, if this region of plasticity remains small in relation to the overall dimensions of the crack and cracked body.

5.3 Loading modes

Consider a cracked body, with a sharp crack along the x-axis. There are generally three modes of loading, which involve different crack surface displacements. The three modes are [34]:

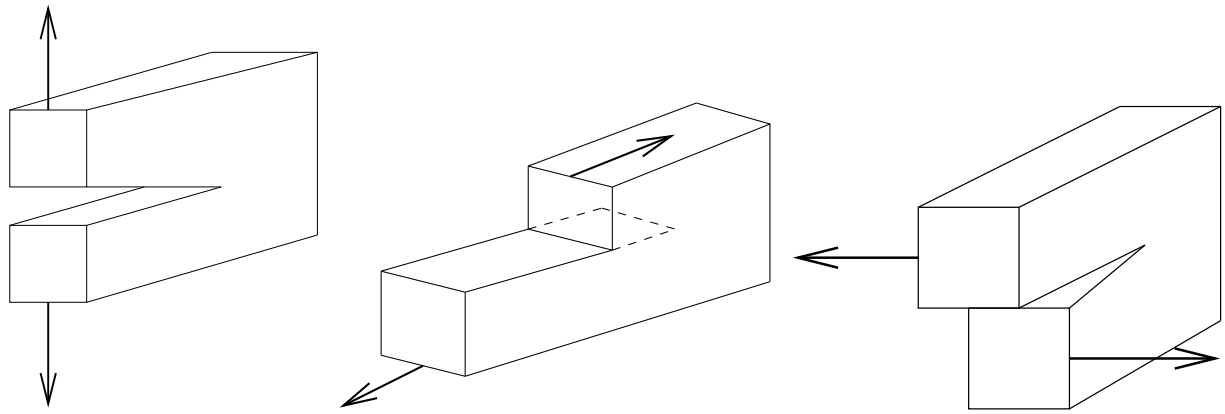

Figure 5.1: The three modes of loading : (a) mode I opening mode (b) mode II sliding mode (c) mode III tearing mode

- Mode I: Opening or tensile mode in which the crack faces are pulled apart in the y direction, but where the deformations are symmetric about the x-z and x-y planes.
- Mode II: Sliding or in plane shear in which the crack surfaces slide over each other in the x direction, but where the deformations are symmetric about the x-y plane and skew symmetric about the x-z plane.
- Mode III: Tearing or anti-plane shear (the crack surfaces move parallel to the leading edge of the crack and relative to each other). The crack surfaces slide over each other in the z direction, but the deformation are skew-symmetric about the x-y and x-z planes.

5.4 Stress intensity factor

Cracks or defects are present to some degree in all structures [34]. They may exist as basic defects in the constituent materials or they may be induced during construction or service life. Therefore a fundamental requirement of fracture mechanics theory is some means of assessing the stability of such cracks. In this respect, the most significant advance has been the introduction of the stress intensity factor as a single parameter for categorizing the onset of crack propagation [34].

The stress-intensity factor uniquely describes the theoretical state of stress at the crack tip. In isotropic materials this is all the information required to predict the critical stress level and the direction of fracture propagation. Thus K can correlate the crack growth and fracture behavior of materials provided that the crack tip stress field remains predominantly elastic. This correlating ability makes the stress intensity factor an extremely important fracture mechanics parameter [35].

The stress intensity factor K, also defines the magnitude of the local stresses around the crack tip. The stress intensity factor depends on loading, crack size, crack shape, and geometric boundaries,

with the general form given by [36]:

$$K = f(g)\sigma\sqrt{(\pi a)} \tag{5.2}$$

where

- σ represents the remote stress applied to the structure,
- a the crack length, and
- $f(g)$ the correction factor that depends on specimen and crack geometry.

Stress intensity factors for a single loading mode can be added algebraically. Consequently, stress intensity factors for complex loading conditions of the same mode can be determined from the superposition of simpler results, such as those readily obtainable from handbooks. In determining K, numerical methods (including finite element methods) have been widely used in recent years. Determination methods for K tend to be approximate [36].

It is the use of the stress intensity factor as the characterizing parameter for crack extension that is the fundamental principle of Linear Elastic Fracture Mechanics (LEFM).

5.5 Fracture toughness

As the stress intensity factor reaches a critical value, K_c, unstable fracture occurs. This critical value of the stress intensity factor is known as the *fracture toughness* of the material. The fracture toughness can be considered the limiting value of stress intensity, similarly the yield stress being the limiting value of stress in a body [36].

The fracture toughness at a given temperature varies with specimen thickness until limiting conditions (maximum condition) are reached. The maximum constraint condition occurs in the plane strain state. The plane strain fracture toughness, K_{1c}, can be considered a material property characterizing the crack resistance, and is therefore called the plane strain fracture toughness.

Thus, the same value of K_{1c} could theoretically be found by testing specimens of the same material with different geometries and with critical combinations of crack size, shape and fracture stress. Within certain limits this is indeed the case. The fracture toughness, K_c, can also be determined under standard conditions, and the value thus found may also be used to predict failure, but only for situations with the same material thickness and constraint [35].

5.6 Finite elements in fracture mechanics

Over the last decade or so, FEM has been firmly established as a standard procedure for the solution of practical fracture problems. The method can easily take account of nonlinearities at the crack tip, e.g small contact zone, finite deformation or scale yielding. The finite element method has become a useful technique for solving elastic fracture mechanics problems [34].

The finite element approaches to fracture mechanics can be divided into either *direct* or *indirect* methods. In the *direct* method, the stress intensity factors are calculated directly from the solution. In most of the *direct* methods adequate representation of the crack tip singularity is a problem. In the *indirect* method, an energy-release rate is calculated and stress intensity factors inferred from it. *Direct* methods can be used with conventional (nonsingular) elements or with elements containing a stress singularity at the crack tip. In the former case, it is necessary to curve fit the stress or displacement behavior away from the crack tip and extrapolate to the crack tip to determine the stress intensity factor (displacement extrapolation). In the latter case, it is calculated directly [37].

The *indirect* approach determines the stress intensity factor by evaluating the energy-release rate. Several techniques for evaluating energy-release rates have been described in the literature. These methods are base on computing the change in potential energy for two crack lengths or computing the change in compliance for two crack lengths. Other approaches are based on evaluating the change in stiffness matrix due to crack extension and require only one analysis. The J integral evaluated for a elastic material, is identical to the energy-release rate and offers a convenient way of evaluating G with a single analysis. In general the *indirect* techniques do not give the mode I and mode II values of K (stress intensity factor) independently, unless it is known *a priori* that the loading produces only mode I or mode II response [37].

The use of finite elements in fracture prediction requires two distinct considerations [34], namely

- crack tip singularity modeling, and
- interpretation of the finite element results.

5.7 Crack tip singularity modeling

Initial studies involving the use of finite element methods in fracture mechanics employed conventional constant stress elements. It was found that substantial mesh refinement is required in the vicinity of the crack tip in order to accurately represent the stress and strain field singularities. It is however expensive in computer time and data preparation effort to use these refined meshes. The development of higher-order elements (elements containing stress singularity at the crack tip) permitted the same order of accuracy to be achieved with coarser meshes. For the efficient numerical solution of fracture problems it is advantageous to develop special crack tip elements which directly model the $1/\sqrt{r}$ near tip strain field singularity because any extrapolation to calculate K is avoided. Many such elements have been developed to date based both on hybrid and displacement formulations [34].

5.8 Interpretation of the finite element results

After the displacement and stress fields throughout the cracked solid or body have been determined, a means of evaluating the stress intensity factor must be found. The most obvious approach is to relate the analytical solutions for the near tip stress and displacement fields to the values obtained from the finite element analysis. This clearly requires extrapolation procedures to provide the

crack tip stress intensity factors. For linear elastic problems, relationships are available which relate the stress intensity factor to strain energy release rate associated with an infinitesimal crack advance. These expressions from the basis of the so-called strain energy release rate and virtual crack extension methods, in which a finite element analysis is preformed for two incrementally different crack lengths and strain energy difference, are evaluated.

A further approach is to derive the stress intensity factors from the value of a path-independent integral. The line integral which has been used most often is Rice's J integral. The J integral evaluated for a linear-elastic material, is identical to the energy-release rate and offers a convenient way of evaluation G with a single analysis. Use of energy methods or a line-integral approach also has the distinct advantage that exact modeling of the crack tip stress and displacement fields is not necessary [34]. The path independence of the J integral expression allows calculation along a contour remote from the crack tip. Such a contour can be chosen to contain only elastic loads and displacements and accurate results can be obtained by the use of relatively coarse meshes with conventional elements [35]. The use of special crack-tip elements is then not necessary [34].

Chapter 6

Fracture mechanics: Displacement extrapolation

In this chapter the displacement extrapolation technique for solving stress intensity factors is outlined. The computer implementation of the theory can be obtained from the author on request.

6.1 Displacement extrapolation basics

The analytical expressions for the displacement variation along radial lines emanating from the crack tip (e.g. see [34]) are given by:

$$u = \frac{K_1}{4\mu}\sqrt{\frac{r}{2\pi}}\left[(2\kappa-1)\cos(\frac{\theta}{2}) - \cos(\frac{3\theta}{2})\right] - \frac{K_2}{4\mu}\sqrt{\frac{r}{2\pi}}\left[(2\kappa+3)\sin(\frac{\theta}{2}) + \sin(\frac{3\theta}{2})\right] \tag{6.1}$$

$$v = \frac{K_1}{4\mu}\sqrt{\frac{r}{2\pi}}\left[(2\kappa+1)\sin(\frac{\theta}{2}) - \sin(\frac{3\theta}{2})\right] - \frac{K_2}{4\mu}\sqrt{\frac{r}{2\pi}}\left[(2\kappa-3)\cos(\frac{\theta}{2}) + \cos(\frac{3\theta}{2})\right]. \tag{6.2}$$

The situation is depicted in Fig 6.1. K_1 and K_2 respectively are the mode I and mode II stress intensity factors, μ is the shear modulus and κ a parameter that depends on the state of stress:

$$\begin{array}{c} \kappa = \frac{(3-\nu)}{(1+\nu)} \text{ for plane stress} \\ \kappa = 3 - 4\nu \text{ for plane strain} \end{array} \tag{6.3}$$

The analytical expressions for the displacement variation along radial lines can be solved to obtain the stress intensity factors:

$$K_1 \begin{pmatrix} (2\kappa-1)\cos(\frac{\theta}{2}) - \cos(\frac{3\theta}{2}) \\ (2\kappa+1)\sin(\frac{\theta}{2}) - \sin(\frac{3\theta}{2}) \end{pmatrix} = 4\mu\sqrt{\frac{2\pi}{r}}\begin{pmatrix} u \\ v \end{pmatrix} \tag{6.4}$$

$$K_2 \begin{pmatrix} -(2\kappa+1)\sin(\frac{\theta}{2}) - \sin(\frac{3\theta}{2}) \\ (2\kappa-3)\cos(\frac{\theta}{2}) + \cos(\frac{3\theta}{2}) \end{pmatrix} = 4\mu\sqrt{\frac{2\pi}{r}}\begin{pmatrix} u \\ v \end{pmatrix} \tag{6.5}$$

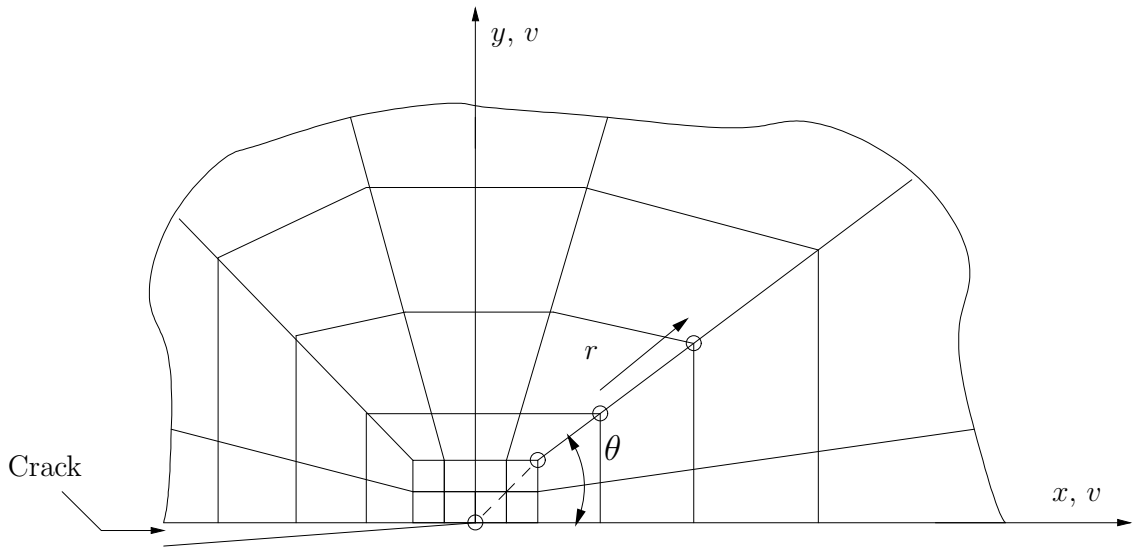

Figure 6.1: Stress intensity factor evaluation by extrapolation. Example of mesh that can be used

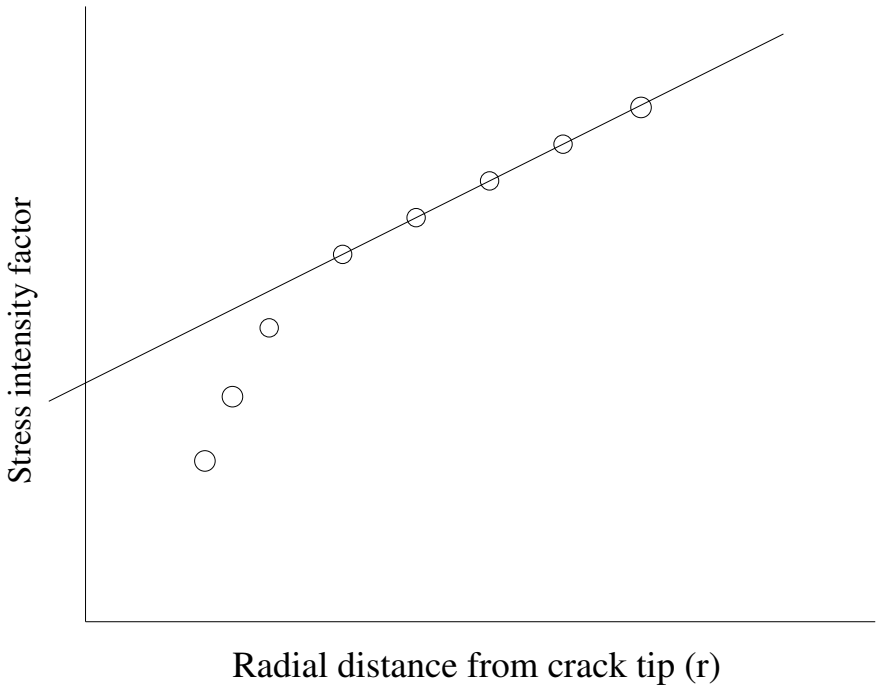

Figure 6.2: Stress intensity factor evaluation by extrapolation. Plot of stress intensity factor K vs. radial distance r from the crack tip

Substituting the values of u or v and r for nodal points along a radial line emanating from the crack tip as shown in Fig 6.1 yields a curve of K_1, K_2 or K_{mixed} against radial distance r (Fig 6.2). By discarding the results for points very close to the crack tip the solutions for K_1 and K_2 can be extrapolated to $r = 0$. Stresses can also be extrapolated to determine the stress intensity factor,

but the displacement extrapolation method is far superior to the stress extrapolation method [34]. The stress intensity values obtained using displacements are far more consistent than those based on stresses [38]. In the displacement extrapolation there is little difference between the accuracy of the results obtained by using different angles [34]. Generally finite element mesh idealization dictates $\theta = 0°$ and $\theta = 90°$ to be the most convenient choices. The extrapolation approach can be employed using either conventional finite elements or with crack tip singularity elements included in the crack tip zone.

6.2 Numerical example

Consider the example of a single edge cracked plate loaded in uniform tension (Fig 6.3(a)). The data are:

- Crack/width ratio $a/W = 0.5$
- Elastic modulus E = 10^7
- Poisson's ratio μ = 0.3
- Force P = 100
- Width W = 1
- Height L = 2.5
- Thickness t = 1

Strictly speaking, this is a rod and not a plate, but this example [38] is used for the sake of verification and comparison with published results.

The stress intensity factor is determined by extrapolation of the displacements (v and u) along the radial lines $\theta = 0°$ and $\theta = 90°$. The plot for extrapolation of the stress intensityy factor along the radial line $\theta = 90°$ is shown in Fig 6.4. The graph for the extrapolation of the stress intensity factor along the radial line $\theta = 0°$ is given in Fig 6.5.

$$K_1 = P\frac{\sqrt{a}}{\sqrt{\pi}}(1.99 - 0.41(\frac{a}{W}) + 18.7(\frac{a}{W})^2 - 38.48(\frac{a}{W})^3 + 53.85(\frac{a}{W})^4) \tag{6.6}$$

The exact value of the Mode I stress intensity factor, as calculated using (6.6), is K_1 = 200 $Pa.m^{0.5}$ [38]. In Table 6.1 the results obtained using the displacements (u,v) on the radial line $\theta = 90°$ are given.

6.3 Discussion

The stress intensity factor obtained through displacement extrapolation is largely dependent on the number of points used to extrapolate the displacement for a particular mesh and radial line

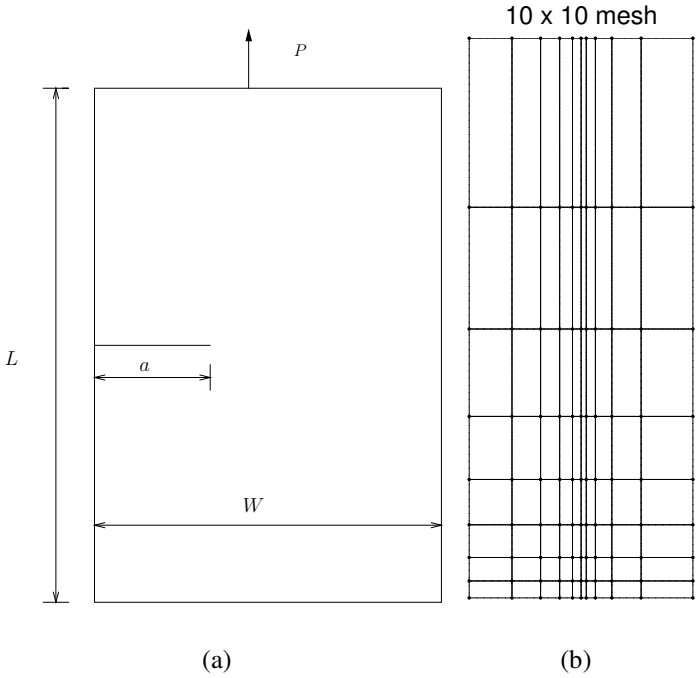

Figure 6.3: Single edge cracked plate used for displacement extrapolation: (a) Geometry of the SECP problem (b) A 10×10 mesh for the single edge crack plate (SECP)

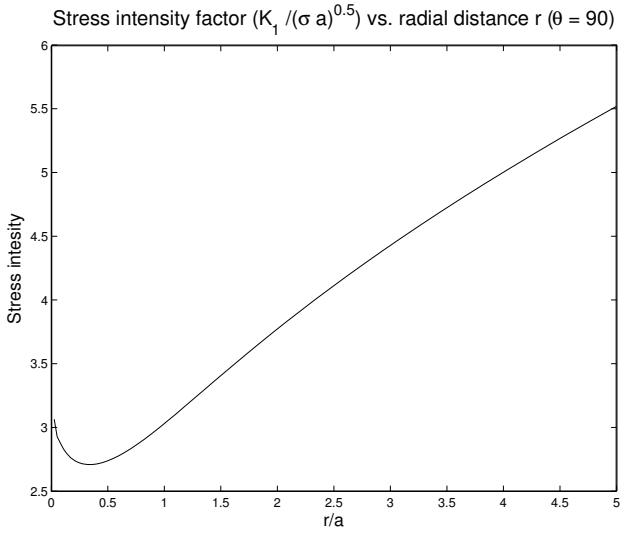

Figure 6.4: Normalized K_I vs. radial distance for $\theta = 90^\circ$

(θ) (see Table 6.1). It may be possible to determine an optimal number of points to be used for extrapolation vs. the number of nodes on the radial line (e.g. $\theta = 0$) emanating from the crack tip. If a radial line from the crack tip other than $\theta = 0^\circ$ or 90° is used for extrapolation, a radial

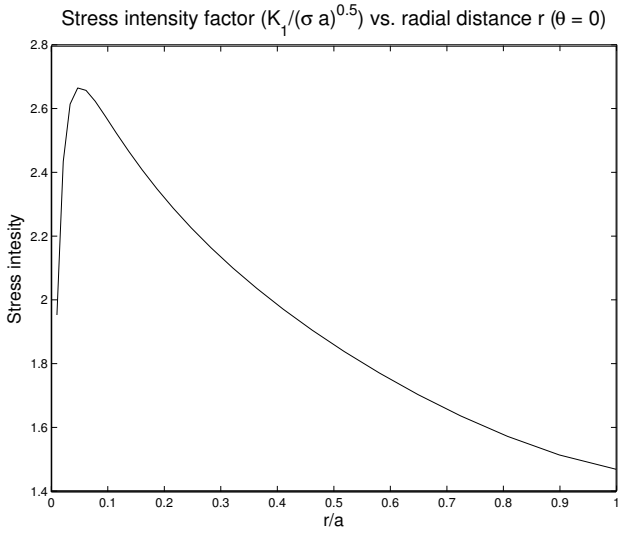

Figure 6.5: Normalized K_I vs. radial distance for $\theta = 0°$

Number of Extrapolation points	Mesh size 10×10	Mesh size 20×20	Mesh size 30×30	Mesh size 40×40	Mesh size 50×50	Mesh size 60×60
10	198.39	196.74	213.40	220.76	224.48	224.69
13	181.77	196.64	209.22	214.00	216.34	217.92
20	—	—	202.53	201.01	200.79	202.77
21	—	—	195.24	188.69	190.97	192.52
25	—	—	—	—	—	200.68

Table 6.1: Stress intensity factor for a SECP determined with displacement extrapolation along the radial line $\theta = 90°$ using different numbers of extrapolation points

mesh should be generated (to generate a radial mesh takes more time than to generate a normal rectangular mesh). It can sometimes be difficult to extrapolate the K vs. r plot obtained for a given radial line.

Chapter 7

Fracture mechanics: J integral

In this chapter, the formulation, proof of path independence, the lower bound theorem and finite element implementation of the J integral is outlined. The computer implementation of the theory is given in Appendix C.

7.1 J integral method

Linear elastic fracture mechanics was originally developed to describe crack growth and fracture under essentially elastic conditions (plain strain conditions). Later it was shown that LEFM concepts could be adapted for limited amounts of plasticity in the crack tip region. However, there are many important classes of materials where the crack tip plastic zone are simply too large for LEFM concepts.

One of the notable successes of LEFM for practical applications is the ability to predict crack initiation using one or two parameters. Of the concepts developed for this purpose two have found a fairly general acceptance: The J integral and the Crack Opening Displacement (COD) approach [35].

Use of energy methods or a line-integral approach has the distinct advantage that an exact model of the crack tip stress and displacement fields is not necessary and accurate results can be obtained by the use of relatively coarse meshes with conventional elements (not crack tip singularity elements).

7.2 J integral definition

The J integral is based on an energy balance approach and is equivalent to the energy release rate during crack extension in a homogeneous elastic body. J.R. Rice first introduced the J integral concept in 1968. The J integral method is an effective method for determining the stress intensity factors (K).

Consider a 2-D homogeneous cracked body of linear or non-linear elastic material free of body forces and tractions on the crack surfaces as shown in Fig 7.1. The total energy content U of the

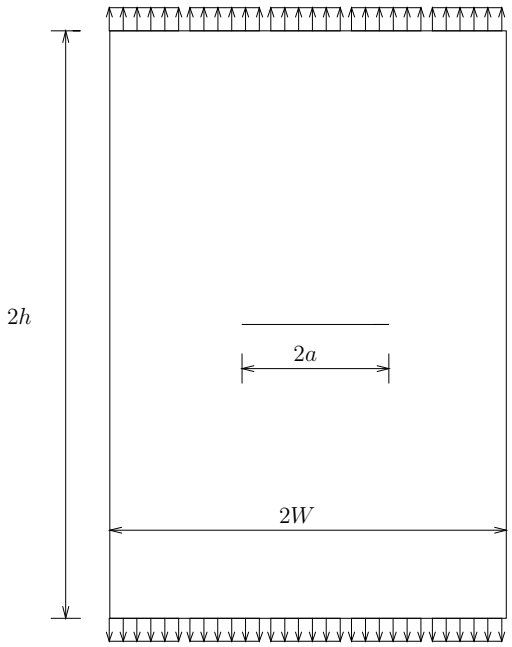

Figure 7.1: Center crack panel

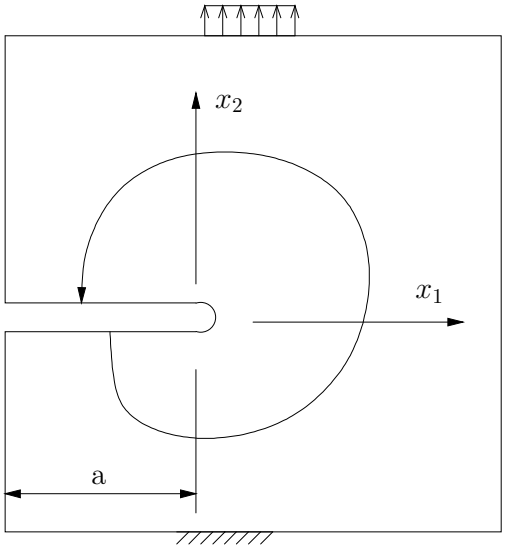

Figure 7.2: A closed contour Γ used in defining the J integral

loaded cracked plate is [35]

$$U = U_o + U_a + U_\gamma - F, \tag{7.1}$$

where

- U_0 = elastic strain energy content of the loaded uncracked plate,
- U_a = change in the elastic strain energy caused by introducing the crack in the plate,

- U_γ = change in elastic surface energy caused by the formation of the crack surfaces, and
- F = work performed by external forces.

Crack growth instability will occur as soon as U no longer increases with increasing crack length a. Thus instability will occur if:

$$\frac{dU}{da} \leq 0, \tag{7.2}$$

or since U_0 is a constant,

$$\frac{d}{da}(U_a + U_\gamma - F) \leq 0. \tag{7.3}$$

Rearranging (7.3) yields:

$$\frac{d}{da}(F - U_a) > \frac{dU_\gamma}{da}. \tag{7.4}$$

The left hand part of (7.4), $\frac{dF}{da}$, represents the energy provided by external work F per unit crack extension and $\frac{dU_a}{da}$ is the increase of elastic energy owing to the external work $\frac{dF}{da}$ .Thus, the left hand part of (7.4) is the amount of energy that remains available for crack extension. The right hand part of (7.4) represents the elastic surface energy of the crack surfaces. This is the energy needed for the crack to grow, i.e. the crack resistance R [35].

The J integral is equal to the energy release rate:

$$J = \frac{d}{da}(F - U_a). \tag{7.5}$$

The J integral is usually defined as

$$J = \int_\Gamma [W(u_i)dy - \bar{T}_i \frac{\partial \bar{u}_i}{\partial x} ds] = \int_\Gamma [W(u_i)dy - \sigma_{ij} n_j \frac{\partial \bar{u}_i}{\partial x} ds], \tag{7.6}$$

with Γ a curve surrounding the notch tip and the integral being evaluated in a counterclockwise sense starting form the lower flat notch surface and continuing along the path Γ to the upper flat surface (see Fig 7.2).

W(u_i) is the strain energy density, defined as:

$$W(\epsilon) = \int_0^\epsilon \sigma_{ij} d\epsilon_{ij}, \tag{7.7}$$

where

$$\epsilon_{ij} = \frac{1}{2}(u_{i,j} + u_{j,i}), \text{ the infinitesimal strain tensor} \tag{7.8}$$

$$\sigma_{ij,j} = 0, \text{ the equilibrium equations for zero body forces} \tag{7.9}$$

$$\sigma_{ij} = \sigma_{ji}, \text{ symmetry of the stress tensor} \tag{7.10}$$

$$T_i = \sigma_{ij} n_j, \text{ the traction on the surface, with } n_j \text{ the components of a unit vector normal to } \Gamma \tag{7.11}$$

The J integral can also be equivalently be defined as the potential energy release rate per unit crack extension, i.e.

$$J = -\frac{d\pi_p}{da}, \tag{7.12}$$

with the system potential energy

$$\pi_p(u_i) = \int_\Omega W(u_i)d\Omega - \int_{S_\sigma} \bar{T}_i u_i ds. \tag{7.13}$$

7.3 Derivation of J

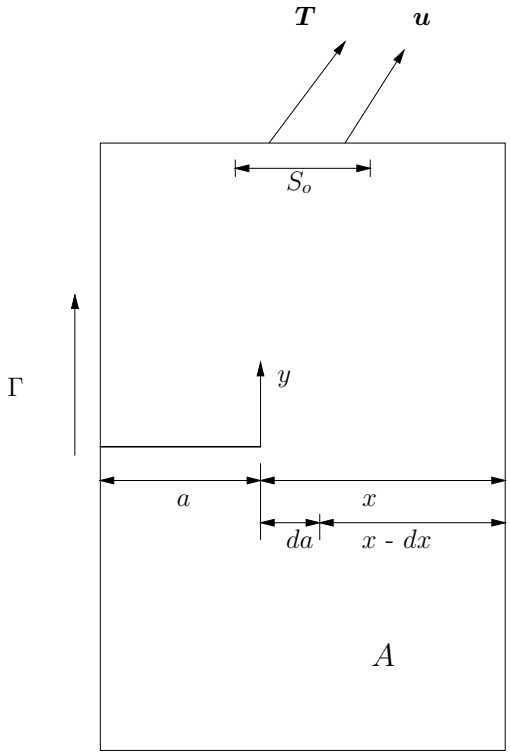

Figure 7.3: A cracked body of unit thickness loaded by a traction T

The derivation of the J integral presented here follows closely the derivation of the J integral presented in [35]. Consider a cracked body of unit thickness (Fig 7.3). The body has a perimeter Γ and a surface A. A traction T acts on a part S_o of the perimeter and performs external work of an amount ΔF. Thus parts of the body undergo a displacement represented as a displacement u. Let U_{01} be the energy contained in the plate before the traction is applied. U_{01} represents the energy contained in the cracked plate owing to any previous history. The effect of applying traction may now be considered for two cases:

- No crack growth:

  - The potential energy is $U_{p1} = U_{01} + \Delta F$

- Crack growth Δa:
  - -$\Delta F = \Delta U_a - \Delta U_\gamma$
  - In this case the potential energy is $U_{p2} = U_{01} + \Delta U_a$
  - U_γ (change in elastic surface energy caused by the formation of the crack surfaces) is irreversible and can not be part of U_{p2}

The change in potential energy due to crack extension Δa is then

$$\Delta U_p = U_{p2} - U_{p1} = \Delta U_a - \Delta F. \tag{7.14}$$

For the limiting case where $\Delta a \to 0$: the change in potential energy due to crack extension Δa is then

$$dU_p = dU_a - dF. \tag{7.15}$$

Integration of (7.15) leads to $U_p = U_a - F$ + constant. The integration constant will be equal to U_{01}, the energy content before ΔF was applied, i.e.

$$U_p = U_a - F + U_{01}. \tag{7.16}$$

$U_a + U_{01}$ is the total strain energy contained in the body. The total strain energy can be represented by

$$U_a + U_{01} = \int_A \int W dx dy, \tag{7.17}$$

and F can be represented by

$$F = \int_\Gamma \bar{T} ds \cdot \bar{u} \tag{7.18}$$

where $\bar{u}$ is the displacement vector. Substituting (7.17) and (7.18) into (7.15) yields

$$U_p = \int_A \int W dx dy - \int_\Gamma \bar{T} ds \cdot \bar{u} \tag{7.19}$$

if the traction applied to the body is constant, this yields

$$\frac{dU_p}{da} = \int_A \int \frac{\partial W}{\partial a} dx dy - \int_\Gamma \bar{T} ds \cdot \frac{\partial \bar{u}}{\partial a} \tag{7.20}$$

$\frac{dU_p}{da}$ is the expression for the change in potential energy per unit crack extension. Constrain the coordinate system such that the origin if fixed at the crack tip a. If the contour Γ is fixed, da = -dx and thus $\frac{d}{da} = -\frac{d}{dx}$. Then

$$\frac{dU_p}{da} = -\int_A \int \frac{\partial W}{\partial x} dx dy + \int_\Gamma \bar{T} ds \cdot \frac{\partial \bar{u}}{\partial x}. \tag{7.21}$$

Next we utilize Green's theorem.

Green's theorem can be stated as follows: Let R be a simply connected region with a piecewise smooth boundary C, oriented counterclockwise. If M and N have continuous partial derivatives in an open region containing R, then

$$\int_C Mdx + Ndy = \int_R \int (\frac{\partial N}{\partial x} - \frac{\partial M}{\partial y})dxdy. \tag{7.22}$$

Writing Green's theorem in parts yields

$$\int_R \int (\frac{\partial N}{\partial x})dxdy = \int_C N(x,y)dy, \tag{7.23}$$

and

$$\int_R \int (\frac{\partial M}{\partial y})dxdy = -\int_C M(x,y)dx. \tag{7.24}$$

With Green's theorem the area integral can be eliminated and $\frac{dU_p}{da}$ can be expressed as a line integral along the contour Γ, hence

$$\frac{dU_p}{da} = -\int_\Gamma W dy + \int_\Gamma \bar{T}\frac{\partial \bar{u}}{\partial x}ds. \tag{7.25}$$

For nonlinear elastic behavior an energy release rate J can be defined as follows

$$J = \frac{d}{da}(F - U_a). \tag{7.26}$$

Substituting (7.25) into (7.12) yields

$$J = \int_\Gamma W dy - \int_\Gamma \bar{T}.\frac{\partial \bar{u}}{\partial x}ds, \tag{7.27}$$

or

$$J = \int_\Gamma W dy - \int_\Gamma T_i\frac{\partial u_i}{\partial x}ds \tag{7.28}$$

which completes the derivation of the J integral.

7.4 Path independence of J

Again, the proof of the path independence of J integral presented here follows the proof presented in [35]. Considering a closed contour as shown in Fig 7.4 and using Green's theorem, it is not difficult to prove that the J value is zero for such a contour.

We have:

$$\sigma_{\mathbf{ij}} = \begin{pmatrix} \sigma_{11} & \sigma_{12} \\ \sigma_{21} & \sigma_{22} \end{pmatrix},$$

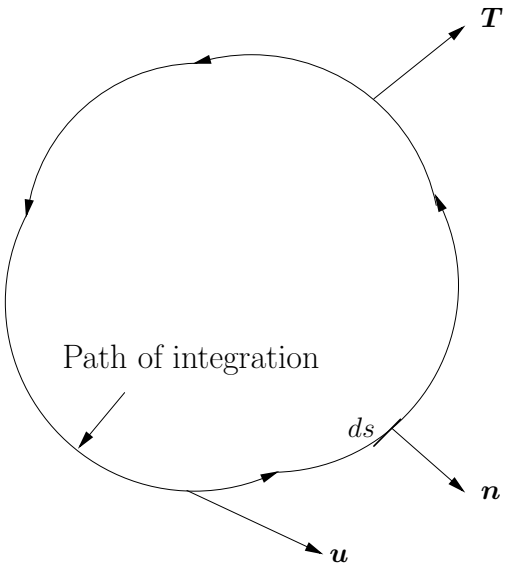

Figure 7.4: A closed contour Γ with parameters used in defining the J integral

and

$$\epsilon_{\mathbf{ij}} = \begin{pmatrix} \epsilon_{11} & \epsilon_{12} \\ \epsilon_{21} & \epsilon_{22} \end{pmatrix}.$$

The infinitesimal strain energy dW is given by:

$$dW = \sum_{ij} \sigma_{ij} d\epsilon_{ij} = \sigma_{11} d\epsilon_{11} + \sigma_{12} d\epsilon_{12} + \sigma_{21} d\epsilon_{21} + \sigma_{22} d\epsilon_{22} = \sigma_{11} d\epsilon_{11} + 2\sigma_{12} d\epsilon_{12} + \sigma_{22} d\epsilon_{22} \quad (7.29)$$

and

$$W = \int_0^{\epsilon_{ij}} dW = \int_0^{\epsilon_{ij}} \sigma_{ij} d\epsilon_{ij}. \quad (7.30)$$

The traction vector T loading a segment of a body may be defined as:

$$T_i = \sigma_{ij} n_j \quad (7.31)$$

or

$$T_1 = \sigma_{11} n_1 + \sigma_{12} n_2 \quad (7.32)$$

$$T_2 = \sigma_{21} n_1 + \sigma_{22} n_2 \quad (7.33)$$

where n_1 and n_2 are the cosines of the angles θ_1 and θ_2 being the angles the vector normal to the surface of the body makes with the positive x and y direction respectively. From this follows

$$dx = -ds \cos(\theta_2), \quad (7.34)$$

and

$$dy = ds \cos(\theta_1). \quad (7.35)$$

Now:

$$J = \int_\Gamma W dy - \int_\Gamma T_i \frac{\partial u_i}{\partial x} ds, \quad (7.36)$$

and from Green's theorem,

$$\int_\Gamma W dy = \int_A \int \frac{\partial W}{\partial x} dx dy \tag{7.37}$$

or

$$\frac{\partial W}{\partial x} = \sigma_{11}\frac{\partial \epsilon_{11}}{\partial x} + 2\sigma_{12}\frac{\partial \epsilon_{12}}{\partial x} + \sigma_{22}\frac{\partial \epsilon_{22}}{\partial x}. \tag{7.38}$$

Since

$$\frac{\partial \epsilon_{11}}{\partial x} = \frac{\partial}{\partial x}\frac{\partial u_1}{\partial x}, \tag{7.39}$$

$$2\frac{\partial \epsilon_{12}}{\partial x} = \frac{\partial}{\partial x}(\frac{\partial u_1}{\partial y} + \frac{\partial u_2}{\partial x}), \tag{7.40}$$

$$\frac{\partial \epsilon_{22}}{\partial x} = \frac{\partial}{\partial x}\frac{\partial u_2}{\partial y}, \tag{7.41}$$

$\frac{dW}{dx}$ can be represented in terms of u_1 and u_2. Hence

$$\frac{\partial W}{\partial x} = \frac{\partial}{\partial x_j}[\sigma_{ij}(\frac{\partial u_i}{\partial x})], \tag{7.42}$$

and

$$\int_\Gamma W dy = \int_A \int \frac{\partial W}{\partial x} dx dy = \int_A \int \frac{\partial}{\partial x_j}[\sigma_{ij}(\frac{\partial u_i}{\partial x})] dx dy. \tag{7.43}$$

The right side (force) of the J integral can be written as

$$\int_\Gamma T_i \frac{\partial u_i}{\partial x} ds = \int_\Gamma [(\sigma_{11}n_1 + \sigma_{12}n_2)\frac{\partial u_1}{\partial x} + (\sigma_{21}n_1 + \sigma_{22}n_2)\frac{\partial u_2}{\partial x}] ds \tag{7.44}$$

$$\int_\Gamma T_i \frac{\partial u_i}{\partial x} ds = \int_\Gamma (\sigma_{11}\frac{\partial u_1}{\partial x} + \sigma_{21}\frac{\partial u_2}{\partial x}) n_1 ds + \int_\Gamma (\sigma_{12}\frac{\partial u_1}{\partial x} + \sigma_{22}\frac{\partial u_2}{\partial x}) n_2 ds, \tag{7.45}$$

with

$$dx = n_2 ds = -\cos\theta_2 ds \tag{7.46}$$

and

$$dy = n_1 ds = \cos\theta_1 ds \tag{7.47}$$

Thus,

$$\int_\Gamma T_i \frac{\partial u_i}{\partial x} ds = \int_\Gamma (\sigma_{11}\frac{\partial u_1}{\partial x} + \sigma_{21}\frac{\partial u_2}{\partial x}) dy - \int_\Gamma (\sigma_{12}\frac{\partial u_1}{\partial x} + \sigma_{22}\frac{\partial u_2}{\partial x}) dx. \tag{7.48}$$

Using Green's theorem, this expression gives

$$\int_\Gamma T_i \frac{\partial u_i}{\partial x} ds = \int_A \int (\sigma_{11}\frac{\partial u_1}{\partial x} + \sigma_{21}\frac{\partial u_2}{\partial x}) dx dy + \int_A \int (\sigma_{12}\frac{\partial u_1}{\partial x} + \sigma_{22}\frac{\partial u_2}{\partial x}) dx dy \tag{7.49}$$

or

$$\int_\Gamma T_i \frac{\partial u_i}{\partial x} ds = \int_A \int \frac{\partial}{\partial x_j}[\sigma_{ij}(\frac{\partial u_i}{\partial x})] dx dy. \tag{7.50}$$

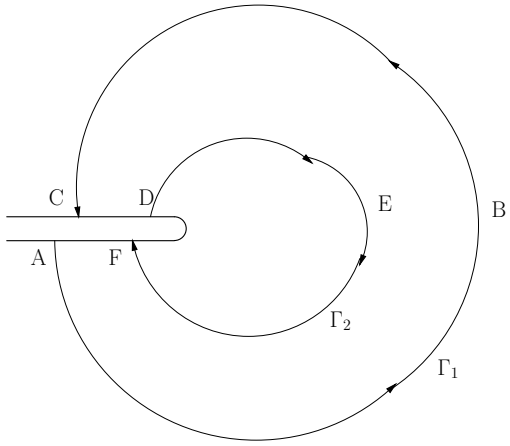

Figure 7.5: A closed contour ABCDEF for a cracked body

Hence

$$J = \int_{\Gamma} W dy - \int_{\Gamma} T_i \frac{\partial u_i}{\partial x} ds = 0 \tag{7.51}$$

Now consider a closed contour in a cracked body (Fig 7.5). The closed contour to be considered is ABCDEF, which includes CD and FA on the crack flanks, and the two paths Γ_1 and Γ_2 in opposite directions to each other. Then, from the knowledge that the total value of J is zero along the closed contour ABCDEF, it follows that

$$J = J_{\Gamma_1} + J_{CD} + J_{\Gamma_2} + J_{FA} = 0. \tag{7.52}$$

Along the crack flanks dy=0 and the traction in zero, i.e. T_i is zero. Thus for CD and FA the open contours J_{CD} and J_{FA} are equal to zero. Then

$$J = J_{\Gamma_1} + J_{\Gamma_2} = 0 \tag{7.53}$$

or

$$J_{\Gamma_1} = -J_{\Gamma_2}. \tag{7.54}$$

Reversing the direction along Γ_2 results in a change of sign. It follows that

$$J_{\Gamma_1} = J_{\Gamma_2} = J, \tag{7.55}$$

i.e. J is path independent when applied around a crack tip from one crack surface to another.

7.5 Lower bound theorem for J

The lower bound theorem can be established for a given linear or nonlinear elastic crack system with homogeneous displacement boundary constraints.

Lower Bound Theorem for J integral: For a given elastic cracked system, if u_i and $\tilde{u_i}$ are, respectively, the exact displacement and the approximate one based on the minimum potential energy principle, the approximate J integral will take a lower bound to the exact integral [39], i.e.

$$J(\tilde{u_i}) \leq J(u_i). \tag{7.56}$$

Therefore, the lower bound for the stress intensity can be obtained by using J integral with *displacement* based elements.

7.5.1 Proof of the lower bound theorem for J

Wu *et al* [1] presented a proof of the lower bound theorem. It is followed closely here without further proof or motivation. Let $\tilde{u_i} = u_i + \delta u_i$, with δu_i compatible virtual displacements. Then the approximate potential energy can be expressed as [7]

$$\Pi_p(\bar{u_i}) = \Pi_p(u_i) + \delta\Pi_p + \delta^2\Pi_p. \tag{7.57}$$

As a stationary condition of $\Pi_p(\tilde{u_i})$, $\delta\Pi_p = 0$. On the other hand, for the given exact displacement u_i which satisfied the boundary condition $\bar{u_i}|_{S_u} = 0$,

$$\int_{S_\sigma} u_i \bar{T_i} ds = \int_\Omega \epsilon_{ij}\sigma_{ij} d\Omega \tag{7.58}$$

should hold, such that

$$\Pi_p = \int_\Omega W(u_i) d\Omega - \int_{S_\sigma} u_i \bar{T_i} ds = -\int_\Omega W(u_i) d\Omega. \tag{7.59}$$

Besides, it is well known that

$$\delta^2\Pi_p = \int_\Omega W(\delta u_i) d\Omega \geq 0. \tag{7.60}$$

In accordance with the definition of J integral and its positive definite attribute, we have

$$J(\tilde{u_i}) = -\frac{d}{da}\Pi_p(\tilde{u_i}) = J(u_i) + \delta^2 J, \tag{7.61}$$

where

$$J(u_i) = -\frac{d}{da}\Pi_p(u_i) = \frac{d}{da}\int_\Omega W(u_i) d\Omega \geq 0, \tag{7.62}$$

$$\delta^2 J = -\frac{d}{da}\delta^2\Pi_p = -\frac{d}{da}\int_\Omega W(\delta u_i) d\Omega. \tag{7.63}$$

Observing that $W(u_i)$ and $W(\delta u_i)$ are all the deformation energy functions, they possess the same function configurations, and must take the same regularity when a stable crack in the system develops. Thus, we see by comparison of (7.62) and (7.63) that $\delta^2 J \leq 0$, hence the inequality (7.56) must be true.

7.5.2 J integral in FEM

In this section the implementation of the J integral in a finite element code (after Owen and Fawkes [34]) is considered. Quadratic isoparamteric elements with a 2×2 point Gauss integration scheme are employed in this example. Since the integral is path-independent, the path can conveniently be chosen to coincide with the line $\zeta = \zeta_p =$ constant, shown in Fig 7.6.

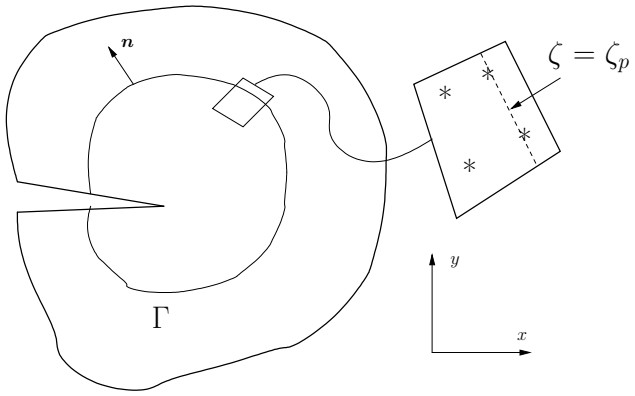

Figure 7.6: Contour path for J integral evaluation

To start, a unit normal vector $\boldsymbol{n}$ to the line $\zeta = \zeta_p$ is defined: The vectors $\boldsymbol{A}$ and $\boldsymbol{B}$ which are respectively directed along the lines $\zeta =$ constant and $\eta =$ constant are given by

$$\boldsymbol{A} = \left[\frac{\partial x}{\partial \eta}, \frac{\partial y}{\partial \eta}, 0\right], \tag{7.64}$$

$$\boldsymbol{B} = \left[\frac{\partial x}{\partial \zeta}, \frac{\partial y}{\partial \zeta}, 0\right]. \tag{7.65}$$

The vector $\boldsymbol{C}$ which is normal to the plane of the element is given by the vector product of $\boldsymbol{A}$ and $\boldsymbol{B}$, so that

$$\boldsymbol{C} = \boldsymbol{A} \times \boldsymbol{B} = \left[0, 0, (\frac{\partial x}{\partial \eta} \cdot \frac{\partial y}{d\zeta} - \frac{\partial y}{\partial \eta} \cdot \frac{\partial x}{\partial \zeta})\right]. \tag{7.66}$$

A vector $\boldsymbol{D}$ normal to the line $\zeta = \zeta_p$ can then be constructed (vector product of $\boldsymbol{C}$ and $\boldsymbol{A}$)

$$\boldsymbol{D} = \left[\frac{\partial y}{\partial \eta}(\frac{\partial y}{\partial \eta} \cdot \frac{\partial x}{d\zeta} - \frac{\partial x}{\partial \eta} \cdot \frac{\partial y}{\partial \zeta}), \frac{\partial x}{\partial \eta}(\frac{\partial x}{\partial \eta} \cdot \frac{\partial y}{\partial \zeta} - \frac{\partial y}{\partial \eta} \cdot \frac{\partial x}{\partial \zeta}), 0\right] = \left[D_1, D_2, 0\right] \tag{7.67}$$

The unit normal vector ($\boldsymbol{n}$) to the line $\zeta = \zeta_p$ can then be obtained

$$\boldsymbol{n} = [n_1, n_2, 0] = \left[\frac{D_1}{N}, \frac{D_2}{N}, 0\right] \text{with N = } \sqrt{D_1^2 + D_2^2}. \tag{7.68}$$

The elemental arc length along the line $\zeta = \zeta_p$ is given by

$$ds = \sqrt{dx^2 + dy^2} = \sqrt{(\frac{\partial x}{\partial \eta})^2 + (\frac{\partial y}{\partial \eta})^2} d\eta \tag{7.69}$$

and similarly,

$$dy = \frac{dy}{d\eta}d\eta. \tag{7.70}$$

For plane stress problems, the strain energy density can be written as

$$U = \frac{E\nu}{2(1+\nu)(1-2\nu)}(\epsilon_x + \epsilon_y)^2 + G(\epsilon_x^2 + \epsilon_y^2) + \frac{G}{2}(\gamma_{xy}^2). \tag{7.71}$$

Also, the traction vector is

$$\boldsymbol{T} = (\sigma_{11}n_1 + \sigma_{12}n_2, \sigma_{21}n_1 + \sigma_{22}n_2, 0) \tag{7.72}$$

so that

$$\boldsymbol{T}\frac{\partial \boldsymbol{d}}{\partial x} = (\sigma_{11}n_1 + \sigma_{12}n_2)\frac{\partial u}{\partial x} + (\sigma_{12}n_1 + \sigma_{22}n_2)\frac{\partial v}{\partial x}. \tag{7.73}$$

where

$$\boldsymbol{d} = (u\ v\ w) \tag{7.74}$$

Substituting (7.69), (7.70), (7.71), (7.72) and (7.73) into the definition of the J integral, we obtain an equation that gives the contribution of an individual element to the J integral:

$$\begin{aligned} J^{(e)} &= \int_{-1}^{+1} \left\{ \left(\frac{E\nu}{2(1+\nu)(1-2\nu)}(\epsilon_x + \epsilon_y)^2 + G(\epsilon_x^2 + \epsilon_y^2) + \frac{G}{2}(\gamma_{xy}^2) \right) \frac{\partial y}{\partial \eta} \right. \\ &\quad \left. - \left[(\sigma_{xx}n_1 + \sigma_{xy}n_2)\frac{\partial u}{\partial x} + (\sigma_{xy}n_1 + \sigma_{yy}n_2)\frac{\partial v}{\partial x} \right] \sqrt{(\frac{\partial x}{\partial \eta})^2 + (\frac{\partial y}{\partial \eta})^2} \right\} d\eta \\ &= \int_{-1}^{+1} X d\eta. \end{aligned} \tag{7.75}$$

The integration for (7.75) must be undertaken numerically:

$$J^{(e)} = \sum_{q=1}^{\text{NGAUS}} X(\zeta_p, \eta_q)W_q, \tag{7.76}$$

in which the integrand X is evaluated at the Gaussian sampling points ζ_p, η_q and W_q is the weighting factor corresponding to η_q. The Cartesian derivatives of the displacement components in (7.75) are given by

$$\frac{\partial(u,v)}{\partial x} = \sum_{i=1}^{n} \frac{\partial N_i^{(e)}}{\partial x}(u_1, v_i), \tag{7.77}$$

$$\frac{\partial(u,v)}{\partial y} = \sum_{i=1}^{n} \frac{\partial N_i^{(e)}}{\partial y}(u_1, v_i), \tag{7.78}$$

in which u_i, v_i are the displacement components of the nodes of the element and $\frac{\partial N_i^{(e)}}{\partial x}, \frac{\partial N_i^{(e)}}{\partial y}$ are the Cartesian derivatives of the element shape functions. The total value of the J integral is given by summing the contribution of all the elements forming the integral path.

7.5.3 Choice of integration path in element

The numerical scheme presented in Section 7.5.2 for evaluating the contribution of an element to the J integral places restrictions on both the finite element mesh that can be used and the order of node numbering of the elements in the path [34]. To be able to use the method presented, the crack geometry must preferably be idealized by a radial fan of elements centered at the crack tip (see Fig 7.7) and the nodal number of the elements, through which the contour is to be taken, must be such that the local ζ coordinate axes follow the tangential direction.

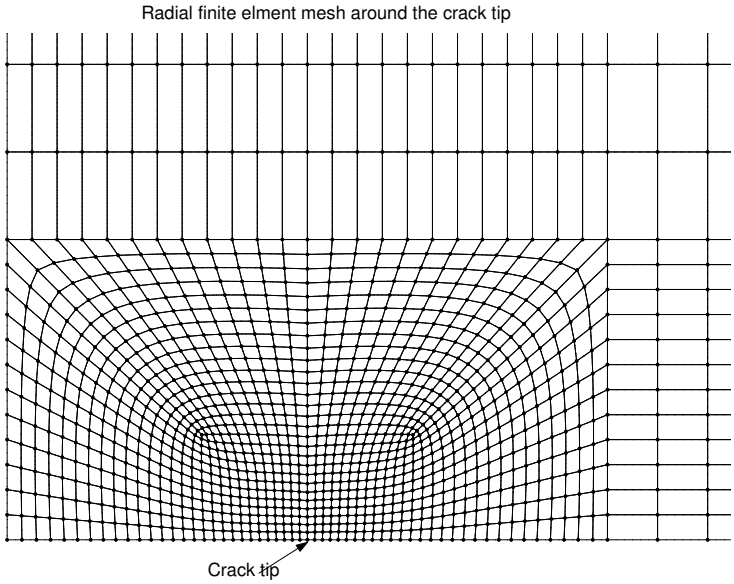

Figure 7.7: Radial finite element mesh around a crack tip

While such an approach allows the numerical process for the evaluation of J to be elegantly formulated, it nevertheless places a considerable restriction on the finite element mesh topology. Therefore a method is required for evaluating the J integral that can be used with any arbitrarily structured finite element mesh is optimum [34]. The most general case for an integration path is illustrated in Fig 7.8.

A typical contour path around the crack tip will be made up of:

- Contributions from elements in which integration is made along paths $\zeta = \zeta_p$ (constant)
- Contributions from elements in which integration is made along paths $\eta = \eta_p$ (constant)
- Contributions from ”corner” elements in which the path changes from the ζ to η direction.

Integration along a path where $\eta = \eta_p$ and a path where $\zeta = \zeta_p$ (see section 7.5.2) can be done in an identical manner [34].

For a corner element where the path changes form ζ to the η direction the contribution of the element to the J integral can be evaluated in a normal manner by integrating across the complete

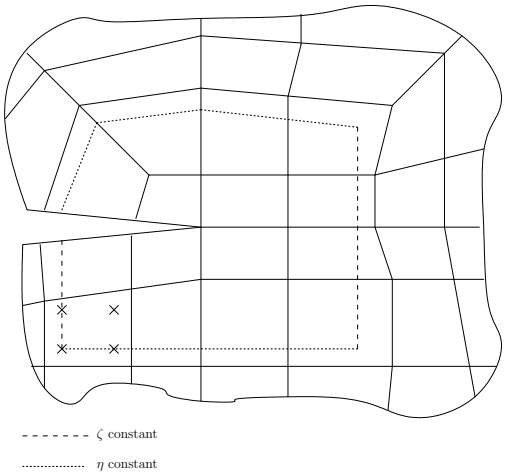

Figure 7.8: Contour for J evaluation involving paths along both ζ and η directions and "corner" elements

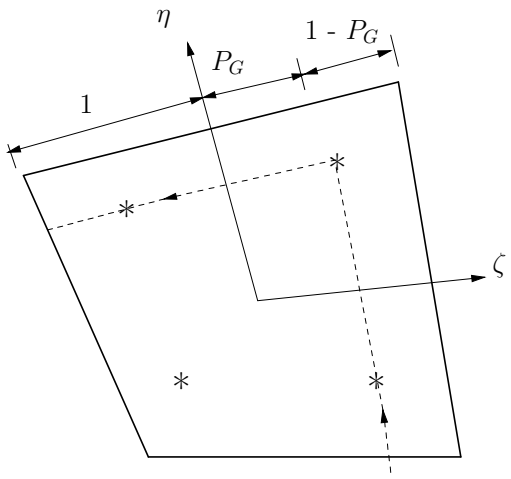

Figure 7.9: Path through corner elements

element dimensions in the ζ and η directions. The values obtained can then be scaled to account for the actual shorter path length. The scaling factor for both the ζ and η directions can be readily obtained for a 2 point Gauss rule to be [34]:

$$S_G = \frac{1 + P_G}{2} = 0.788675 \text{ where } P_G = 0.57735. \tag{7.79}$$

Obviously some degree of numerical inaccuracy is introduced by this scaling process, but since the contribution of such a corner element to the complete J integral will be small, the error involved is acceptable.

To avoid the error introduced by the corner elements the J integral path can be selected on the boundary of the element. If the element edge is chosen as the integral path, no scaling of corner node elements needs to be done. This approach can also be used with any arbitrary mesh.

Chapter 8

Fracture mechanics: The I^* integral as the dual form of the J integral

In this chapter, the formulation, path independence, lower bound theorem and finite element implementation of the I^* integral is outlined. The computer implementation of the theory is reflected in Appendix C.

8.1 The I^* integral

Based on the energy foundation of the path-independent integral there must exist a dual version of Rice's J integral, which should also be a path-independent integral, be identical to J in value and be dependent on the system complementary energy. The I^* integral presented by Wu *et al.* [39] is such an integral. The J integral is equivalent to the release rate of strain energy $\Pi(u_i)$ with respect to the crack area, and the I^* integral is equivalent to the release rate of the complementary energy $\Pi_c(\sigma_{ij})$ with respect to the crack area. An interesting application of the I^* integral is that it is able to provide the approximate upper bound solution for crack problems. Equilibrium based elements (based on the complementary energy principle) should be used to estimate the I^* integral.

8.2 Derivation of the I^* integral

The derivation of the I^* integral presented here follows the derivation of the I^* integral presented by [39]. Consider a 2-D homogeneous cracked system of linear or non-linear elastic material free of body forces and traction on the crack surface as shown in Fig 7.3. For the purpose of developing the dual integral of J, one may use the Legendre transformation

$$W(u_i) + B(\sigma_{ij}) = \sigma_{ij}\epsilon_{ij}, \tag{8.1}$$

thus

$$W(u_i) = \sigma_{ij}\epsilon_{ij} - B(\sigma_{ij}). \tag{8.2}$$

Introducing (8.2) into the J integral formulation (7.6), the I^* integral can be formulated as follows

$$I^* = \int_\Gamma [[\sigma_{ij}\epsilon_{ij} - B(\sigma_{ij})]dy - \sigma_{ij}n_j\frac{\partial u_i}{\partial x}ds]. \tag{8.3}$$

with $n_1 ds = \cos\theta_1 ds = dy$ and $n_2 ds = -\cos\theta_2 ds = -dx$. Viz.,

$$I^* = \int_\Gamma [-B(\sigma_{ij})dy + \sigma_{ij}\epsilon_{ij}dy - \sigma_{i1}\frac{\partial u_i}{\partial x}dy + \sigma_{i2}\frac{\partial u_i}{\partial x}dx], \tag{8.4}$$

hence

$$I^* = \int_\Gamma [-B(\sigma_{ij})dy + \sigma_{i2}\frac{\partial u_i}{\partial y}dy + \sigma_{i2}\frac{\partial u_i}{\partial x}dx], \tag{8.5}$$

or

$$I^* = \int_\Gamma [-B(\sigma_{ij})dy + (\frac{\partial u_1}{\partial y}\sigma_{12} + \frac{\partial u_2}{\partial y}\sigma_{22})dy + (\frac{\partial u_1}{\partial x}\sigma_{12} + \frac{\partial u_2}{\partial x}\sigma_{22})dx]. \tag{8.6}$$

The I^* integral can also be defined as a complementary energy release rate

$$I^* = \frac{d\Pi_c}{da}, \tag{8.7}$$

where the system complementary energy is given by:

$$\Pi_c(\sigma_{ij}) = \int_\Omega B(\sigma_{ij})d\Omega - \int_{S_u} \bar{u_i}\sigma_{ij}n_j ds. \tag{8.8}$$

8.3 Path independence of I^*

Again consider the cracked body shown in Fig 7.5. The domain $\Delta\Omega$ is enclosed by the paths Γ_1, Γ_2 and the crack surface CD and AF. With respect to (8.5) the I^* integrals related to the different paths Γ_1 and Γ_2 yields (no sum on i)

$$\begin{aligned}\Delta I^* &= I^*(\Gamma) - I^*(\Gamma') \\ &= \oint \Big[- B(\sigma_{ij})dy + u_i\frac{\partial \sigma_{ij}}{\partial x}n_j ds + \frac{\partial}{\partial x_j}(u_i\sigma_{12})dx_j\Big] \\ &\quad - \int_{CD+AF} \Big[- B(\sigma_{ij})dy + u_i\frac{\partial \sigma_{ij}}{\partial x}n_j ds + \frac{\partial}{\partial x_j}(u_i\sigma_{12})dx_j\Big]\end{aligned} \tag{8.9}$$

For the assumed stress finite elements employed to calculate I^*, it is assumed that the equilibrium equations $\sigma_{ij,j} = 0$ are satisfied (exactly or in a least-squares sense). Thus

$$\oint \Big[- B(\sigma_{ij})dy + u_i\frac{\partial \sigma_{ij}}{\partial x}n_j ds + \frac{\partial}{\partial x_j}(u_i\sigma_{12})dx_j\Big] \tag{8.10}$$

$$= \int_{\Delta\Omega} \Big[- \frac{\partial B}{\partial \sigma_{ij}}\frac{\partial \sigma_{ij}}{\partial x} + u_{i,j}\frac{\partial \sigma_{ij}}{\partial x} + u_i\frac{\partial}{\partial x}\sigma_{ij,j}\Big]d\Omega \tag{8.11}$$

$$= \int_{\Delta\Omega} \Big[-\frac{\partial B}{\partial \sigma_{ij}} + u_{i,j} \Big] \frac{\partial \sigma_{ij}}{\partial x} d\Omega \tag{8.12}$$

Observing that the traction-free condition $(\sigma_{ij} n_j = T_i)|_{CD+AF} = 0$ and $\sigma_{22} = \sigma_{12} = 0$ can be imposed by the assumed stress elements, the second term in (8.9) vanishes, since $dy = 0$ on CD and AF. Using

$$\epsilon_{ij} = \frac{\partial}{\partial \sigma_{ij}} \tag{8.13}$$

then (8.9) becomes

$$\Delta I^* = \int_{\Delta\Omega} (-\epsilon_{ij} + u_{i,j}) \frac{\partial \sigma_{ij}}{\partial x} d\Omega. \tag{8.14}$$

For a given discrete system, it takes the form

$$\Delta I^* = \sum_e \int_{\Delta\Omega} (-\epsilon_{ij} + u_{i,j}) \frac{\partial \sigma_{ij}}{\partial x} d\Omega. \tag{8.15}$$

In accordance with (8.15), we have another equivalent relation:

$$\Delta I^* = 0 \Leftrightarrow \epsilon_{ij} = \frac{1}{2}(u_{i,j} + u_{j,i}) \text{ in } \Delta\Omega^e. \tag{8.16}$$

As for the assumed stress elements, the path independence for the numerical solution of I^* are conditioned by meeting the $\epsilon_{ij} - u_i$ compatibility constraints within individual elements.

The assumed stress finite elements are able to guarantee the numerical solution of I^* to be path-independent.

8.4 Upper bound theorem for I^*

The upper bound theorem as given in [39] is formulated as follows: For a given elastic cracked system, if σ_{ij} and $\tilde{\sigma}_{ij}$ are, respectively, the exact stresses and the approximate stresses based on the minimum complementary energy principle, the approximate I^* integral will take the upper bound of its exact integral:

$$I^*(\tilde{\sigma}_{ij}) \geq I^*(\sigma_{ij}). \tag{8.17}$$

Therefore, the upper bound of I^* can be obtained by using stress equilibrium elements.

8.5 Proof of the upper bound theorem

Let $\tilde{\sigma_{ij}} = \sigma_{ij} + \delta\sigma_{ij}$, where $\delta\sigma_{ij}$ are virtual stresses, hence we can write:

$$\Pi_c(\tilde{\sigma_{ij}}) = \Pi_c(\sigma_{ij}) + \delta\Pi_c + \delta^2\Pi_c. \tag{8.18}$$

As a stationary condition of $\Pi_c(\tilde{\sigma}_{ij})$, we have $\delta\Pi_c = 0$. On the other hand, due to $\bar{u_i}|_{S_u} = 0$, the complementary energy functional

$$\Pi_c(\sigma_{ij}) = \int_\Omega B(\sigma_{ij}) d\Omega - \int_{S_u} \bar{u}_i \sigma_{ij} n_j ds, \tag{8.19}$$

becomes

$$\Pi_c(\sigma_{ij}) = \int_\Omega B(\sigma_{ij})d\Omega. \tag{8.20}$$

and

$$\delta^2\Pi_c = \int_\Omega B(\delta\sigma_{ij})d\Omega \geq 0. \tag{8.21}$$

With respect to the exact solutions, $I^*(\sigma_{ij}) = J(u_i) \geq 0$. Thus, by means of $I^* = \frac{d\Pi_c}{da}$ and (8.18) through to (8.21), the following can be obtained:

$$I^*(\tilde{\sigma}_{ij} = I^*(\sigma_{ij}) + \delta^2 I^*, \tag{8.22}$$

with

$$I^*(\sigma_{ij}) = \frac{d}{da}\Pi_c(\sigma_{ij}) = \frac{d}{da}\int_\Omega B(\sigma_{ij})d\Omega \geq 0, \tag{8.23}$$

and

$$\delta^2 I^* = \frac{d}{da}\delta^2\Pi_c = \frac{d}{da}\int_\Omega B(\delta\sigma_{ij})d\Omega. \tag{8.24}$$

Observing that both $B(\sigma_{ij})$ and $\delta B(\sigma_{ij})$ are positive definite complementary energy functions, they possess the same function configurations. Therefore, they must exhibit the same variation when the system is experiencing stable crack growth. By comparison of (8.23) and (8.24), it can be found that $\delta^2 I^* \geq 0$ and that the inequality (8.17) must be true.

The stress equilibrium element is based on the complementary energy formulation $\Pi_c(\sigma)$, while the stress hybrid element is based on the Reissner formulation $\Pi_R(\sigma, u)$. However, $\Pi_R(\sigma, u)$ is identical to $\Pi_c(\sigma)$. Thus a hybrid model may degenerate into an equilibrium model when the stress equilibrium equations are enforced in the hybrid element.

8.5.1 Determination of the stress intensity factor K_I using the J and I^* integrals

For ease of comparison the J- or I^* integrals are expressed in terms of stress intensity factors. The relationship between the J and I^* integral values and the stress intensity factor can be stated as follows:

Linear isotropic elasticity

For linear elastic isotropic materials in elastic conditions the J and I^* integrals can be written in terms of Mode I and Mode II stress intensity factors as follows:

$$J = I^* = \frac{K_I^2 + K_{II}^2}{E'} \tag{8.25}$$

where E' = E for plane stress and E' = $E/(1-\nu^2)$ for plane strain, where ν is Poisson's ratio [40].

Linear orthotropic elasticity

Formulating the constitutive relations of a linear elastic orthotropic material in global coordinates as follows (for the definition of a_{11} - a_{66} see (11.7)):

$$\boldsymbol{\epsilon} = \begin{bmatrix} a_{11} & a_{12} & 0 \\ a_{12} & a_{22} & 0 \\ 0 & 0 & a_{66} \end{bmatrix} \boldsymbol{\sigma}. \tag{8.26}$$

the J and I^* integrals can be expressed as follows in terms of the Mode I and Mode II stress intensity factors [40]:

$$J = I^* = \left[K_I^2 \left(\frac{a_{11} a_{22}}{2} \right)^{1/2} + K_{II}^2 \left(\frac{a_{11}}{\sqrt{2}} \right) \right] \left[\left(\frac{a_{22}}{a_{11}} \right)^{1/2} + \frac{2a_{12} + a_{66}}{2a_{11}} \right]^{1/2}. \tag{8.27}$$

Chapter 9

Fracture mechanics: Isotropic results

In this chapter, numerical results are presented for isotropic fracture mechanics problems using the developed code in Appendix C. The problems are evaluated using the J and I^* integrals with the different displacement based and assumed stress elements presented in earlier chapters. The results obtained are compared with known exact solutions. A convergence study is done to determine the effect of mesh refinement on the values of the J and I^* integrals.

9.1 Problem description

Four different problems (three Mode I problems and a Mode II crack problem) with known "exact" solutions are investigated. These are

- a center cracked panel (CCP) with unit thickness subjected to uniform tension, see Fig 9.1(a),
- a single edge cracked panel (SECP) with unit thickness subjected to uniform tension, see Fig 9.1(b),
- a double edge cracked panel (DECP) with unit thickness subjected to uniform tension, see Fig 9.1(c), and
- a center cracked panel (CCP) subjected to uniform shearing, see Fig 9.1(d).

Due to the symmetry of the cracked panels, only a quarter of the CCP and DECP and one half of the SECP are modelled with a discrete finite element mesh (see Fig 9.2(a) and Fig 9.2(b) for Mesh 1 and Mesh 3). For the mode I problems (CCP, SECP and DECP with uniform tension) the normal nodal displacements are fixed on the axes of symmetry. For the mode II problem (CCP with uniform shear), the tangential nodal displacements are fixed on the axis of symmetry and the upper right hand corner node's x and y displacement are constrained with an MPC.

Five integration contours (numbered 1, 2, 3, 4 and 5 beginning with the innermost contour) were used. The contours are shown in Fig 9.2(a) and Fig 9.2(b) for Mesh 1 and Mesh 3.

To evaluate the J integral, the following elements, based on the minimum potential energy principle, are used:

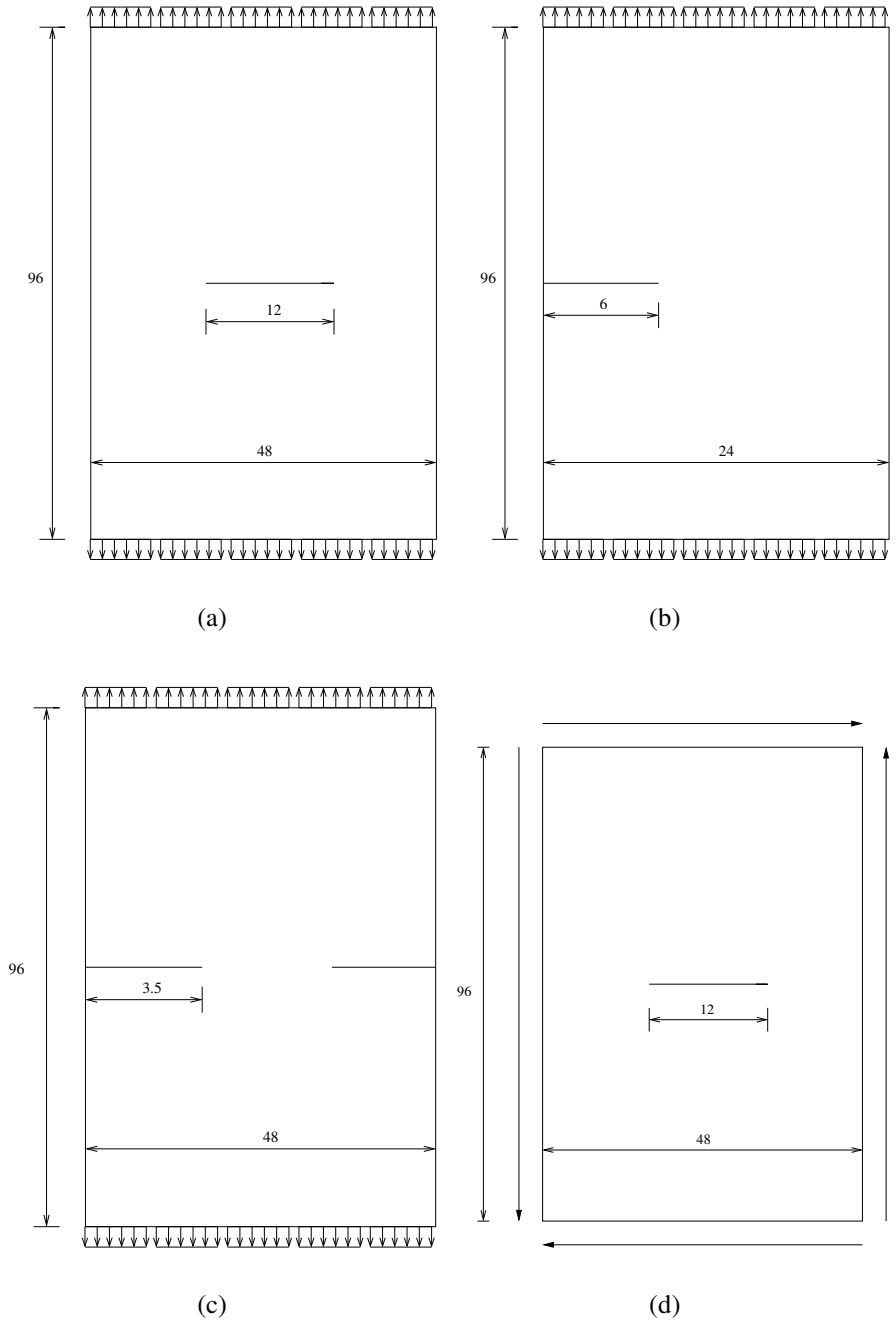

Figure 9.1: Cracked panels: (a) Center cracked panel (CCP) that is subjected to tension (b) Single edge cracked panel (SECP) subjected to uniform tension (c) Double edge cracked panel (DECP) subjected to uniform tension (d) Center cracked panel (CCP) subjected to uniform shear

- Q4 (A displacement based quadrilateral element) and
- Q4X (A displacement based quadrilateral element with drilling degrees of freedom)

The value of the I^* integral was calculated using the following elements, in accordance with the complementary energy principle:

- PS (The assumed stress quadrilateral element proposed by Pian and Sumihara [5]),
- PS(α) (A penalized version of the assumed stress quadrilateral element proposed by Pian and Sumihara [5]),
- 8β (A assumed stress quadrilateral element with drilling degrees of freedom and 8 β parameters),
- 8$\beta(\alpha)$ (A penalized version of the assumed stress quadrilateral element with drilling degrees of freedom and 8 β parameters),
- 9β (A assumed stress quadrilateral element with drilling degrees of freedom and 9β parameters) and
- 9$\beta(\alpha)$ (A penalized version of the assumed stress quadrilateral element with drilling degrees of freedom and 9 β parameters).

The J and I^* integral values calculated are converted to stress intensity factors (K) for convenient comparison. The exact solutions of the stress intensity factor K_1 and K_2 are adopted from [1].

The stress intensity factor is independent of the material constants in principle [40]. For computational ease, the following material properties were used throughout:

- Young's modulus E = 1,
- Poisson's ratio ν = 0.3, and
- the distributed loads $\sigma = \tau = 1$.

The units of loading are consistent with that of E.

9.2 Analytical stress intensity factors expressions

- a center cracked panel (CCP) with unit thickness subjected to uniform tension:
  - where σ is the remote stress applied to the component, 2a is the crack length and f(g) is a correction factor that depends on the specimen and crack geometry.

$$K_I = f(g)\sigma\sqrt{(\pi a)} \tag{9.1}$$

$$f(g) = \sqrt{(\sec\frac{\pi a}{2b})} \tag{9.2}$$

- a single edge cracked panel (SECP) with unit thickness subjected to uniform tension:

- where σ is the remote stress applied to the component, a is the crack length and f(g) is a correction factor that depends on the specimen and crack geometry.

$$K_I = f(g)\sigma\sqrt{(\pi a)} \tag{9.3}$$

$$f(g) = 1.12 - 0.231(\frac{a}{b}) + 10.55(\frac{a}{b})^2 - 21.72(\frac{a}{b})^3 + 30.39(\frac{a}{b})^4 \tag{9.4}$$

- a double edge cracked panel (DECP) with unit thickness subjected to uniform tension:
  - where σ is the remote stress applied to the component, a is the crack length and f(g) is a correction factor that depends on the specimen and crack geometry.

$$K_I = f(g)\sigma\sqrt{(\pi a)} \tag{9.5}$$

$$f(g) = 1.12 + 0.203(\frac{a}{b}) - 1.197(\frac{a}{b})^2 + 1.930(\frac{a}{b})^3 \tag{9.6}$$

9.3 Convergence study

The effect of mesh refinement on the stress intensity factor is of interest. The convergence study is done for a center cracked panel (see Fig 9.1(a)) using 3 different meshes (Mesh 1, Mesh 2 and Mesh 3) with different densities. The stress intensity factor is obtained for the different meshes using 5 independent integral paths. Mesh 2 is a bisection of Mesh 1, and Mesh 3, in turn, is a bisection of Mesh 2.

Mesh 1 consists of 17 $\times$ 9 elements in total and a radial fan of element around the crack tip of 7 $\times$ 3 elements as shown in Fig 9.2(a). The five selected integration contours for the quarter CCP are shown in Fig 9.2(a) and Fig 9.2(b).

The effect of the mesh refinement on the J integral is investigated for displacement base finite elements Q4 and Q4X. The stress intensity factor calculated with the J integral for the CCP plate are listed in Table 9.1 for the Q4 element and in Table 9.2 for the Q4X elements. The results are plotted in Fig 9.3(a) and Fig 9.3(b).

Path	Mesh 1	Mesh 2	Mesh 3
Path 1	4.377	4.474	4.494
Path 2	4.377	4.474	4.494
Path 3	4.450	4.503	4.501
Path 4	4.463	4.496	4.505
Path 5	4.459	4.495	4.504
Exact		4.506	

Table 9.1: Convergence of K_1 for an isotropic CCP subjected to uniform tension with Q4 elements

It is evident that the stress intensity factor obtained with the J integral converges to the analytical value as the mesh is refined. It is also confirmed that the stress intensity factor calculated with the

Path	Mesh 1	Mesh 2	Mesh 3
Path 1	4.391	4.468	4.494
Path 2	4.375	4.467	4.494
Path 3	4.443	4.494	4.501
Path 4	4.390	4.470	4.496
Path 5	4.392	4.471	4.496
Exact		4.506	

Table 9.2: Convergence of K_1 for an isotropic CCP subjected to uniform tension with Q4X elements

J integral, with the displacement based elements, presents a lower bound to the true value of K_1. The path-independence of J integral is also confirmed.

Next we consider the I^* integral with assumed stress elements: The mixed formulation elements PS, PS(α), 8β, 8$\beta(\alpha)$, 9β and 9$\beta(\alpha)$ elements are used in combination with the I^* integral to calculate the stress intensity factor for the center cracked panel.

The calculated stress intensity factors for the CCP plate obtained using all the mixed formulation elements are listed in Table 9.3, Table 9.4, Table 9.5, Table 9.6, Table 9.7 and Table 9.8 and plotted in Fig 9.3(c), Fig 9.3(d), Fig 9.4(a), Fig 9.4(b), Fig 9.4(c) and Fig 9.4(d).

Path	Mesh 1	Mesh 2	Mesh 3
Path 1	4.441	4.485	4.500
Path 2	4.444	4.485	4.500
Path 3	4.486	4.513	4.507
Path 4	4.469	4.496	4.505
Path 5	4.473	4.497	4.505
Exact		4.506	

Table 9.3: Convergence of K_1 for an isotropic CCP subjected to uniform tension with PS elements

It is evident that the stress intensity factor obtained with all the mixed formulation elements using the I^* integral converge to the analytical value as the mesh is refined. It is also confirmed that the stress intensity factor calculated with the I^* integral using the elements with penalized equilibrium (PS(α), 8$\beta(\alpha)$ and 9$\beta(\alpha)$ elements) forms a upper bound for the true value of K_1. The stress intensity factors obtained when the PS, 8β and 9β elements are used tends to under predicted the K_1 value. The stress intensity factor calculated with the I^* integral using unpenalized assumed stress elements with drilling degrees of freedom do not form a upper bound for the stress intensity factor for the (relatively fine) meshes considered. The path-independence of the I^* integral as obtained with all the mixed formulation elements is, however, confirmed.

It is noted that the solution of J converges to the analytical solution from below, while the solution of I^* using the penalized equilibrium elements converges to the analytical solution from above.

Path	Mesh 1	Mesh 2	Mesh 3
Path 1	4.485	4.528	4.512
Path 2	4.491	4.508	4.512
Path 3	4.534	4.538	4.518
Path 4	4.517	4.520	4.516
Path 5	4.521	4.521	4.516
Exact		4.506	

Table 9.4: Convergence of K_1 for an isotropic CCP subjected to uniform tension with PS(α) elements

Path	Mesh 1	Mesh 2	Mesh 3
Path 1	4.442	4.481	4.498
Path 2	4.429	4.482	4.498
Path 3	4.419	4.476	4.495
Path 4	4.434	4.480	4.498
Path 5	4.436	4.480	4.498
Exact		4.506	

Table 9.5: Convergence of K_1, for an isotropic CCP subjected to uniform tension with 8β elements

This demonstrates the bound theorems nicely.

9.4 Results for different panels

In Fig 9.5(a) to Fig 9.5(d) the displaced geometry of the different cracked plate problems are plotted against their undisplaced geometry.

From the convergence study it is noted that the results obtained using Mesh 3 are superior to the results obtained using Mesh 1 or Mesh 2, hence all the results given below are obtained using Mesh 3.

Fig 9.6(b), Fig 9.7(a) and Fig 9.7(b) presents a summary of the numerical results for the individual specimens. All of them confirm that the J integral using elements with drilling d.o.f and Q4 element gives a lower bound on the stress intensity and that the I^* integral using the 8$\beta(\alpha)$, 9$\beta(\alpha)$ and PS(α) elements gives a upper bound on the stress intensity factor.

1. Center cracked panel subjected to a uniform stretching load

   In Table 9.9 the results for the center cracked plate subjected to tension are tabulated. The results for the CCP are plotted in Fig 9.6(a). Clearly, the stress intensity factor calculated with the I^* integral and penalized equilibrium elements forms an upper bound and the J integral forms a lower bound to the analytical stress intensity factor.

Path	Mesh 1	Mesh 2	Mesh 3
Path 1	4.483	4.508	4.512
Path 2	4.492	4.509	4.512
Path 3	4.506	4.519	4.516
Path 4	4.517	4.524	4.516
Path 5	4.524	4.527	4.517
Exact		4.506	

Table 9.6: Convergence of K_1 for an isotropic CCP subjected to uniform tension with $8\beta(\alpha)$ elements

Path	Mesh 1	Mesh 2	Mesh 3
Path 1	4.442	4.481	4.498
Path 2	4.429	4.482	4.498
Path 3	4.419	4.476	4.495
Path 4	4.434	4.480	4.498
Path 5	4.437	4.480	4.498
Exact		4.506	

Table 9.7: Convergence of K_1 for an isotropic CCP subjected to uniform tension with 9β elements

2. Single edge cracked panel

   In Table 9.10 the results obtained for the single edge cracked plate subjected to uniform tension are tabulated. The results for the SECP are plotted in Fig 9.6(b). The stress intensity factor calculated with the I^* integral using the first 3 integration contours under predicts the stress intensity factor rather than forming an upper bound. This seems to be the result of selecting the integration paths to close to the crack tip.

3. Double edge cracked panel

   In Table 9.11 the results for the double edge cracked plate under uniform tension are tabulated. The results for the DECP are plotted in Fig 9.7(a). The upper and lower bounds predicted for the stress intensity factor of the DECP are clearly depicted in Fig 9.7(a).

4. Center cracked panel subjected to uniform shear

   In Table 9.12 the results for the center cracked plate under uniform shear are tabulated. The results for the CCP under uniform shear are plotted in Fig 9.7(b). Using a finer mesh may improve the results obtained. The elements all under predicts K_{II}, in particular as r, is increased.

Path	Mesh 1	Mesh 2	Mesh 3
Path 1	4.476	4.503	4.508
Path 2	4.487	4.501	4.508
Path 3	4.488	4.512	4.512
Path 4	4.502	4.515	4.512
Path 5	4.504	4.515	4.513
Exact		4.506	

Table 9.8: Convergence of K_1 for an isotropic CCP subjected to uniform tension with $9\beta(\alpha)$ elements

Path	Q4	Q4X	PS	PS(α)	8β	$8\beta(\alpha)$	9β	$9\beta(\alpha)$
Path 1	4.494	4.494	4.500	4.512	4.498	4.512	4.498	4.508
Path 2	4.494	4.494	4.500	4.512	4.498	4.512	4.498	4.508
Path 3	4.501	4.501	4.507	4.518	4.495	4.516	4.495	4.512
Path 4	4.505	4.496	4.505	4.516	4.498	4.517	4.498	4.512
Path 5	4.504	4.496	4.505	4.516	4.498	4.517	4.498	4.513
Exact				4.506				

Table 9.9: K_1 results for the isotropic CCP subjected to uniform tension (Mesh 3)

Path	Q4	Q4X	PS	PS(α)	8β	$8\beta(\alpha)$	9β	$9\beta(\alpha)$
Path 1	6.457	6.456	6.469	6.496	6.461	6.498	6.463	6.484
Path 2	6.455	6.455	6.469	6.495	6.460	6.497	6.463	6.483
Path 3	6.512	6.492	6.482	6.508	6.465	6.516	6.467	6.504
Path 4	6.508	6.486	6.502	6.529	6.496	6.531	6.498	6.517
Path 5	6.507	6.486	6.503	6.529	6.496	6.531	6.499	6.517
Exact				6.517				

Table 9.10: K_1 results for the isotropic SECP subjected to uniform tension (Mesh 3)

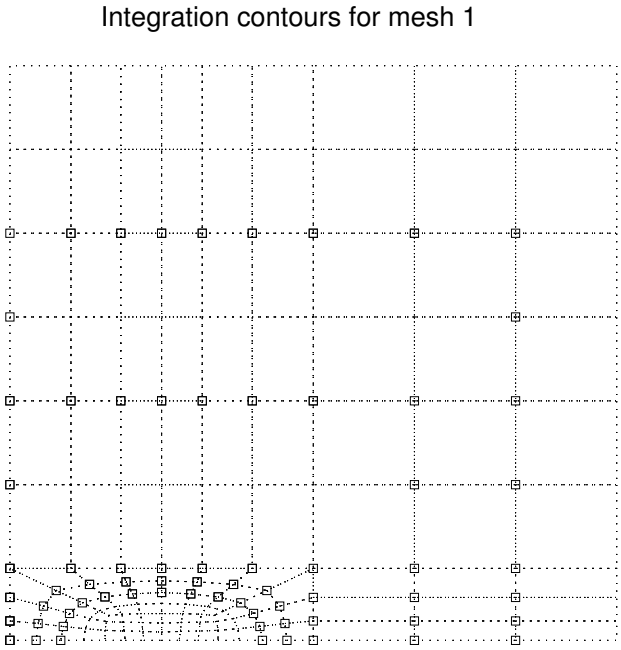

(a)

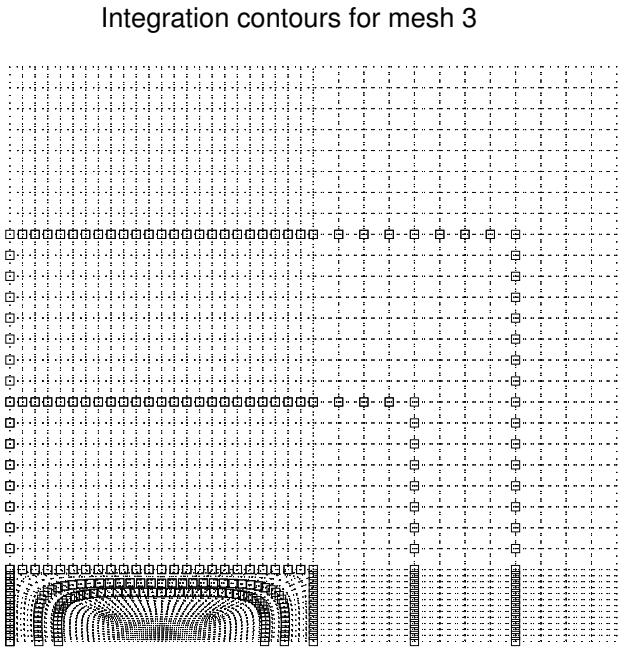

(b)

Figure 9.2: Finite element mesh and five selected integration contours for one-quarter of the CCP and one half of the SECP and the DECP. (a) Mesh 1 (b) Mesh 3

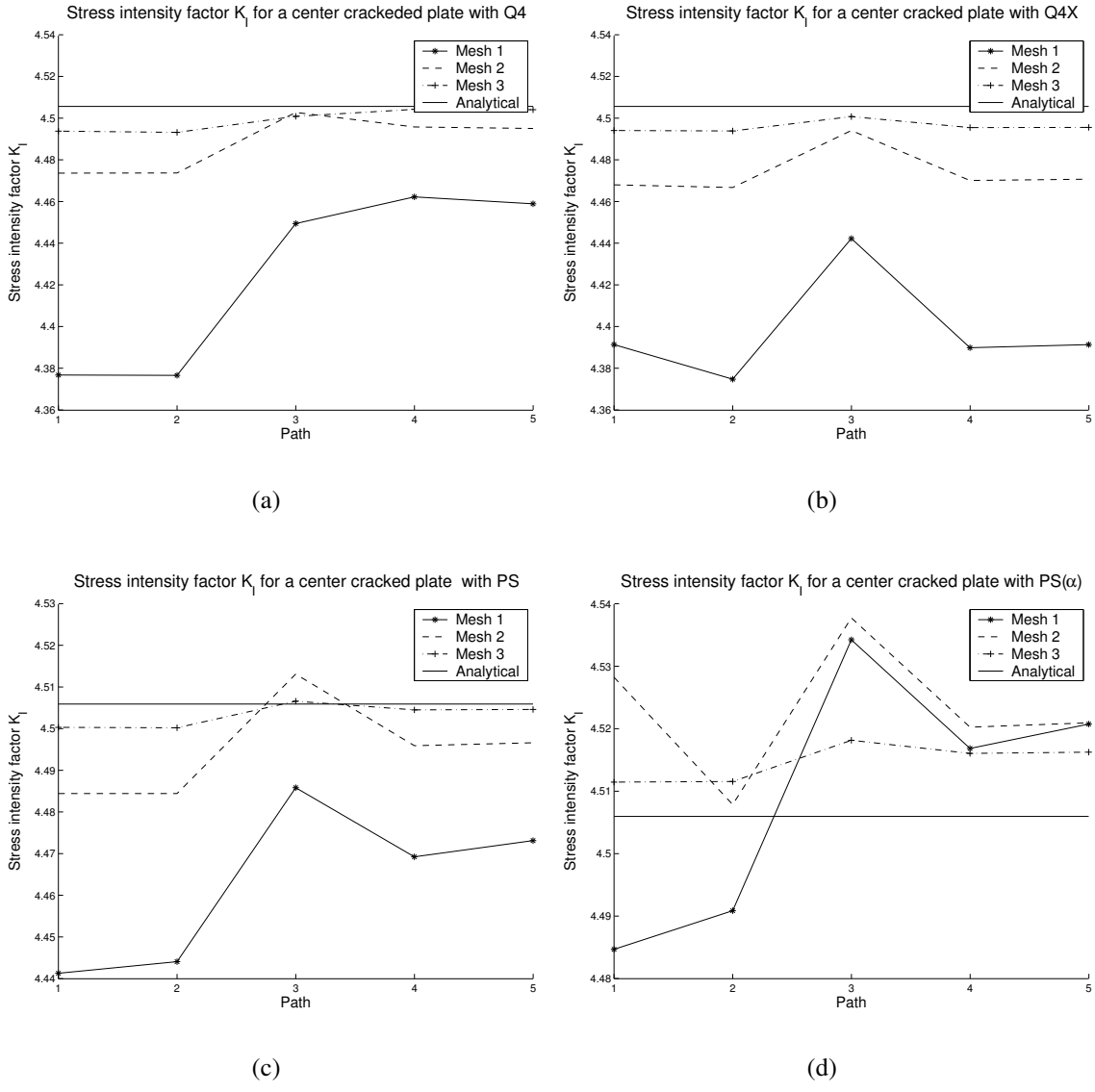

Figure 9.3: Convergence study for the CCP with different elements: (a) Q4 (b) Q4X (c) PS, and (d) PS(α)

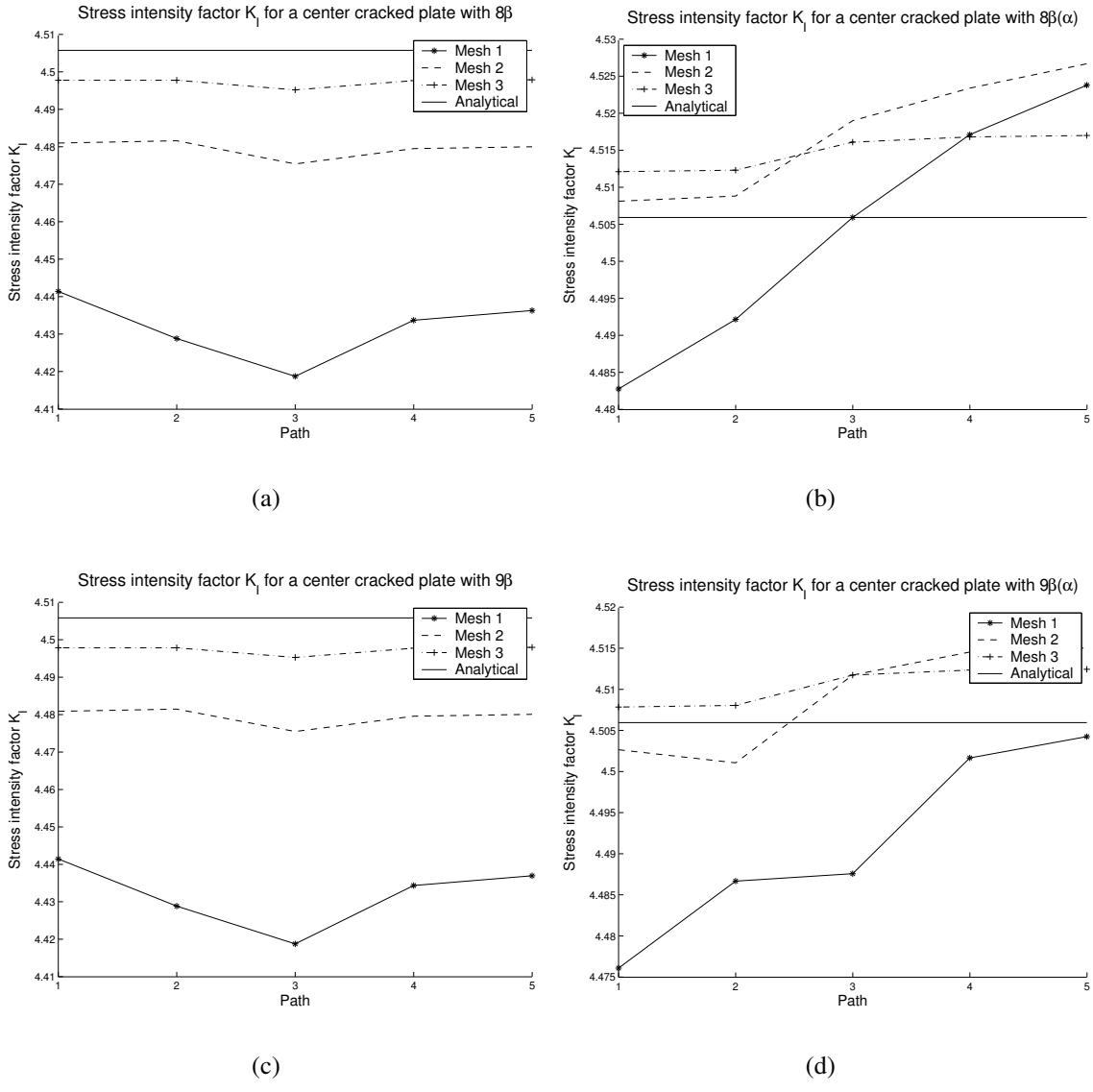

Figure 9.4: Convergence study for the CCP with different elements: (a) 8β (b) $8\beta(\alpha)$ (c) 9β (d) $9\beta(\alpha)$

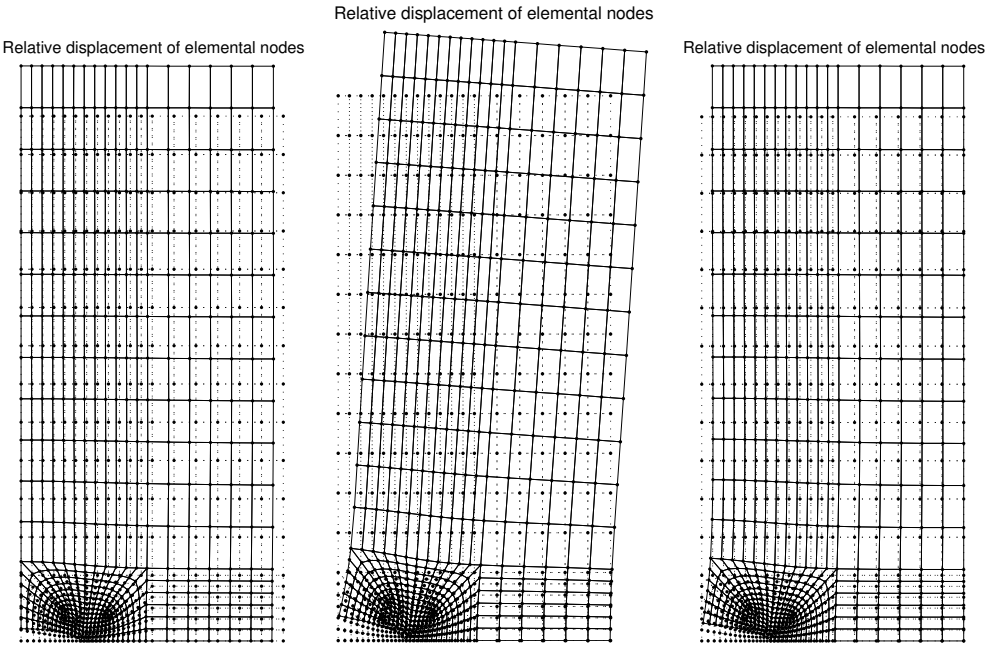

(a) (b) (c)

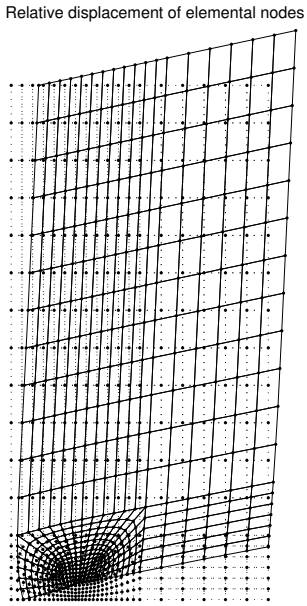

(d)

Figure 9.5: Displacement of cracked panels ($\times$ 0.1): (a) Center cracked panel (CCP) (b) Single edge cracked panel (SECP) (c) Double edge cracked panel (DECP) (d) Center cracked panel (CCP) with uniform shear

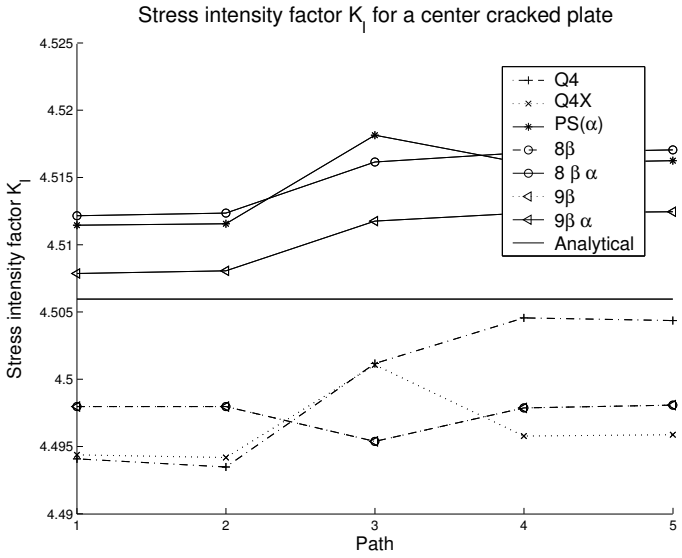

(a)

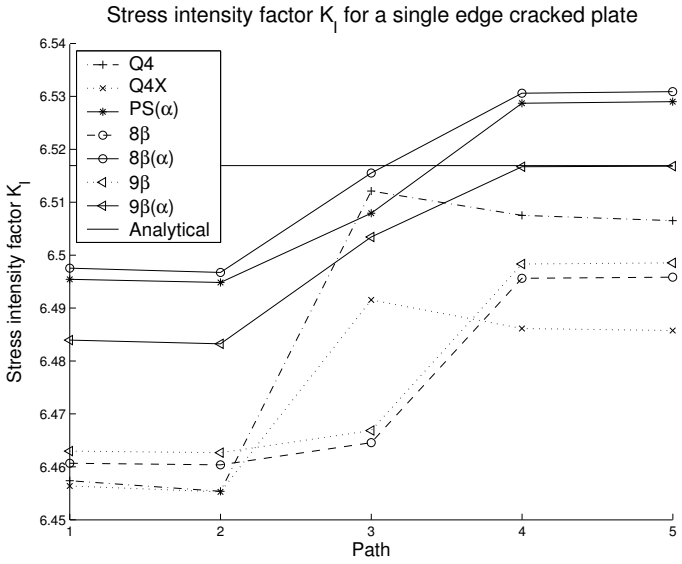

(b)

Figure 9.6: Summary of results for cracked isotropic panels with different elements: (a) CCP subjected to uniform tension (b) SECP subjected to uniform tension

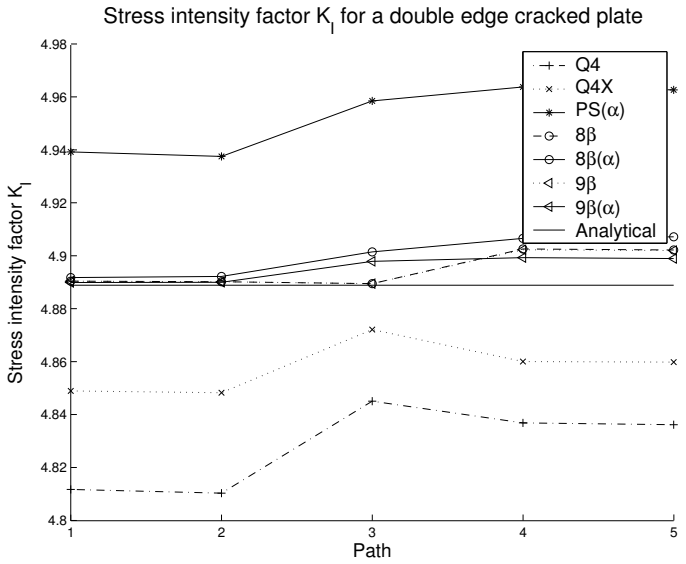

(a)

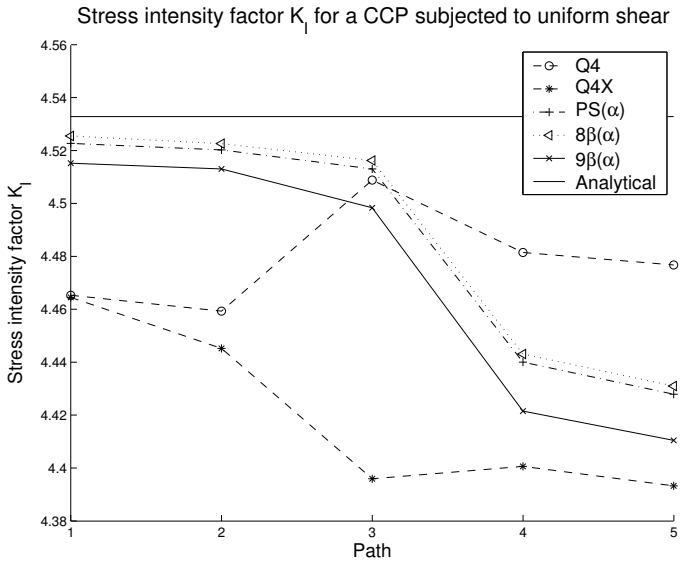

(b)

Figure 9.7: Summary of results for cracked isotropic panels with different elements: (a) DECP subjected to uniform tension (b) CCP subjected to uniform shear

Path	Q4	Q4X	PS	PS(α)	8β	8β(α)	9β	9β(α)
Path 1	4.812	4.849	4.817	4.940	4.891	4.892	4.891	4.890
Path 2	4.810	4.848	4.817	4.938	4.890	4.892	4.890	4.890
Path 3	4.845	4.872	4.825	4.959	4.890	4.902	4.890	4.898
Path 4	4.837	4.860	4.828	4.964	4.903	4.907	4.903	4.900
Path 5	4.836	4.860	4.827	4.963	4.902	4.907	4.902	4.899
Exact				4.889				

Table 9.11: K_1 results for the isotropic DECP subjected to uniform tension (Mesh 3)

Path	Q4	Q4X	PS	PS(α)	8β	8β(α)	9β	9β(α)
Path 1	4.465	4.465	4.486	4.523	4.489	4.526	4.486	4.515
Path 2	4.459	4.445	4.484	4.520	4.484	4.523	4.484	4.513
Path 3	4.509	4.396	4.479	4.513	4.428	4.516	4.426	4.499
Path 4	4.482	4.401	4.412	4.440	4.415	4.443	4.414	4.422
Path 5	4.477	4.393	4.400	4.428	4.404	4.431	4.403	4.411
Exact				4.533				

Table 9.12: K_1 results for the isotropic CCP subjected to uniform shear (Mesh 2)

Chapter 10

On the stability of drilling elements

The stability of elements with drilling degrees of freedom in fracture mechanics is largely influenced by two factors: The integration scheme used (i.e. reduced or full integration) and the value of the penalty parameter γ.

10.1 Effect of reduced integration

Reduced integration is frequently used in evaluating the element stiffness matrix of quadratically interpolated displacement based finite elements. Using reduced integration 'softens' the element, thereby increasing elemental accuracy. (Softening comes about because certain higher-order polynomial terms happen to vanish at Gauss points of a low-order rule. Simply stated, with fewer sampling points, some of the more complicated displacement modes offer less resistance to deformation [41].)

Reduced integration should be used with caution due to the fact that it can result in the introduction of spurious zero energy modes on the element level.

For Q4X, the matrix $\boldsymbol{K}^e = \boldsymbol{G}^{eT}\boldsymbol{H}^{e-1}\boldsymbol{G}^e$ can be integrated using either full or reduced integration. Integrating the $\boldsymbol{K}^e$ matrix with a 3×3 Gaussian quadrature prevents any spurious modes (full integration). Alternatively, $\boldsymbol{K}^e$ may be integrated by the reduced 5-point rule proposed by Dovey [42]. (A 2×2 Gaussian quadrature is not suitable, since a communicable mechanism is introduced [43].) The reduced 5-point rule is outlined below. This scheme also prevents spurious modes in linear elastostatics for the Q4X element [43].

It is noted that reduced integration in mixed/hybrid finite elements is in general not considered advantageous.

10.1.1 5-Point integration rule

The 5-point integration rule is depicted in Figure 10.1. Due to the symmetry of the integration scheme, the weights W_α are identical. The rule is indicated by:

$$I^* = W_0 F(0,0) + W_\alpha F(\pm\alpha, \pm\alpha) \tag{10.1}$$

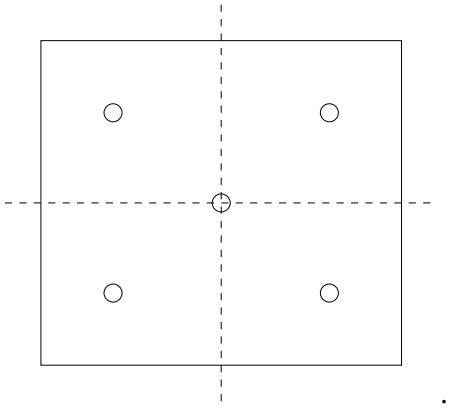

Figure 10.1: 5-Point integration scheme

$$W_\alpha = 1 - \frac{W_0}{4} \tag{10.2}$$

$$\alpha = (\frac{1}{3W_\alpha})^{0.5} \tag{10.3}$$

The scheme only has physical meaning while $0 < W_0 < 4$, but is often restricted to $0 < W_0 < 8/3$. The 5-point scheme converges to the 2×2 Gaussian scheme as $W_0 \to 0$.

10.1.2 Influence of center point weight W_0

To investigate the effect of reduced integration on elements with drilling degrees of freedom in fracture mechanics, the 5-point integration scheme is now applied with different values for the center point weight W_0. In performing this study, $\gamma = G$ is used throughout. We study the nodal values of rotation; results are depicted in Figs 10.2(a) through 10.2(c).

Figs 10.2(a) and 10.2(b) illustrate that a checkerboard-like pattern is introduced when W_0 is small (e.g. $W_0 \leq 0.1 \times 8/3$). By increasing the weight W_0 of the center point, the checkerboard-like effect is reduced. A sensible value for the center point weight W_0 is in the vicinity of $8/3$ (Fig 10.2(c)). In fact, when using a center point weight of $W_0 = 8/3$, the results compare closely with the results for full integration (Fig 10.2(d)). This suggests that full integration is preferable, since reduced computational effort should probably not be the sole motivation for selecting reduced integration [15].

10.2 Different values for γ

Next, we study the effect of the penalty parameter γ on the rotations in the vicinity of the crack tip. A 9-point full integration scheme is now used to integrate $\boldsymbol{K}^e$.

Recall that the formulation of the element with drilling degrees of freedom depends on the parameter γ as follows:

$$[\boldsymbol{K}^e + \boldsymbol{P}^e_\gamma]\boldsymbol{q} = \boldsymbol{r} \tag{10.4}$$

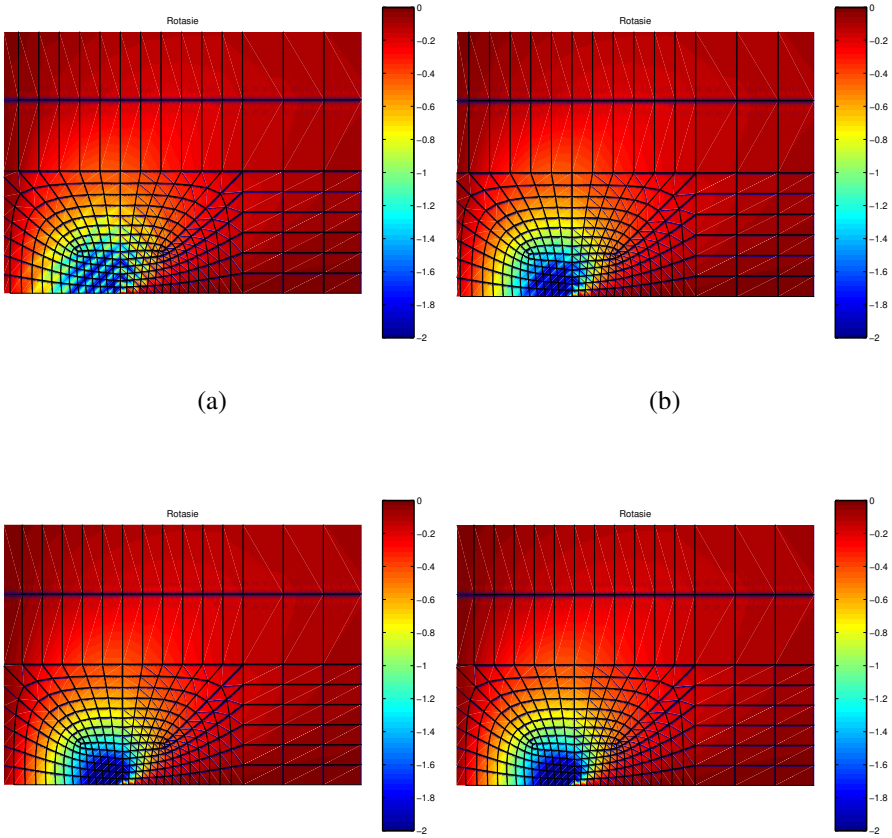

(a) (b)

(c) (d)

Figure 10.2: Nodal rotation for a center cracked panel using different integration schemes: (a) 5 point integration, $W_0 = 0.01 \times 8/3$ (b) 5 point integration, $W_0 = 0.1 \times 8/3$ (c) 5 point integration, $W_0 = 8/3$ (d) 9 point integration, (all with $\gamma = G$)

with

$$\boldsymbol{P}^e = \gamma \int_{\Omega_e} \begin{pmatrix} \boldsymbol{b}^e \\ \boldsymbol{g}^e \end{pmatrix} [\boldsymbol{b}^e \; \boldsymbol{g}^e] d\Omega. \tag{10.5}$$

The parameter γ is problem dependent, since it is a part of a penalty term. For linear elastic isotopic problems, the formulation is relatively insensitive to the value of γ [21, 22, 43] and the patch test is passed for any $\gamma > 0$. However, in linear elastic fracture mechanics, the material in the vicinity of the crack tip contains a stress singularity, and different values for γ may apply.

In addition, a further important argument applies when evaluating suitable values of γ. Recall that the variational expression (4.11) contains the skew part of the stress tensor, skew τ. This is interpolated in the discrete problem as τ_0, which is selected constant over an element. Clearly, it is required that $\tau_0 \approx 0$. To assess this aspect, the dependency of τ_0 on γ is depicted in Fig 10.3 for the center cracked panel.

Fig 10.3 suggests that $\gamma < G$, or even $\gamma < G/10$ is desirable to ensure $\tau_0 \approx 0$. This is confirmed

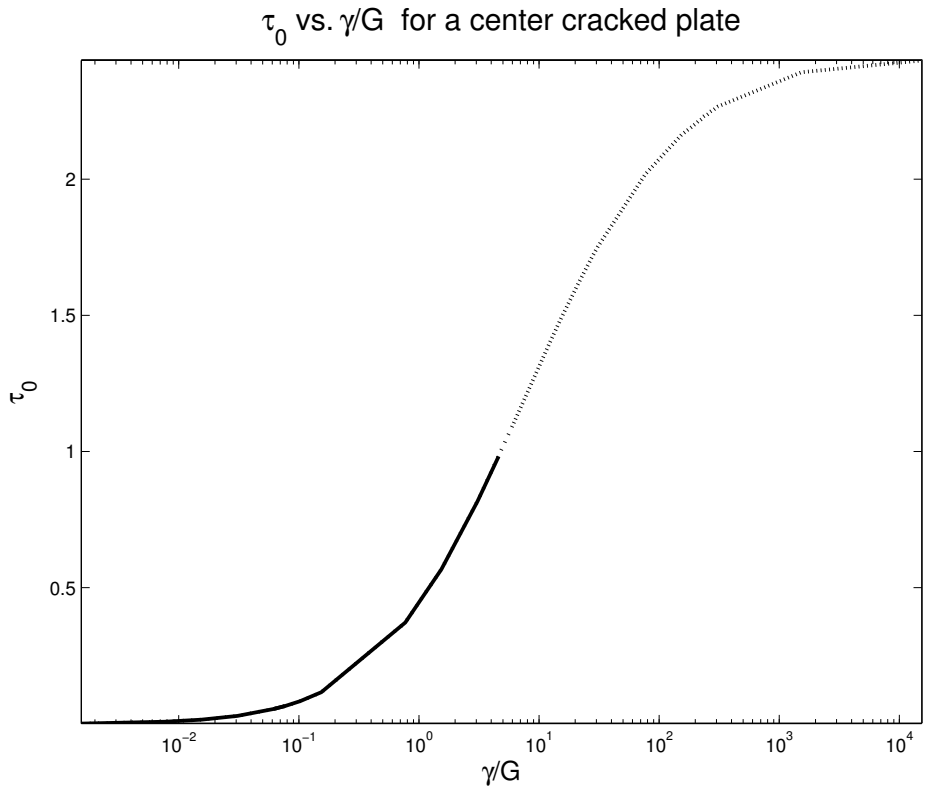

Figure 10.3: τ_0 vs. γ for a center cracked panel with full integration, for γ = 6.5 $\times$ 10^{-4} through γ = 6.5 $\times$ 10^{3}. The solid line indicates the optimal range for γ

by Fig 10.4. However, this figure illustrates that γ has a marked influence on the shape and size of the rotations in the 'plastic zone'. While approximate relationships exist which relate the size of the plastic zone to a material specific stress intensity value, it is not clear what the true value of rotations in the plastic zone are. It is recommended that this is addressed in a future study.

To assess the effect of γ on τ_0 for a different geometry, we now also study a single edge cracked plate. Results are depicted in Fig 10.5, which illustrates that the trend is similar to that of the center cracked plate, although the maximum value of τ_0 for the single edge cracked plate is notably higher than τ_0 for the center cracked plate.

Finally, Fig 10.6 illustrates that the predicted accuracy of K_1 decreases as γ/G is increased, viz. as τ_0 increases. Based on the foregoing, it is recommended that γ is selected from the range $\gamma = G/100$ through $\gamma = G/10$.

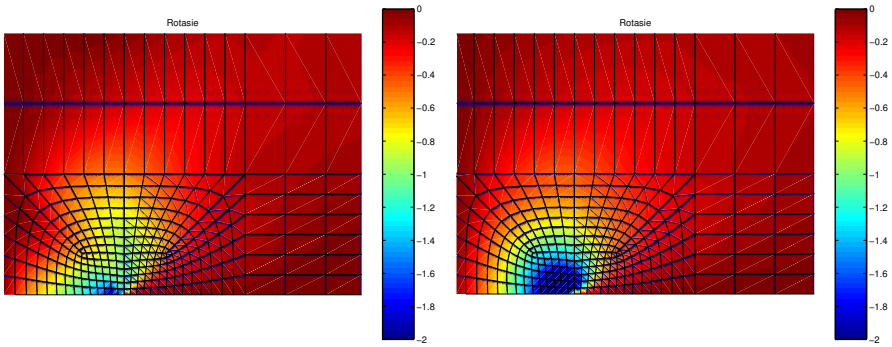

(a)

(b)

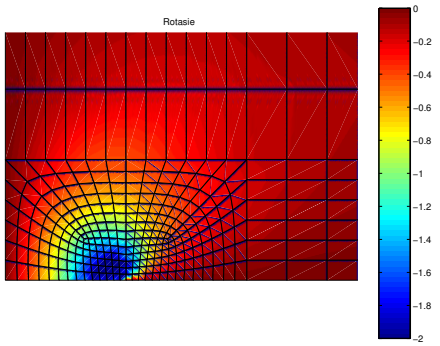

(c)

Figure 10.4: Nodal rotations for a center cracked panel: (a) $\gamma = G/1000$ (b) $\gamma = G$ (c) $\gamma = G \times 1000$ (9-point integration scheme)

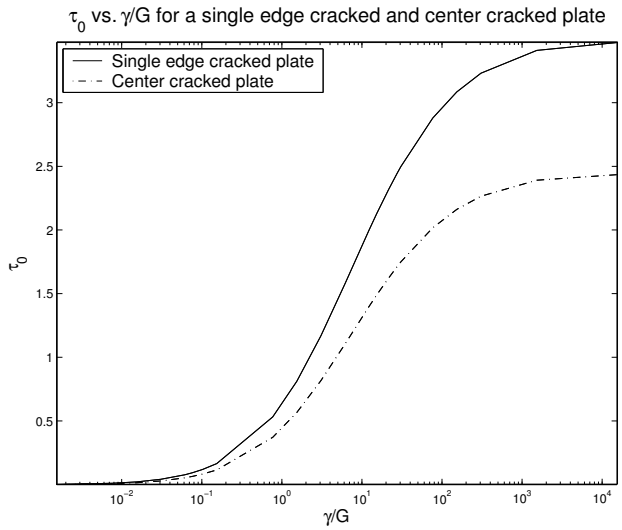

Figure 10.5: τ_0 vs. γ for a center cracked panel and a single edge cracked panel with full integration

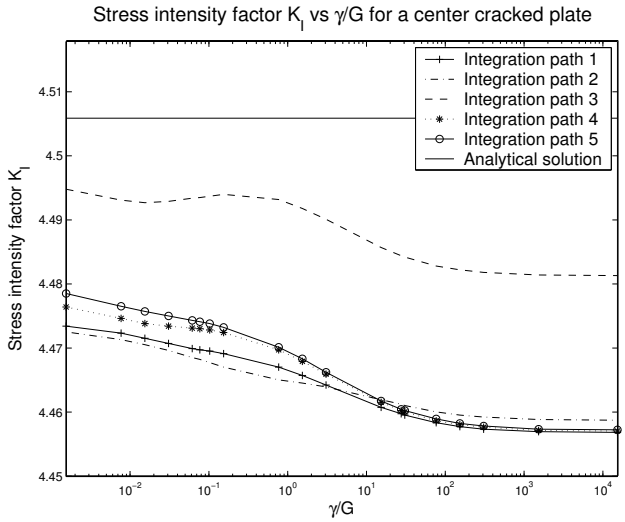

(a)

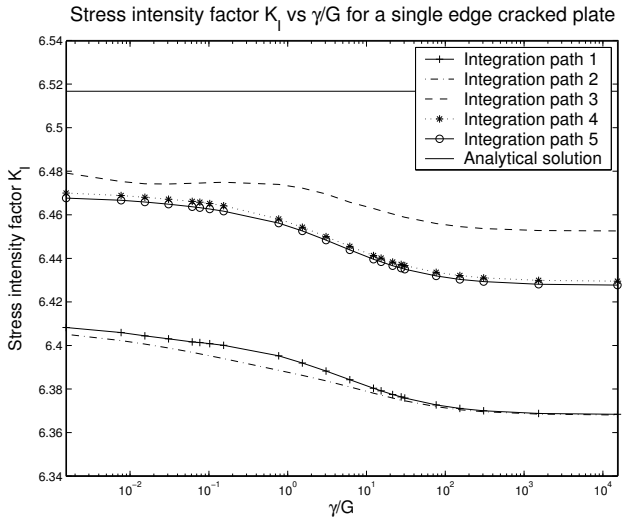

(b)

Figure 10.6: Stress intensity factor K_I vs. γ for the 5 different integration paths: (a) Center cracked panel (b) Single edge cracked panel

Chapter 11

Fracture mechanics: Orthotropic materials

In this chapter, fracture mechanics in orthotropic plates, stress and displacement distributions around the crack tip in an anisotropic material are considered.

11.1 Introduction

With the growth in applications of composite materials, a problem of continuing interest is the calculation of the stress intensity factor in cracked orthotropic plates modeling fiber reinforced composites. The fracture of composite materials is an important and complex engineering problem. Significant defects can be built into a composite laminate during manufacturing of a new component. The material used can also be relatively fragile and large cracks can result from minor service mishaps. High performance composites often consist of high strength fibers in a weak matrix. Hence, crack formation and growth is constrained by the fiber direction, resulting in mixed mode crack deformation growth.

Several numerical methods for determining stress intensity factors in cracked anisotropic plates have been developed by extending the methods originally developed for isotropic materials. The J integral can be used to develop a failure analysis approach which is applicable to both single and mixed mode crack problems in orthotropic materials. In a mixed mode, however, a simple application of the J integral does not provide sufficient information for a separate determination of mixed mode stress intensity factors. Various other methods are used to determine stress intensity factors for anisotropic materials: the J_k integral, the hybrid mongrel formulation, contour integrals based on Betti's reciprocal work theorem, etc.

11.2 Anisotropic stress and displacement field near a crack tip

The stress and displacement expressions in the neighborhood of the crack tip in homogeneous anisotropic media under a plane stress condition with zero body forces are given by Saxce and Kang [44] as:

$$\sigma_x = \frac{\beta_I}{\sqrt{r}}\text{Re}\left[\frac{s_1 s_2}{s_1 - s_2}\left(\frac{s_2}{z_2} - \frac{s_1}{z_1}\right)\right] + \frac{\beta_{II}}{\sqrt{r}}\text{Re}\left[\frac{1}{s_1 - s_2}\left(\frac{s_2^2}{z_2} - \frac{s_1^2}{z_1}\right)\right], \tag{11.1}$$

$$\sigma_y = \frac{\beta_I}{\sqrt{r}}\text{Re}\left[\frac{1}{s_1 - s_2}\left(\frac{s_2}{z_2} - \frac{s_1}{z_1}\right)\right] + \frac{\beta_{II}}{\sqrt{r}}\text{Re}\left[\frac{1}{s_1 - s_2}\left(\frac{1}{z_2} - \frac{1}{z_1}\right)\right], \tag{11.2}$$

$$\tau_{xy} = \frac{\beta_I}{\sqrt{r}}\text{Re}\left[\frac{s_1 s_2}{s_1 - s_2}\left(\frac{1}{z_1} - \frac{1}{z_2}\right)\right] + \frac{\beta_{II}}{\sqrt{r}}\text{Re}\left[\frac{1}{s_1 - s_2}\left(\frac{s_2}{z_2} - \frac{s_1}{z_1}\right)\right], \tag{11.3}$$

and

$$u = \beta_I\sqrt{r}\text{Re}\left[\frac{1}{s_1 - s_2}(s_1 p_2 z_2 - s_2 p_1 z_a)\right] + \beta_{II}\sqrt{r}\text{Re}\left[\frac{1}{s_1 - s_2}(p_2 z_2 - p_1 z_a)\right], \tag{11.4}$$

$$v = \beta_I\sqrt{r}\text{Re}\left[\frac{1}{s_1 - s_2}(s_1 q_2 z_2 - s_2 q_1 z_a)\right] + \beta_{II}\sqrt{r}\text{Re}\left[\frac{1}{s_1 - s_2}(q_2 z_2 - q_1 z_a)\right], \tag{11.5}$$

with

$$\begin{array}{ll} z_1 = \sqrt{\cos\theta + s_1 \sin\theta} & z_2 = \sqrt{\cos\theta + s_2 \sin\theta} \\ p_1 = a_{11}s_1^2 + a_{12} - a_{16}s_1 & p_2 = a_{11}s_2^2 + a_{12} - a_{16}s_2 \\ q_1 = a_{11}s_1 + \frac{a_{22}}{s_1} - a_{26} & q_2 = a_{11}s_1 2 + \frac{a_{22}}{s_2} - a_{26} \end{array}$$

where Re denotes the real part of the complex function between brackets. s_1, s_2 and their conjugates are roots of the fourth order characteristic equation

$$a_{11}s^4 + 2a_{16}s^3 + (2a_{12} + a_{66})s^2 - 2a_{26}s + a_{22} = 0, \tag{11.6}$$

where the a_{ij} are the elastic compliance coefficients, which can be written in terms of Young's moduli E_{ij}, Poisson's ratios ν_{ij} and shear moduli G_{ij}. For an orthotropic material, a_{ij} are given as

$$\begin{array}{lll} a_{11} = \dfrac{1}{E_{11}} & a_{12} = -\dfrac{\nu_{21}}{E_{22}} = -\dfrac{\nu_{12}}{E_{11}} & a_{13} = \dfrac{\nu_{31}}{E_{33}} = -\dfrac{\nu_{13}}{E} \\ a_{22} = \dfrac{1}{E_{22}} & a_{12} = -\dfrac{\nu_{32}}{E_{33}} = -\dfrac{\nu_{23}}{E_{22}} & a_{33} = \dfrac{1}{E_{33}} \\ a_{44} = \dfrac{1}{G_{23}} & a_{55} = \dfrac{1}{G_{13}} & a_{66} = \dfrac{1}{G_{12}} \end{array} \tag{11.7}$$

and $a_{16} = a_{26} = a_{36} = 0$.

Chapter 12

Fracture mechanics: Orthotropic results

In this chapter, numerical results for orthotropic fracture mechanics problems are presented. Again the problems are evaluated using the J and I^* integrals with different displacement based and assumed stress elements. Results are compared to known solutions where possible. The effect of fiber orientation and the degree of anisotropy on the stress intensity factors are also described.

12.1 Overview

To allow comparison with results presented in literature, the problems considered are mode I crack problems. For an orthotropic material crack problem to be a mode I problem, one of the principal axes of the material must be parallel to the crack axis. Therefore, only $0°$, $90°$ or symmetric angle ply laminates can be considered. The fiber orientation in orthotropic material is defined as the angle between the crack axis and the fiber in a counterclockwise direction, see Fig 12.1.

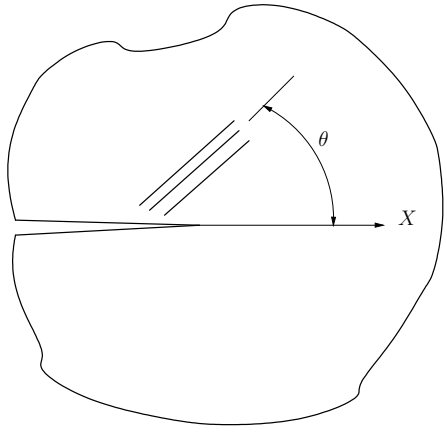

Figure 12.1: Definition of the fiber orientation in an orthotropic material

Three test problems are investigated, namely

- a center cracked panel (CCP) with $0°$ ply arrangement, uniformly loaded in tension (the

reference solution is taken from [40]),

- a single edge cracked panel (SECP) with 0° ply arrangement, uniformly loaded in tension (the reference solution is taken from [40]), and
- a double edge cracked panel (DECP) with symmetric angle ply arrangements, uniformly loaded in tension (the reference solution is taken from [3] and [45]).

The in-plane lines of material symmetry for the first two problems coincide with the x-y axis. The material constants are set to be $E_1 = 1$, $E_2 = 10$, $\beta_1 = 1$ and $\beta_2^2 = 0.1$, where $\beta_1\beta_2 = (E_1/E_2)^{\frac{1}{2}}$ and $\beta_1 + \beta_2 = \sqrt{2}[(E_1/E_2)^{\frac{1}{2}} + E_1/2G_{12} - v_{12}]^{\frac{1}{2}}$ [40]. The units of loading are consistent with that of E.

12.2 Convergence study

To study the influence of mesh refinement on the prediction of the stress intensity factor in orthotropic materials, a convergence study is firstly done. For the convergence study the center cracked panel with 0° ply arrangement is considered. Three different meshes (the same meshes as for the isotropic problems) are used with the same 5 integration contours (see Fig 9.2(a) and Fig 9.2(b)).

For the convergence study we only consider the following elements (for the sake of convenience, the elemental descriptions are again given):

- J integral: Q4 (A displacement based quadrilateral element)
- J integral: Q4X (A displacement based quadrilateral element with drilling degrees of freedom)
- I^* integral: PS(α) (A penalized version of the assumed stress quadrilateral element proposed by Pian and Sumihara [5])
- I^* integral: $8\beta(\alpha)$ (A penalized version of the assumed stress quadrilateral element with drilling degrees of freedom and 8 β parameters)
- I^* integral: $9\beta(\alpha)$ (A penalized version of the assumed stress quadrilateral element with drilling degrees of freedom and 9 β parameters)

The assumed stress elements without penalized equilibrium (PS, 8β and 9β) are not considered, since they do not predict an upper bound for the stress intensity factor for reasonably fine meshes. (The results obtained with these elements are of course still path-independent and the calculated stress intensity factor converges with mesh refinement.)

For the meshes considered, the stress intensity factor calculated using the Q4 element violates the bound theorem, (see Fig 12.2(a)), and the results reveal a notable path dependency. This is due to the material orthotropy, which requires a very fine mesh for the Q4 elements [40].

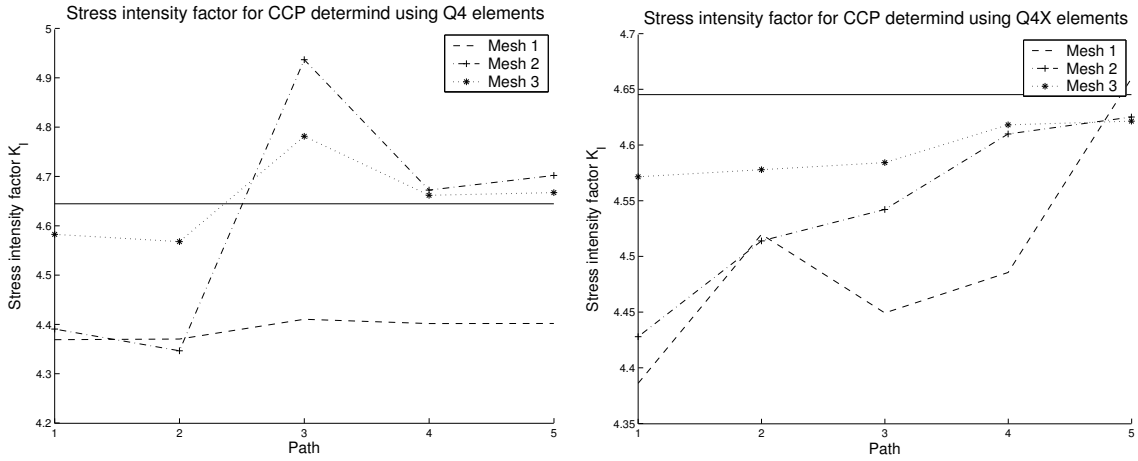

(a) (b)

Figure 12.2: Convergence study of K_I for the orthotropic CCP with different displacement based elements: (a) Q4 (b) Q4X

With Q4X elements, the J integral is path-independent and satisfies the bound theorem (see Fig 12.2(b)). As expected, the stress intensity factors calculated with the J integral and Q4X form a lower bound to the true value of the stress intensity factor, but the calculated stress intensity factor does converge to the analytical value with mesh refinement.

When evaluating the J integral for orthotropic materials, the Q4X element seems superior to the Q4 element.

We now turn the attention to the assumed stress based elements: For PS(α), 8$\beta(\alpha)$ and 9$\beta(\alpha)$, a convergence study is presented in Figs 12.3(a), 12.3(b) and 12.3(c). The results confirm the path independence of the elements, while an upper bound to the stress intensity factor is predicted, as may be expected. Again, the calculated stress intensity factors do converge to the analytical solutions with mesh refinement. Clearly, the results obtained with mesh 3 are superior to the

Path	Mesh 1	Mesh 2	Mesh 3
Path 1	4.370	4.392	4.584
Path 2	4.371	4.347	4.569
Path 3	4.411	4.939	4.783
Path 4	4.403	4.674	4.663
Path 5	4.403	4.704	4.669
Reference		4.646	

Table 12.1: Convergence of K_1 for an orthotropic CCP subjected to uniform tension with Q4 elements

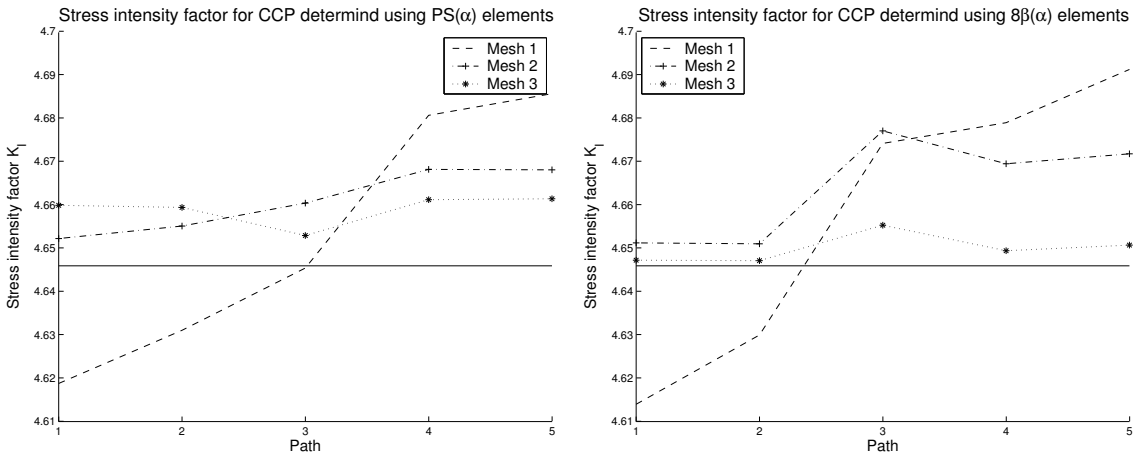

(a) (b)

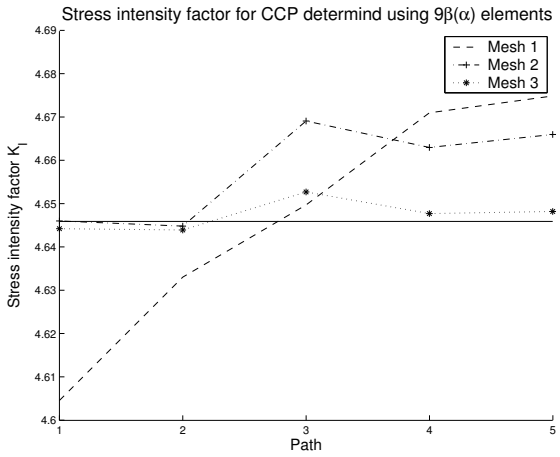

(c)

Figure 12.3: Convergence study of K_I for the orthotropic CCP with different assumed stress elements: (a) PS(α) (b) $8\beta(\alpha)$ (c) $9\beta(\alpha)$

results obtained using mesh 1 or mesh 2.

12.3 Selected results demonstrating path independence

General results for the problems of interest are now presented. Throughout, mesh 3 is used.

1. Center cracked panel with a 0° ply arrangement

   The results obtained for the CCP are listed in Table 12.6. The reference solution is K_1 =

Path	Mesh 1	Mesh 2	Mesh 3
Path 1	4.386	4.428	4.572
Path 2	4.520	4.514	4.579
Path 3	4.450	4.543	4.585
Path 4	4.486	4.611	4.619
Path 5	4.661	4.626	4.622
Reference		4.646	

Table 12.2: Convergence of K_1 for an orthotropic CCP subjected to uniform tension with Q4X elements

Path	Mesh 1	Mesh 2	Mesh 3
Path 1	4.619	4.652	4.660
Path 2	4.631	4.655	4.660
Path 3	4.646	4.661	4.653
Path 4	4.681	4.668	4.661
Path 5	4.686	4.668	4.662
Reference		4.646	

Table 12.3: Convergence of K_1 for an orthotropic CCP subjected to uniform tension with PS(α) elements

4.646. The results demonstrate adherence to the bound theorems: The stress intensity factor determined with the I^* integral using penalized equilibrium elements forms an upper bound to the K_I factor, while the stress intensity factor determined with the J integral and Q4X elements forms a lower bound to K_I.

2. Single edge crack panel with 0° ply arrangement

   Results are given in Table 12.7 for the SECP. Unfortunately, no theoretical reference solution could be found for this problem, but the results compare well with those obtained by Xiao *et al* [40].

12.4 The effect of fiber orientation on the stress intensity factor

The effect of fiber orientation on a double edge cracked panel with a symmetric ply arrangement is now studied. Symmetric fiber orientations of $\pm 0^\circ$, $\pm 10^\circ$, $\pm 20^\circ$ ... $\pm 90^\circ$ are considered.

The calculated stress intensity factors for this problem are listed in Tables 12.8, 12.9 and 12.10. The results are compared with the results obtained by [45] and [3] where possible.

For the double edge cracked plate problem, the material constants used are:

Path	Mesh 1	Mesh 2	Mesh 3
Path 1	4.614	4.651	4.647
Path 2	4.630	4.651	4.647
Path 3	4.674	4.677	4.655
Path 4	4.679	4.670	4.650
Path 5	4.691	4.672	4.651
Reference		4.646	

Table 12.4: Convergence of K_1 for an orthotropic CCP subjected to uniform tension with $8\beta(\alpha)$ elements

Path	Mesh 1	Mesh 2	Mesh 3
Path 1	4.605	4.646	4.644
Path 2	4.633	4.645	4.644
Path 3	4.650	4.669	4.653
Path 4	4.671	4.663	4.648
Path 5	4.675	4.666	4.648
Reference		4.646	

Table 12.5: Convergence of K_1 for an orthotropic CCP subjected to uniform tension with $9\beta(\alpha)$ elements

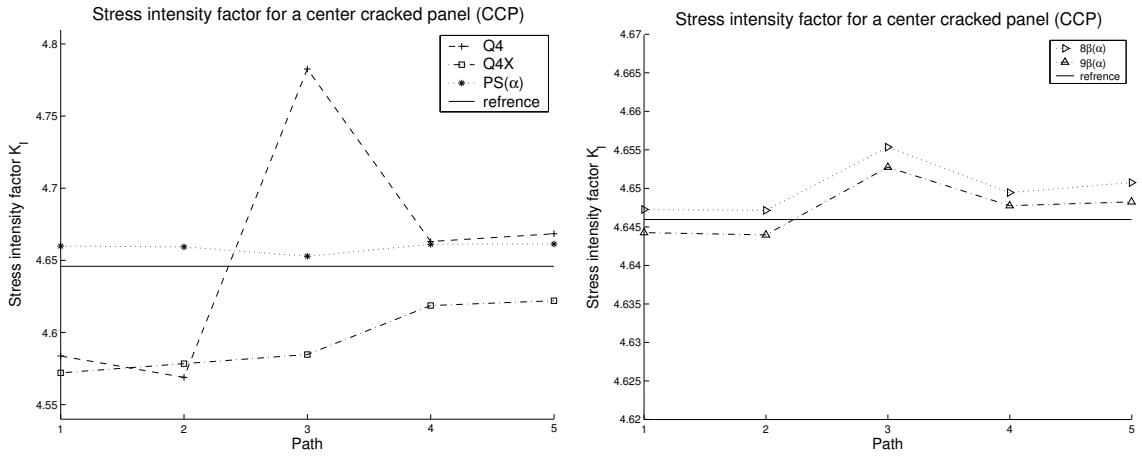

(a) (b)

Figure 12.4: Summary of results for an orthotropic center cracked panel with $\theta = 0^\circ$ fiber angle: (a) Q4, Q4X and PS(α) elements (b) $8\beta(\alpha)$ and $9\beta(\alpha)$ elements

Element	Path 1	Path 2	Path 3	Path 4	Path 5
Q4	4.584	4.569	4.783	4.663	4.669
Q4X	4.572	4.579	4.585	4.619	4.622
PS	4.650	4.650	4.645	4.652	4.652
PS(α)	4.660	4.660	4.653	4.661	4.662
8β	4.634	4.633	4.583	4.631	4.632
8$\beta(\alpha)$	4.647	4.647	4.655	4.650	4.651
9β	4.633	4.633	4.583	4.633	4.633
9$\beta(\alpha)$	4.644	4.644	4.653	4.648	4.648
Reference			4.646		

Table 12.6: K_1 results for the orthotropic CCP with 0° laminate under uniform tension (mesh 3)

Element	Path 1	Path 2	Path 3	Path 4	Path 5
Q4	6.351	6.351	6.382	6.385	6.383
Q4X	6.350	6.348	6.371	6.371	6.372
PS	6.3641	6.363	6.374	6.383	6.382
PS(α)	6.393	6.398	6.422	6.415	6.415
8β	6.325	6.352	6.363	6.378	6.378
8$\beta(\alpha)$	6.393	6.393	6.405	6.425	6.429
9β	6.352	6.352	6.363	6.376	6.376

Table 12.7: K_1 results for the orthotropic SECP with 0° laminate under uniform tension (mesh 3)

- E_1 = 144.798 GPa,
- E_2 = 11.722 GPa,
- G_{12} = 9.6532 GPa, and
- ν = 0.21.

The double edge cracked plate dimensions used are:

- Crack length: $a = 3.5$,
- Width: $2b = 14$,
- Height: $2c = 14$,

The units of loading are consistent with that of E.

For the double edge cracked panel, the results are summarized in Figs 12.6(a) and 12.6(b). The results reveal a slight (unimportant) path dependence.

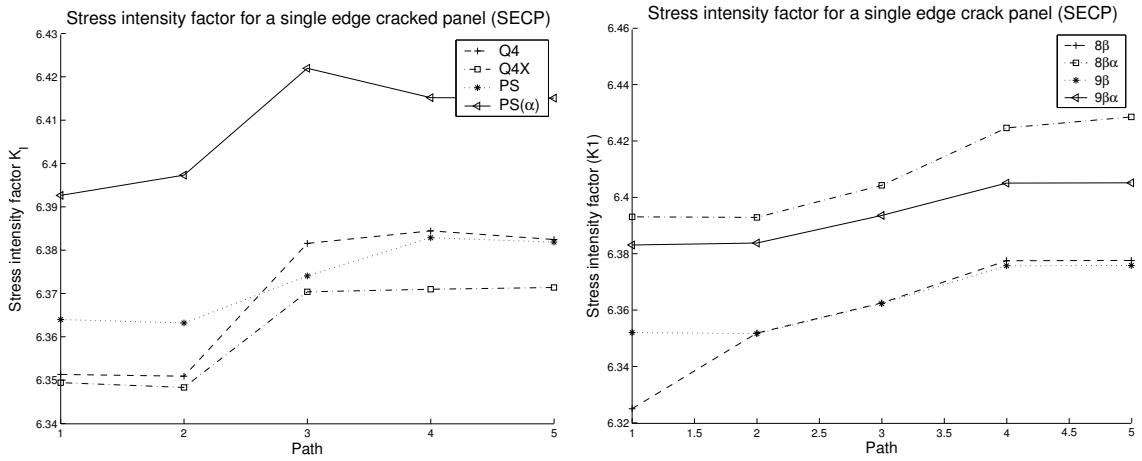

(a) (b)

Figure 12.5: Summary of results for an orthotropic single edge cracked panel with $\theta = 0^\circ$ fiber angle: (a) SECP with $\theta = 0^\circ$ Q4, Q4X, PS and PS(α) elements (b) SECP with $\theta = 0^\circ$ 8β, $8\beta(\alpha)$, 9β and $9\beta(\alpha)$ elements

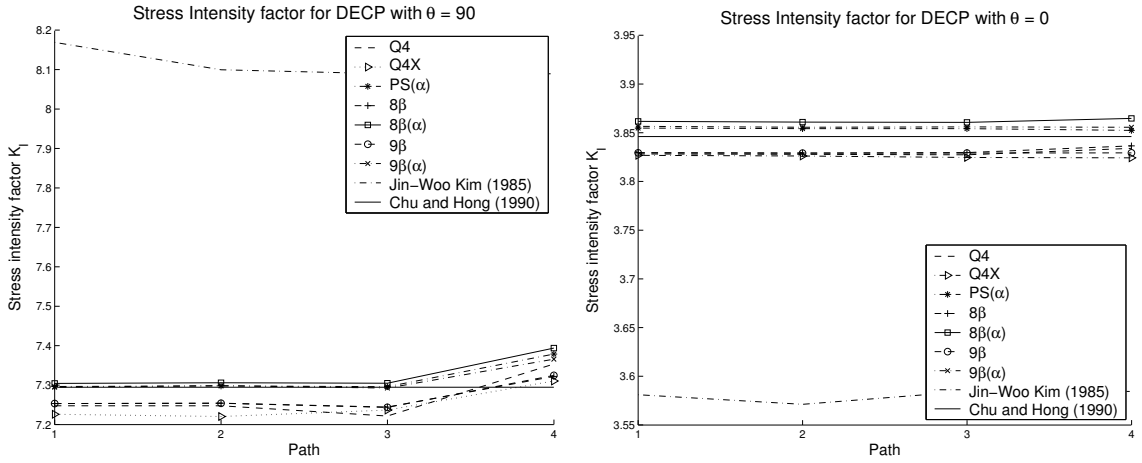

(a) (b)

Figure 12.6: Summary of results for an orthotropic double edge cracked panel: (a) fiber angle $\theta = 90^\circ$ (b) fiber angle $\theta = 0^\circ$

The results obtained for the DECP with symmetric angle ply lamina (see Table 12.10 and Fig 12.10), compare very well with the results obtained by Chu and Hong [45]. Comparing the results obtained by Chu and Hong with the results obtained by Kim [3], it is noted that large discrepancies exist between these results, which peak around angles of $\pm 60^\circ_s$. According to Chu and Hong [45]

Element	Path 1	Path 2	Path 3	Path 4
Q4	7.248	7.248	7.222	7.354
Q4X	7.226	7.221	7.237	7.311
PS(α)	7.297	7.298	7.297	7.379
8β	7.254	7.255	7.245	7.323
8$\beta(\alpha)$	7.305	7.306	7.305	7.394
9β	7.254	7.254	7.244	7.325
9$\beta(\alpha)$	7.295	7.299	7.293	7.366
Reference [3]	8.171	8.101	8.091	—
Reference [45]	7.295	7.295	7.295	7.295

Table 12.8: K_1 results for the orthotropic DECP with a 90° laminate under uniform tension (mesh 3)

Element	Path 1	Path 2	Path 3	Path 4
Q4	3.829	3.828	3.828	3.834
Q4X	3.827	3.827	3.825	3.825
PS(α)	3.855	3.855	3.855	3.853
8β	3.830	3.830	3.830	3.837
8$\beta(\alpha)$	3.862	3.861	3.861	3.865
9β	3.830	3.830	3.830	3.830
9$\beta(\alpha)$	3.857	3.856	3.856	3.856
Reference [3]	3.581	3.571	3.585	—
Reference [45]	3.847	3.847	3.847	3.847

Table 12.9: K_1 results for the orthotropic DECP with a 0° laminate under uniform tension (mesh 3)

it seems that these discrepancies are due to Kim's [3] miscalculation of compliance coefficients. (The compliance coefficients for a laminate must be determined by inversion of the equivalent modulus for a laminate, which is the average of the modulus of the constituent plies, and must not be determined by averaging the compliance coefficients of the constituent plies.)

The agreement with the results presented by Chu and Hong seems to indicate that the current implementation is correct.

12.5 The effect of the degree of anisotropy on K

To consider the effect of the degree of anisotropy on the stress intensity factor, a center cracked plate under uniform tensile stress is now considered. This problem was also considered by Su and Sun [46]. The ratio $\frac{E_1}{E_2}$ is varied to determine the influence of the degree of anisotropy on the stress

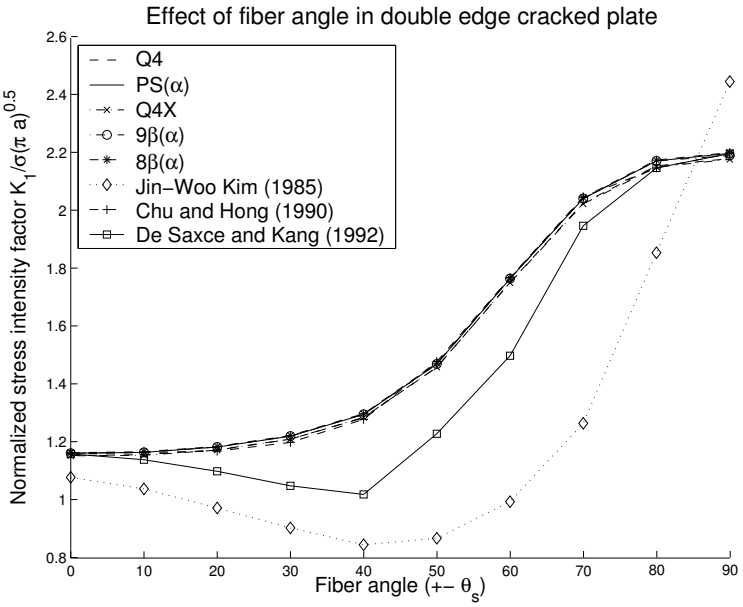

(a)

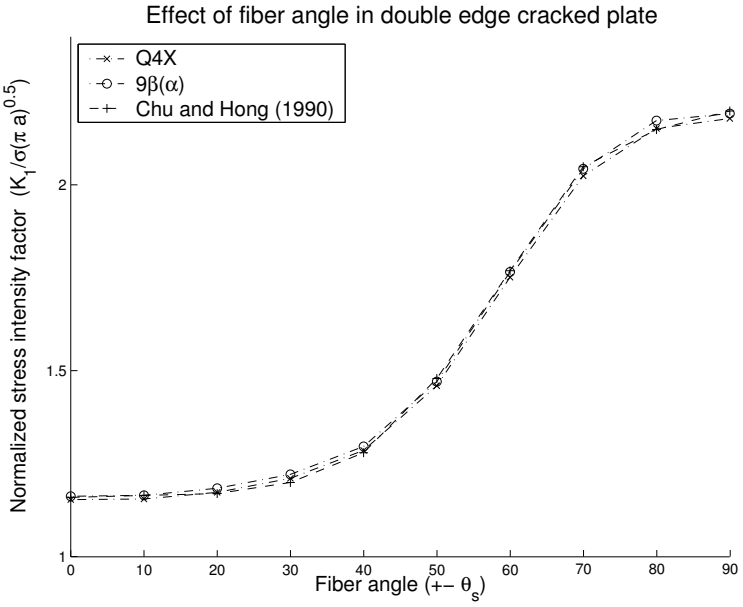

(b)

Figure 12.7: Results for the effect of fiber orientation on a double edge crack plate, $\theta = \pm 0^\circ_s$ through $\theta = \pm 90^\circ_s$ (a) Solution for all elements (b) Solution for Q4X and $9\beta\alpha$ only

intensity factor.

Fiber orientation	Q4	Q4X	PS(α)	8β(α)	9β(α)
$\pm 0^\circ_s$	1.1546	1.1538	1.1624	1.1645	1.1628
$\pm 10^\circ_s$	1.1576	1.1555	1.1656	1.1677	1.1654
$\pm 20^\circ_s$	1.1746	1.1734	1.1838	1.1860	1.1843
$\pm 30^\circ_s$	1.2111	1.2111	1.2215	1.2239	1.2218
$\pm 40^\circ_s$	1.2855	1.2864	1.2969	1.2993	1.2971
$\pm 50^\circ_s$	1.4601	1.4604	1.4716	1.4740	1.4715
$\pm 60^\circ_s$	1.7540	1.7525	1.7667	1.7693	1.7669
$\pm 70^\circ_s$	2.0291	2.0256	2.0443	2.0471	2.0444
$\pm 80^\circ_s$	2.1574	2.1531	2.1744	2.1772	2.1743
$\pm 90^\circ_s$	2.1824	2.1797	2.2006	2.2031	2.1930

Table 12.10: K_1 results for the isotropic CCP under uniform tension (mesh 3)

The height to width ratio h/w and the crack length to width ratio a/w are varied to estimate the effect of geometry on the stress intensity factor. Height to width ratios of $h/w = 1.0$, 1.5, and 2.0 are considered.

The material properties used are:

- Young's modulus E_1 = 30.0, and
- Poisson's ratio ν_{12} = 0.3.

The values of E_2 and G_{12} are obtained from

$$\frac{E_1}{E_2} = \sqrt{2}\left(\sqrt{\frac{E_1}{E_2}} + \frac{E_1}{2G_{12}} - \nu_{12}\right)^{\frac{1}{2}}. \tag{12.1}$$

The material properties are summarized in Table 12.11.

In the tabulated results that follow, the reported stress intensity factor values are average normalized values, calculated as

$$\frac{(K_{I,path1} + K_{I,path2} + K_{I,path3} + K_{I,path4} + K_{I,path5})}{(5 \times \sqrt{\pi \times a})}. \tag{12.2}$$

The results are summarized in Figs 12.8 and 12.9. When comparing the results with those obtained by Su and Sun [46], it is noted that the correlation between the results is very high.

A study of Figs 12.8 and 12.9 reveals the following:

- As the ratio of the crack length to plate width a/w increases, the stress intensity factor increases.
- An increase in the height to width ratio h/w of the cracked plate decreases the stress intensity factor significantly.

E_1/E_2	E_1 (PSi $\times 10^6$)	E_2 (PSi $\times 10^6$)	v_{12}	G_{12} (PSi $\times 10^6$)
0.3	30.0	100.00	0.3	15.789
0.5	30.0	60.000	0.3	14.286
0.7	30.0	42.860	0.3	13.043
0.9	30.0	33.333	0.3	12.000
1.0	30.0	30.000	0.3	11.538
1.1	30.0	27.273	0.3	11.111
1.5	30.0	20.000	0.3	9.677
2.5	30.0	12.000	0.3	7.317
3.5	30.0	8.571	0.3	5.882
4.5	30.0	6.667	0.3	4.918

Table 12.11: Material constants for cracked rectangular plate

- The effect of the degree of anisotropy decreases as a/w decreases and h/w increases.
- The effect of the degree of anisotropy on the stress intensity factor is considerable for ratios of E_1/E_2 less than 1.
- The stress intensity factor is only influenced significantly when $E_1/E_2 > 1$ for a/w large and h/w small.

For the sake of clarity, the tabulated results are summarized as follows:

1. Height to width ratio h/w = 1

   Results are shown in Fig 12.8(a) and tabulated in Tables 12.12 through 12.16. In Table 12.17, the results obtained by Su and Sun [46] are listed.

2. Height to width ratio h/w = 1.5

   Results are shown in Fig 12.8(b) and tabulated in Tables 12.18 through 12.22. In Table 12.23, the results obtained by Su and Sun [46] are listed.

3. Height to width ratio h/w = 2

   Results are shown in Fig 12.5 and tabulated in Tables 12.24 through 12.28. In Table 12.29, the results obtained by Su and Sun [46] are listed.

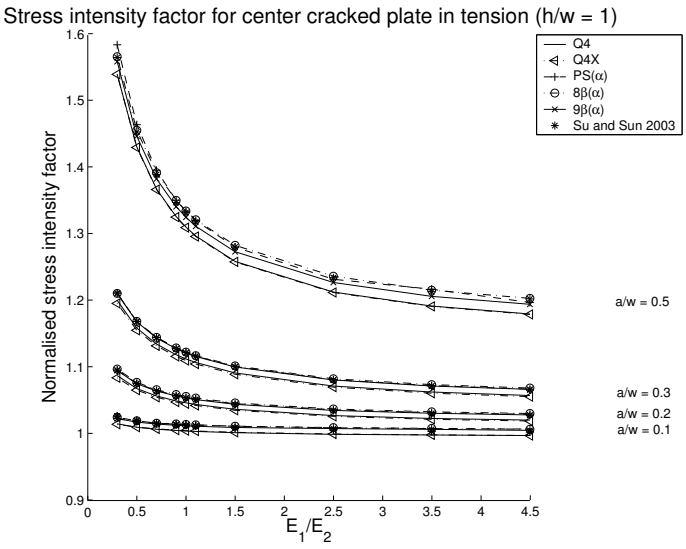

(a)

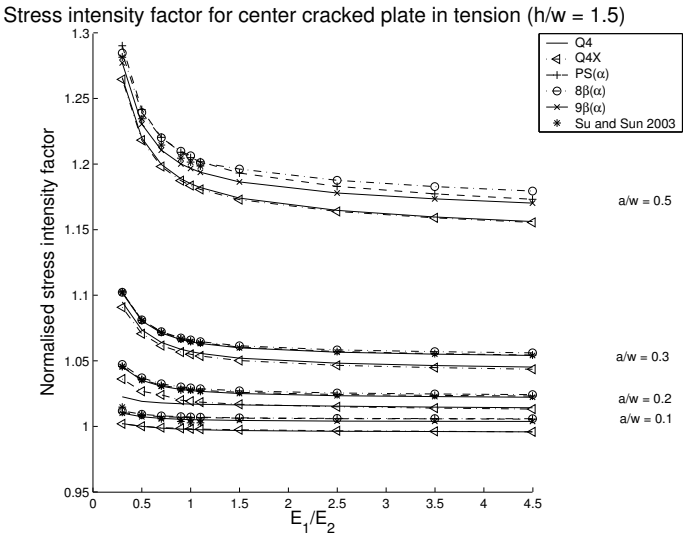

(b)

Figure 12.8: The effect of the degree of anisotropy and height to width ratio for the orthotropic CCP with 0° ply arrangement: (a) Height to width ratio h/w = 1 (b) Height to width ratio h/w = 1.5

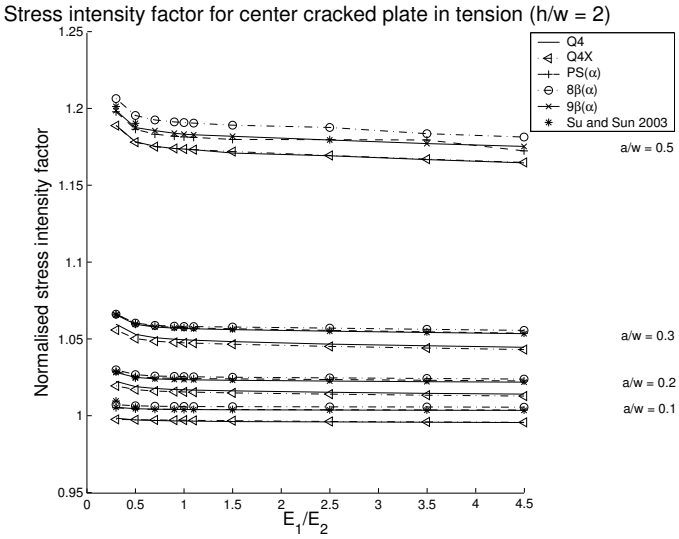

Figure 12.9: The effect of the degree of anisotropy and height to width ratio for the orthotropic CCP with 0° ply arrangement: Height to width ratio h/w = 2

	a/w			
E_x/E_y	0.1	0.2	0.3	0.5
0.3	1.0152	1.0878	1.2009	1.5405
0.5	1.0101	1.0682	1.1592	1.4314
0.7	1.0071	1.0571	1.1351	1.3682
0.9	1.0053	1.0497	1.1190	1.3268
1.0	1.0045	1.0468	1.1127	1.3110
1.1	1.0038	1.0443	1.1074	1.2976
1.5	1.0029	1.0370	1.0917	1.2594
2.5	0.9995	1.0277	1.0721	1.2133
3.5	0.9984	1.0233	1.0630	1.1923
4.5	0.9977	1.0208	1.0577	1.1803

Table 12.12: The effect of the degree of anisotropy on K_1 for an orthotropic CCP with 0° ply arrangement and height to width ratio h/w = 1, different crack length to width ratios a/w, using Q4 elements

	a/w			
E_x/E_y	0.1	0.2	0.3	0.5
0.3	1.0145	1.0845	1.1962	1.5406
0.5	1.0102	1.0659	1.1559	1.4307
0.7	1.0076	1.0552	1.1324	1.3673
0.9	1.0058	1.0480	1.1165	1.3259
1.0	1.0050	1.0453	1.1104	1.3102
1.1	1.0044	1.0428	1.1051	1.2968
1.5	1.0025	1.0356	1.0897	1.2587
2.5	0.9999	1.0264	1.0703	1.2126
3.5	0.9986	1.0220	1.0613	1.1917
4.5	0.9977	1.0195	1.0561	1.1797

Table 12.13: The effect of the degree of anisotropy on K_1 for an orthotropic CCP with 0° ply arrangement and height to width ratio h/w = 1, different crack length to width ratios a/w, using Q4X elements

	a/w			
E_x/E_y	0.1	0.2	0.3	0.5
0.3	1.0237	1.0959	1.2116	1.5850
0.5	1.1089	1.0762	1.1693	1.4650
0.7	1.0163	1.0653	1.1450	1.3963
0.9	1.0146	1.0580	1.1287	1.3515
1.0	1.0139	1.0551	1.1225	1.3348
1.1	1.0133	1.0527	1.1170	1.3208
1.5	1.0115	1.0455	1.1013	1.2809
2.5	1.0092	1.0364	1.0817	1.2326
3.5	1.0081	1.0321	1.0726	1.2176
4.5	1.0075	1.0296	1.0673	1.1977

Table 12.14: The effect of the degree of anisotropy on K_1 for an orthotropic CCP with 0° ply arrangement and height to width ratio h/w = 1, different crack length to width ratios a/w, using PS(α) elements

	a/w			
E_x/E_y	0.1	0.2	0.3	0.5
0.3	1.0249	1.0975	1.2113	1.5672
0.5	1.0198	1.0777	1.1693	1.4564
0.7	1.0162	1.0666	1.1453	1.3927
0.9	1.0150	1.0592	1.1293	1.3511
1.0	1.0143	1.0564	1.1231	1.3353
1.1	1.0137	1.0539	1.1178	1.3219
1.5	1.0118	1.0467	1.1023	1.2836
2.5	1.0095	1.0375	1.0830	1.2372
3.5	1.0084	1.0333	1.0741	1.2161
4.5	1.0071	1.0308	1.0690	1.2039

Table 12.15: The effect of the degree of anisotropy on K_1 for an orthotropic CCP with 0° ply arrangement and height to width ratio h/w = 1, different crack length to width ratios a/w, using $8\beta(\alpha)$ elements

	a/w			
E_x/E_y	0.1	0.2	0.3	0.5
0.3	1.0230	1.0954	1.2110	1.5596
0.5	1.0178	1.0755	1.1686	1.4476
0.7	1.0149	1.0645	1.1443	1.3834
0.9	1.0130	1.0571	1.1281	1.3416
1.0	1.0123	1.0542	1.1216	1.3257
1.1	1.0116	1.0517	1.1164	1.3122
1.5	1.0098	1.0445	1.1007	1.2739
2.5	1.0080	1.0354	1.0811	1.2277
3.5	1.0069	1.0311	1.0721	1.2068
4.5	1.0055	1.0287	1.0670	1.1949

Table 12.16: The effect of the degree of anisotropy on K_1 for an orthotropic CCP with 0° ply arrangement and height to width ratio h/w = 1, different crack length to width ratios a/w, using $9\beta(\alpha)$ elements

	a/w			
E_x/E_y	0.1	0.2	0.3	0.5
0.3	1.027	1.096	1.212	1.566
0.5	1.020	1.076	1.169	1.454
0.7	1.016	1.065	1.145	1.390
0.9	1.014	1.057	1.128	1.348
1.0	1.013	1.054	1.122	1.333
1.1	1.012	1.052	1.117	1.319
1.5	1.009	1.044	1.101	1.281
2.5	1.006	1.035	1.081	1.235
3.5	1.004	1.030	1.072	1.214
4.5	1.003	1.028	1.066	1.203

Table 12.17: Reference solution for the effect of the degree of anisotropy on K_1 for an orthotropic CCP with 0° ply arrangement and height to width ratio h/w = 1, different crack length to width ratios a/w

	a/w			
E_x/E_y	0.1	0.2	0.3	0.5
0.3	1.0024	1.0228	1.0952	1.2665
0.5	1.0003	1.0194	1.0739	1.2204
0.7	0.9989	1.0182	1.0643	1.2002
0.9	0.9982	1.0175	1.0591	1.1893
1.0	0.9979	1.0173	1.0574	1.1855
1.1	0.9977	1.0171	1.0560	1.1825
1.5	0.9971	1.0166	1.0523	1.1745
2.5	0.9965	1.0157	1.0485	1.1651
3.5	0.9963	1.0150	1.0567	1.1601
4.5	0.9961	1.0145	1.0455	1.1566

Table 12.18: The effect of the degree of anisotropy on K_1 for an orthotropic CCP with 0° ply arrangement and height to width ratio h/w = 1.5, different crack length to width ratios a/w, using Q4 elements

	a/w			
E_x/E_y	0.1	0.2	0.3	0.5
0.3	1.0022	1.0364	1.0912	1.2651
0.5	1.0004	1.0271	1.0710	1.2187
0.7	0.9993	1.0243	1.0619	1.1986
0.9	0.9987	1.0203	1.0570	1.1878
1.0	0.9984	1.0195	1.0553	1.1841
1.1	0.9982	1.0188	1.0540	1.1811
1.5	0.9977	1.0171	1.0505	1.1733
2.5	0.9969	1.0152	1.0469	1.1643
3.5	0.9965	1.0142	1.0451	1.1594
4.5	0.9961	1.0135	1.0439	1.1559

Table 12.19: The effect of the degree of anisotropy on K_1 for an orthotropic CCP with 0° ply arrangement and height to width ratio h/w = 1.5, different crack length to width ratios a/w, using Q4X elements

	a/w			
E_x/E_y	0.1	0.2	0.3	0.5
0.3	1.0110	1.0460	1.1027	1.2908
0.5	1.0087	1.0360	1.0814	1.2421
0.7	1.0077	1.0316	1.0721	1.2209
0.9	1.0072	1.0293	1.0671	1.2094
1.0	1.0070	1.0285	1.0654	1.2054
1.1	1.0069	1.0278	1.0641	1.2022
1.5	1.0065	1.0262	1.0608	1.1936
2.5	1.0061	1.0246	1.0574	1.1834
3.5	1.0060	1.0239	1.0558	1.1777
4.5	1.0058	1.0234	1.0547	1.1736

Table 12.20: The effect of the degree of anisotropy on K_1 for an orthotropic CCP with 0° ply arrangement and height to width ratio h/w = 1.5, different crack length to width ratios a/w, using PS(α) elements

	a/w			
E_x/E_y	0.1	0.2	0.3	0.5
0.3	1.0121	1.0475	1.1026	1.2852
0.5	1.0095	1.0373	1.0816	1.2398
0.7	1.0083	1.0328	1.0725	1.2205
0.9	1.0077	1.0304	1.0677	1.2103
1.0	1.0074	1.0296	1.0662	1.2068
1.1	1.0073	1.0290	1.0649	1.2016
1.5	1.0068	1.0274	1.0618	1.1967
2.5	1.0064	1.0257	1.0586	1.1881
3.5	1.0062	1.0250	1.0573	1.1833
4.5	1.0061	1.0245	1.0564	1.1799

Table 12.21: The effect of the degree of anisotropy on K_1 for an orthotropic CCP with 0° ply arrangement and height to width ratio h/w = 1.5, different crack length to width ratios a/w, using $8\beta(\alpha)$ elements

	a/w			
E_x/E_y	0.1	0.2	0.3	0.5
0.3	1.0103	1.0456	1.1022	1.2777
0.5	1.0076	1.0354	1.0808	1.2310
0.7	1.0064	1.0309	1.0715	1.2111
0.9	1.0057	1.0285	1.0665	1.2006
1.0	1.0054	1.0276	1.0648	1.1972
1.1	1.0053	1.0270	1.0635	1.1942
1.5	1.0048	1.0253	1.0602	1.1868
2.5	1.0043	1.0237	1.0569	1.1784
3.5	1.0041	1.0230	1.0554	1.1739
4.5	1.0040	1.0225	1.0544	1.1707

Table 12.22: The effect of the degree of anisotropy on K_1 for an orthotropic CCP with 0° ply arrangement and height to width ratio h/w = 1.5, different crack length to width ratios a/w, using $9\beta(\alpha)$ elements

	a/w			
E_x/E_y	0.1	0.2	0.3	0.5
0.3	1.015	1.046	1.103	1.282
0.5	1.009	1.036	1.081	1.235
0.7	1.006	1.031	1.072	1.215
0.9	1.004	1.028	1.067	1.205
1.0	1.003	1.028	1.065	1.202
1.1	1.003	1.027	1.064	1.199

Table 12.23: Reference solution for the effect of the degree of anisotropy on K_1 for an orthotropic CCP with 0° ply arrangement and height to width ratio h/w = 1.5, different crack length to width ratios a/w

	a/w			
E_x/E_y	0.1	0.2	0.3	0.5
0.3	0.9988	1.0228	1.0601	1.1896
0.5	0.9977	1.0194	1.0535	1.1790
0.7	0.9973	1.0182	1.0513	1.1760
0.9	0.9970	1.0175	1.0503	1.1746
1.0	0.9970	1.0173	1.0499	1.1742
1.1	0.9969	1.0171	1.0496	1.1738
1.5	0.9966	1.0166	1.0487	1.1726
2.5	0.9964	1.0157	1.0471	1.1698
3.5	0.9962	1.0150	1.0460	1.1673
4.5	0.9960	1.0145	1.0450	1.1652

Table 12.24: The effect of the degree of anisotropy on K_1 for an orthotropic CCP with 0° ply arrangement and height to width ratio h/w = 2, different crack length to width ratios a/w, using Q4 elements

	a/w			
E_x/E_y	0.1	0.2	0.3	0.5
0.3	0.9980	1.0199	1.0563	1.1895
0.5	0.9978	1.0174	1.0507	1.1787
0.7	0.9977	1.0165	1.0490	1.1758
0.9	0.9975	1.0161	1.0482	1.1746
1.0	0.9975	1.0159	1.0479	1.1742
1.1	0.9974	1.0158	1.0477	1.1738
1.5	0.9972	1.0153	1.0470	1.1726
2.5	0.9967	1.0145	1.0456	1.1700
3.5	0.9964	1.0138	1.0445	1.1676
4.5	0.9961	1.0132	1.0435	1.1655

Table 12.25: The effect of the degree of anisotropy on K_1 for an orthotropic CCP with 0° ply arrangement and height to width ratio h/w = 2, different crack length to width ratios a/w, using Q4X elements

	a/w			
E_x/E_y	0.1	0.2	0.3	0.5
0.3	1.0056	1.0294	1.0666	1.1985
0.5	1.0048	1.0260	1.0605	1.1871
0.7	1.0046	1.0251	1.0587	1.1839
0.9	1.0046	1.0248	1.0580	1.1826
1.0	1.0045	1.0247	1.0578	1.1821
1.1	1.0045	1.0246	1.0576	1.1818
1.5	1.0045	1.0244	1.0571	1.1805
2.5	1.0043	1.0240	1.0560	1.1803
3.5	1.0042	1.0235	1.0551	1.1801
4.5	1.0041	1.0231	1.0542	1.1730

Table 12.26: The effect of the degree of anisotropy on K_1 for an orthotropic CCP with 0° ply arrangement and height to width ratio h/w = 2, different crack length to width ratios a/w, using PS(α) elements

	a/w			
E_x/E_y	0.1	0.2	0.3	0.5
0.3	1.0076	1.0303	1.0666	1.2071
0.5	1.0069	1.0272	1.0608	1.1961
0.7	1.0066	1.0263	1.0593	1.1932
0.9	1.0065	1.0261	1.0588	1.1919
1.0	1.0065	1.0259	1.0586	1.1915
1.1	1.0064	1.0258	1.0585	1.1911
1.5	1.0063	1.0255	1.0582	1.1898
2.5	1.0062	1.0251	1.0575	1.1883
3.5	1.0061	1.0247	1.0567	1.1842
4.5	1.0060	1.0243	1.0560	1.1820

Table 12.27: The effect of the degree of anisotropy on K_1 for an orthotropic CCP with 0° ply arrangement and height to width ratio h/w = 2, different crack length to width ratios a/w, using $8\beta(\alpha)$ elements

	a/w			
E_x/E_y	0.1	0.2	0.3	0.5
0.3	1.0059	1.0286	1.0662	1.1993
0.5	1.0050	1.0254	1.0600	1.1882
0.7	1.0047	1.0244	1.0582	1.1862
0.9	1.0045	1.0240	1.0575	1.1845
1.0	1.0045	1.0239	1.0573	1.1839
1.1	1.0044	1.0238	1.0571	1.1835
1.5	1.0043	1.0235	1.0565	1.1825
2.5	1.0041	1.0230	1.0555	1.1801
3.5	1.0040	1.0226	1.0547	1.1778
4.5	1.0039	1.0223	1.0539	1.1759

Table 12.28: The effect of the degree of anisotropy on K_1 for an orthotropic CCP with 0° ply arrangement and height to width ratio h/w = 2, different crack length to width ratios a/w, using $9\beta(\alpha)$ elements

	a/w			
E_x/E_y	0.1	0.2	0.3	0.5
0.3	1.010	1.029	1.066	1.202
0.5	1.006	1.025	1.060	1.191

Table 12.29: Reference solution for the effect of the degree of anisotropy on K_1 for an orthotropic CCP with 0° ply arrangement and height to width ratio h/w = 2, different crack length to width ratios a/w

Chapter 13

Conclusions

The conclusions of this study are summarized as follows: It is well known that isotropic and orthotropic fracture mechanics problems can effectively be solved by combining the finite element method and the path independent integrals J and I^*.

Not as well known, is that assumed stress finite elements, combined with the I^* integral, can be used to predict an upper bound to the stress intensity factor. Assumed stress elements without penalized equilibrium tend to under predict the stress intensity factor if the mesh is not highly refined; to predicted the upper bound, assumed stress elements with penalized equilibrium are an attractive modeling option.

Solving the J integral with displacement based elements, yields a lower bound to the stress intensity factor. A lower bound in isotropic fracture mechanics problems can be predicted accurately with Q4 or Q4X elements. In orthotropic fracture problems however, Q4 elements reveal a notable path dependency, for such problems, elements with drilling degrees of freedom represent a superior modeling option to Q4 elements.

When using elements with drilling degrees of freedom to solve fracture mechanics problems, the integration scheme used and the value of the penalty parameter γ in the elements, needs consideration. Reduced integration, with a small center point weight, or a too large penalty parameter, can introduce a checkerboard like locking pattern. Both the integration scheme and the penalty parameter γ influence the stability of elements with drilling degrees of freedom. For these elements, it is proposed that full integration is used, combined with a γ value selected from the range $G/100$ through $G/10$.

From a mechanics of material point of view, it is shown that the degree of anisotropy and the fiber orientation in orthotropic fracture mechanics problems have a large influence on the stress intensity factor. The influence of the degree of anisotropy decreases as the ratio of E_1/E_2 increases. When the degree of anisotropy is larger than 1, the stress intensity factor is only influenced significantly for large a/w and small h/w ratios.

13.1 Recommendations for further studies

- In the section on displacement based elements with penalized equilibrium we only considered regular geometries; a treatment for irregular (generally distorted geometries) is awaiting. This can probably be done using

  1. analytical or symbolic techniques to find the characteristic polynomial, or
  2. through approximate relationships derived from the mapping to a 'regular' parent element.

- While approximate relationships exist which relate the size of the plastic zone to a material specific stress intensity value, it is not clear what the true value of rotations in the plastic zone are. It is recommended that this is addressed in a future study.

- A further study on the effect of fiber orientation on the stress intensity factor in orthotropic materials is recommended.

- The use of elements with drilling degrees of freedom in more complicated fracture mechanics problems will be a interesting study.

- A further study using path independent integrals (e.g. J_k) that can split the mixed mode stress intensity factor into Mode I and Mode II stress intensity factors is recommended.

Bibliography

[1] C.C. Wu, Q.Z. Xiao, and G. Yagawa. Finite element methodology for path integrals in fracture mechanics. *International journal for numerical methods in engineering*, 43:69–91, 1998.

[2] G.C. Sih, Paris P.C., and G.R. Irwin. On cracks in rectilinearly anisotropic bodies. *International Journal of Fracture Mechanics*, 1(3):189–203, 1965.

[3] J.W. Kim. A contour integral computation of stress intensity factors in the cracked orthotropic elastic plates. *Engineering Fracture Mechanics*, 21:353–364, 1985.

[4] O.C. Zienkiewicz. *MATLAB 6.5*. The MathWorks Inc., November 2002.

[5] T.H.H. Pain and K. Sumihara. Rational approach for assumed stress finite elements. *Int. J. Numer. Methods Eng.*, 20:1685 – 1695, 1984.

[6] K.-J. Bathe. *Finite Element Procedures in Engineering Analysis*. Prentice-Hall, New Jersey, 1996.

[7] K. Washizu. *Variational Methods in Elasticity and Plasticity*. Pergamon Press, 1982.

[8] C. Lanczos. *The Variational Principles of Mechanics*. Univ. of Toronto Press, 1970.

[9] J.N. Reddy. *Energy and Variational Methods in Applied Mechanics*. John Wiley and Sons, 1984.

[10] T.J.R. Hughes. *The finite element method: Linear static and dynamic analysis*. Prentice-Hall, London, 1987.

[11] S. Geyer and A.A. Groenwold. Two hybrid stress membrane finite element families with drilling rotations. *Int. J. Num. Meth. Eng.*, 53:583–601, 2002.

[12] S. Geyer and A.A. Groenwold. On reduced integration and locking of flat shell finite elements with drilling rotations. *Commun. Num. Meth. Eng.*, 19:85–97, 2003.

[13] B. Fraeijs du Veubeke. Displacement and equilibrium models in the finite element method. In O.C. Zienkiewicz and G.C. Holister, editors, *Stress analysis*, pages 145–197, Chichester, 1965. John Wiley.

[14] C.-C. Wu and Y.K. Cheung. On optimization approaches of hybrid stress elements. *Finite Elem. Anal. Des.*, 21:111–128, 1995.

[15] R.D. Cook, D.S. Malkus, M.E. Plesha, and R.J. Witt. *Concepts and applications of finite element analaysis*. John Wiley & Sons, New York, 2002.

[16] E.L. Wilson, R.L. Taylor, W.P. Doherty, and J. Ghaboussi. Incompatible displacement models. In S.J. Fenves et al., editor, *Numerical and computer methods in structural mechanics*, pages 43–57, New York, 1973. Academic Press.

[17] T.H.H. Pian. Derivation of element stiffness matrices by assumed stress distributions. *AIAA J.*, 2:1333–1336, 1964.

[18] T.H.H. Pian. State-of-the-art development of the hybrid/mixed finite element method. *Fin. Elem. Anal. Des.*, 21:5–20, 1995.

[19] J.C. Simo and M.S. Rifai. A class of mixed assumed strain methods and the method of incompatible modes. *Int. J. Numer. Methods Eng.*, 29:1595–1638, 1990.

[20] D.J. Allman. A compatible triangular element including vertex rotations for plane elasticity analysis. *Comp. Struc.*, 19:1–8, 1984.

[21] T.J.R. Hughes and F. Brezzi. On drilling degrees of freedom. *Comp. Methods Appl. Mech. Eng.*, 72:105–121, 1989.

[22] A. Ibrahimbegovic, R.L. Taylor, and E.L. Wilson. A robust quadrilateral membrane finite element with drilling degrees of freedom. *Int. J. Numer. Methods Eng.*, 30:445–457, 1990.

[23] A.A Groenwold. Finite element analysis of composite plates and shells. Master's project, Pretoria University, June-August 1993.

[24] E. Reissner. A note on variational principles in elasticity. *Int. J. Solids. Struct.*, 1:93–95, 1965.

[25] O.C Zienkiewicz. *The Finite Element method*. McGraw-Hill, London, 1982.

[26] E.L Wilson. The static condensation algorithm. *Int. J. Num. Meth. Eng*, 8:199–203, 1974.

[27] N. Stander and E.L. Wilson. A 4-node quadrilateral membrane element with in-plane vertex rotations and modified reduced quadrature. *Eng. Comput*, 6:266–271, 1989.

[28] R.L. Taylor and J.C Simo. Bending and membrane elements for analysis of thick and thin shells. *Proc. NUMETA Conference, Swansea 7-11 Jan*, 1985.

[29] R.H. MacNeal and R.L Harder. A refined four-noded membrane element with rotational degrees of freedom. *Comp. Struc*, 19:1–8, 1988.

[30] R.L. Taylor. Finite element analysis of linear shell problems. In J.R. Whiteman, editor, *Proceedings of the Mathematics in Finite Elements and Applications*, pages 191–203, New York, 1987. Academic Press.

[31] A.A. Groenwold, Q.Z. Xiao, and N.J. Theron. Accurate solution of traction free boundaries using hybrid stress membrane elements with drilling degrees of freedom. *Comput. Struct.*, 82:2071–2081, 2004.

[32] S.P. Timoshenko. History of the strength of materials. *New York*, 1953.

[33] C.E Inglis. Stresses in a plate due to the presence of cracks and sharp corners. *Proc. Inst. Naval Architects*, 60, 1913.

[34] D.R.J. Owen and A.J. Fawkes. *Engineering fracture mechanics, numerical methods and applications*. Swansea Pineridge Press Ltd. Uk, second edition, 1983.

[35] H.L. Ewalds and R.J.H. Wanhill. *Fracture Mechanics*. Edward Arnold (Publishers) Ltd, third edition, 1984.

[36] Bannantine J.A, J.J Comer, and Handrock J.L. *Fundamentals of metal fatigue analysis*. Prestice-Hall, Inc, Englewood Cliffs, New Jersey, first edition, 1990.

[37] E.F. Rybicki and M.F. Kanninen. A finite element calculation of stress intensity factors by a modified crack closure integral. *Engineering Fracture Mechanics*, 9:1931 – 938, 1977.

[38] A.J Fawkes, Owen D.R.J, and Luxmoore A.R. An assessment of crack tip singularity models for use with isoparametric elements. *Engineering Fracture Mechanics*, 11:143–159, 1979.

[39] C.C. Wu, Xiao Q.Z., and Z.R. Li. Fracture estimation: bound theorem and numerical strategy. In Cheng F.Y. and Y. Gu, editors, *Proceedings of 2nd Sino-Us Joint symposium on recent Advancement of Computational Mechanics in Structural Engineering*, Dalian, China, May 1998.

[40] Q.Z. Xiao, B.L. Karihaloo, and F.W. Williams. Application of penalty-equilibrium hybrid stress element method to crack problems. *Engineering Fracture Mechanics*, 63:1–22, 1999.

[41] C.S. Long and A.A. Groenwold. Reduced modified quadrature for quadratic membrane finite elements. *Int. J. Num. Meth. Eng.*, 61:837–855, 2004.

[42] H.H. Dovey. *Extension of three dimensional analysis to shell structures using the finite element idealization*. PhD dissertation, University of California, Berkeley, 1974. (Report no. UC SESM 74-2).

[43] A.A. Groenwold and N. Stander. An efficient 4-node 24 d.o.f. thick shell finite element with 5-point quadrature. *Eng. Comput.*, 12:723–748, 1995.

[44] G. De Saxce and C.H. Kang. Application of the hybrid mongrel displacement finite method to the computation of stress intensity factors in anisotropic material. *Engineering Fracture Mechanics*, 41:71–83, 1992.

[45] S.J. Chu and Hong C.S. Application of the j_k integral to mixed mode crack problems for anisotropic composite laminates. *Engineering Fracture Mechanics*, 35:1093 – 1103, 1990.

[46] R.K.L. Su and H.Y. Sun. Numerical solutions of two-dimensional anisotropic crack problems. *International Journal of Solids and Structures*, 40:4615–4635, 2003.

Appendix A

Eigenvalues of Q4(α) and 5β

In this chapter the symbolic eigenvalues (used in Chapter 3) for square and rectanguler Q4, 5β, Q4(α) and Q4($\alpha_x\alpha_y$) elements are given.

A.1 Square Q4(α) element with side lengths $2a$

$$\lambda_1 = 1/2\,\frac{\left(-2\,a^2-\sqrt{4}\sqrt{a^4\nu^2}\right)E}{-a^2+a^2\nu^2} \tag{A.1}$$

$$\lambda_2 = \frac{E}{\nu+1} \tag{A.2}$$

$$\lambda_3 = 1/2\,\frac{\left(-2\,a^2+\sqrt{4}\sqrt{a^4\nu^2}\right)E}{-a^2+a^2\nu^2} \tag{A.3}$$

$$\lambda_4 = 1/12\,\frac{E\,(-3\,v\,A\,E^2-3\,A\,E^2+2\,v^2a^2+6\,a^2-8\,v\,a^2)}{a^2\,(-v^2+1-v+v^3)} \tag{A.4}$$

$$\lambda_5 = 1/12\,\frac{E\,(-3\,v\,A\,E^2-3\,A\,E^2+2\,v^2a^2+6\,a^2-8\,v\,a^2)}{a^2\,(-v^2+1-v+v^3)} \tag{A.5}$$

A.2 Square 5β element with side lengths $2a$

$$\lambda_1 = 1/2\,\frac{\left(-2\,a^2-\sqrt{4}\sqrt{a^4\nu^2}\right)E}{-a^2+a^2\nu^2} \tag{A.6}$$

$$\lambda_2 = \frac{E}{\nu+1} \tag{A.7}$$

$$\lambda_3 = 1/2\,\frac{\left(-2\,a^2+\sqrt{4}\sqrt{a^4\nu^2}\right)E}{-a^2+a^2\nu^2} \tag{A.8}$$

$$\lambda_4 = 1/3\,E \tag{A.9}$$

$$\lambda_5 = 1/3\,E \tag{A.10}$$

A.3 Rectangular Q4(α) element with side lengths $2a$, $2b$, $a \geq b$

$$\lambda_1 = 1/2\,\frac{\left(-b^2-a^2+\sqrt{b^4-2\,b^2a^2+a^4+4\,b^2a^2\nu^2}\right)E}{-a\,b+a\,b\,\nu^2} \tag{A.11}$$

$$\lambda_2 = 1/2\,\frac{E\,(b^2+a^2)}{a\,b\,(\nu+1)} \tag{A.12}$$

$$\lambda_3 = 1/2\,\frac{\left(-b^2-a^2-\sqrt{b^4-2\,b^2a^2+a^4+4\,b^2a^2\nu^2}\right)E}{-a\,b+a\,b\,\nu^2} \tag{A.13}$$

$$\lambda_4 = 1/12\,\frac{E\,(-3\,v\,A\,E^2-3\,A\,E^2+2\,a^2-4\,a^2v+2\,a^2v^2+4\,b^2-4\,b^2v)}{a\,b\,(v^3-v^2-v+1)} \tag{A.14}$$

$$\lambda_5 = 1/12\,\frac{E\,(-3\,A\,E^2-3\,v\,A\,E^2+4\,a^2-4\,a^2v+2\,b^2-4\,b^2v+2\,v^2b^2)}{a\,b\,(v^3-v^2-v+1)} \tag{A.15}$$

A.4 Rectangular 5β element with side lengths $2a$, $2b$, $a \geq b$

$$\lambda_1 = 1/2\,\frac{\left(-b^2-a^2+\sqrt{b^4-2\,b^2a^2+a^4+4\,b^2a^2\nu^2}\right)E}{-a\,b+a\,b\,\nu^2} \tag{A.16}$$

$$\lambda_2 = 1/2\,\frac{E\,(b^2+a^2)}{a\,b\,(\nu+1)} \tag{A.17}$$

$$\lambda_3 = 1/2\,\frac{\left(-b^2-a^2-\sqrt{b^4-2\,b^2a^2+a^4+4\,b^2a^2\nu^2}\right)E}{-a\,b+a\,b\,\nu^2} \tag{A.18}$$

$$\lambda_4 = 1/3\,\frac{b\,E}{a} \tag{A.19}$$

$$\lambda_5 = 1/3\,\frac{a\,E}{b} \tag{A.20}$$

A.5 Rectangular Q4($\alpha_x\alpha_y$) element with side lengths $2a$, $2b$, $a \geq b$

$$\lambda_1 = 1/2\,\frac{\left(-b^2-a^2+\sqrt{b^4-2\,b^2a^2+a^4+4\,b^2a^2\nu^2}\right)E}{-a\,b+a\,b\,\nu^2} \tag{A.21}$$

$$\lambda_2 = 1/2\,\frac{E\,(b^2+a^2)}{a\,b\,(\nu+1)} \tag{A.22}$$

$$\lambda_3 = 1/2\,\frac{\left(-b^2-a^2-\sqrt{b^4-2\,b^2a^2+a^4+4\,b^2a^2\nu^2}\right)E}{-a\,b+a\,b\,\nu^2} \tag{A.23}$$

$$\begin{aligned}\lambda_4 = {} & \frac{E(-2\,b^2v^3+(12\,E^2\alpha_x+4\,a^2+2\,b^2+3\,E^2\alpha_y))v^2}{-12\,a\,b\,(v^4-2\,v^2+1)} \\ & + \frac{E((-6\,E^2\alpha y+2\,b^2)v-2\,b^2-4\,a^2+3\,E^2\alpha_y)}{-12\,a\,b\,(v^4-2\,v^2+1)}\end{aligned} \tag{A.24}$$

$$\begin{aligned}\lambda_5 = {} & \frac{E(2\,v^3a^2+(-3\,E^2\alpha_x-2\,a^2-4\,b^2-12\,E^2\alpha_y)v^2)}{12ab(v^4-2\,v^2+1)} \\ & + \frac{E((-2\,a^2+6\,E^2\alpha_x)v+2\,a^2+4\,b^2-3\,E^2\alpha x)}{12\,a\,b\,(v^4-2\,v^2+1)}\end{aligned} \tag{A.25}$$

Appendix B

Sample input file

An example of an input file is presented below. The input file is for an isotropic center cracked panel under uniform tension. (Note: Not all the element connectivity and node coordinates are given.)

```
function [elprop,gcoord,loads,nnode,restraints,nodes,begin_Jnode] = Drilling

nload=1; % number of load cases
begin_Jnode = 1;

nodes = [
       20      19      9     10
       19      17      7     9
       17      15      5     7
       30      29      19    20
       29      27      17    19
       ...

       106     120     119   105
       120     134     133   119
       134     144     143   133
       144     150     147   143
       150     152     149   147];


gcoord = [  -6.      48.     0
            -3.58378 48.     0
            -1.61089 48.     0
             0.      48.     0
             18.     48.     0
             ...

             .744958 .743769 0
             0.      .693522 0
            -.693522 0.      0
             .693503 0.      0
             0.      0.      0];

nnode=length(gcoord); % number of nodes

restraints=[
    46  0 1 1 1 1 1  0 0 0 0 0 0
    60  0 1 1 1 1 1  0 0 0 0 0 0
    72  0 1 1 1 1 1  0 0 0 0 0 0
    85  0 1 1 1 1 1  0 0 0 0 0 0
    98  0 1 1 1 1 1  0 0 0 0 0 0
    111 0 1 1 1 1 1  0 0 0 0 0 0
    124 0 1 1 1 1 1  0 0 0 0 0 0
```

```
    137 0 1 1 1 1 1  0 0 0 0 0 0
    146 0 1 1 1 1 1  0 0 0 0 0 0
    151 0 1 1 1 1 1  0 0 0 0 0 0
    152 0 1 1 1 1 1  0 0 0 0 0 0
    1   1 0 1 1 1 1  0 0 0 0 0 0
    11  1 0 1 1 1 1   0 0 0 0 0 0
    21  1 0 1 1 1 1   0 0 0 0 0 0
    31  1 0 1 1 1 1   0 0 0 0 0 0
    47  1 0 1 1 1 1   0 0 0 0 0 0
    62  1 0 1 1 1 1   0 0 0 0 0 0
    75  1 0 1 1 1 1   0 0 0 0 0 0
    76  1 0 1 1 1 1   0 0 0 0 0 0
    77  1 0 1 1 1 1   0 0 0 0 0 0
    78  1 0 1 1 1 1   0 0 0 0 0 0]; % constraints
% format
% node no. :: ux - rx :: val ux - rx

ff=zeros(length(gcoord)*2,1);
Force = 24*1;
Upper = [1 2 3 4 6 8 10 9 7 5];
L = length(Upper);

for i = 1:(L-1)
    nd1 = Upper(1,i);
    nd2 = Upper(1,i+1);
    xcoord1 = gcoord(nd1,1);
    xcoord2 = gcoord(nd2,1);
    Bydrae = abs(xcoord2 - xcoord1);

    Frac = Bydrae/24;

    ff(nd1*2) = ff(nd1*2) + (Force*Frac)/2;
    ff(nd2*2) = ff(nd2*2) + (Force*Frac)/2;

end

elprop=[1.0 1 0.3 5]; % element properties
% format
% element no. :: thickness :: E :: poisson's ratio :: integration scheme

loads=[
1 1  0 ff(1*2)  0 0 0 0
1 2  0 ff(2*2)  0 0 0 0
1 3  0 ff(3*2)  0 0 0 0
1 4  0 ff(4*2)  0 0 0 0
1 6  0 ff(6*2)  0 0 0 0
1 8  0 ff(8*2)  0 0 0 0
1 10 0 ff(10*2) 0 0 0 0
1 9  0 ff(9*2)  0 0 0 0
1 7  0 ff(7*2)  0 0 0 0
1 5  0 ff(5*2)  0 0 0 0
]; % loads
% format
% load case :: node :: fx :: fy :: fz :: mx :: my :: mz

clear ff
```

Appendix C

Source code listings

For the sake of brevity, only representative code fragments are presented; other code fragments may be obtained from the author upon request.

C.1 Element routines: J integral (for a Q4 element)

For the sake of brevity, only the implementation for Q4 is shown.

```
function [K1,J] = J_integral(nnel,matmtx,nodes,gcoord,disp,iopt,poisson,emodule,begin_Jnode,Type)

if  Type ~= 0
%-------------------------------------------------------------------------
%           J Integraal
%-------------------------------------------------------------------------
[Path_element] = path_element_def(Type);
[Junk1,Stress_eq] = size(Path_element);
Path_plot(disp,gcoord,nodes,begin_Jnode,Path_element);

%-------------------------------------------------------------------------
% Initialize constants
%-------------------------------------------------------------------------
a11 = matmtx(1,1);
a12 = matmtx(1,2);
a13 = matmtx(1,3);
a21 = matmtx(2,1);
a22 = matmtx(2,2);
a23 = matmtx(2,3);
a31 = matmtx(3,1);
a32 = matmtx(3,2);
a33 = matmtx(3,3);

number_of_elm = length(Path_element);
J = zeros(number_of_elm,1);
Sy_lengte = zeros(number_of_elm,1);
%-------------------------------------------------------------------------
% Choose integration path
%-------------------------------------------------------------------------
choose_int=menu('Choose the integration scheme to be used',...
   ' 1 Point quadrature rule  ','  2 Point quadrature rule  ',...
   ' 3 Point quadrature rule ','  4 Point quadrature rule  ',...
   ' 5 Point quadrature rule ');

 if (choose_int == 1)
```

```
     nglx=1; ngly=1;
     nglxy=nglx*ngly;
 end
 if (choose_int == 2)
     nglx=2; ngly=2;
     nglxy=nglx*ngly;
 end
 if (choose_int == 3)
     nglx=3; ngly=3;
     nglxy=nglx*ngly;
 end
 if (choose_int == 4)
     nglx=4; ngly=4;
     nglxy=nglx*ngly;
 end
 if (choose_int == 5)
     nglx=5; ngly=5;
     nglxy=nglx*ngly;
 end

[point2,weight2]=feglqd2(nglx,ngly);             % sampling points & weights

choose_x = menu('Specify path in element','Positive integrasion points','Negative integration points',' -1 ',' 1 ');
if choose_x == 1
    x_path = nglx;
end
if choose_x == 2
    x_path = 1;
end
if choose_x == 3;
    x_path = 1;
end
if choose_x == 4
    x_path = 1;
end
%---------------------------------------------------------------------------
%               Loop over all the elements in path
%---------------------------------------------------------------------------
for E = 1:number_of_elm                          % Loop over all the elements in path

     teller = 1;
     geval = 0;

    for i=1:nnel
        nd(i)=nodes(Path_element(E,1),i);        % extract connected node for (iel)-th element
    end

    if Path_element(E,2) ==1                    % Change the node connectivity, for element on the left
        nd2(:,:) = nd(:,:);
        nd(1,1) = nd2(1,3);
        nd(1,2) = nd2(1,4);
        nd(1,3) = nd2(1,1);
        nd(1,4) = nd2(1,2);
    end

    if Path_element(E,2) ==3                     % Change the node connectivity, for elements on the top
        nd3(:,:) = nd(:,:);
        nd(1,1) = nd3(1,2);
        nd(1,2) = nd3(1,3);
        nd(1,3) = nd3(1,4);
        nd(1,4) = nd3(1,1);
    end

    for i=1:nnel
        xcoord(i)=gcoord(nd(i),1);               % extract x value of the node
        ycoord(i)=gcoord(nd(i),2);               % extract y value of the node
        eldisp(teller,1) = disp(nd(i)*2-1);      % extract u displacement of node
        eldisp(teller+ 1,1) = disp(nd(i)*2);     % extract v displacement of node
```

```
        teller = teller + 2;
    end
%-------------------------------------------------------------------------
%             Adjacent element (for integration on element bound)
%-------------------------------------------------------------------------
   if Stress_eq ==3
       if choose_x == 4
           if Path_element(E,1) ~= Path_element(E,3)

           teller2 = 1;

           for i=1:nnel
               nd2(i)=nodes(Path_element(E,3),i);     % Extract connected node for (iel)-th element
           end

           if Path_element(E,2) ==1                   % Change the node connectivity, for element on the left
              nd3(:,:) = nd2(:,:);
              nd2(1,1) = nd3(1,3);
              nd2(1,2) = nd3(1,4);
              nd2(1,3) = nd3(1,1);
              nd2(1,4) = nd3(1,2);
           end

           if Path_element(E,2) ==3                    % Change the node connectivity, for elements on the top
              nd3(:,:) = nd2(:,:);
              nd2(1,1) = nd3(1,2);
              nd2(1,2) = nd3(1,3);
              nd2(1,3) = nd3(1,4);
              nd2(1,4) = nd3(1,1);
           end

           for i=1:nnel
               xcoord2(i)=gcoord(nd2(i),1);               % extract x value of the node
               ycoord2(i)=gcoord(nd2(i),2);               % extract y value of the node
               eldisp2(teller2,1) = disp(nd2(i)*2-1);     % extract u displacement of node
               eldisp2(teller2+ 1,1) = disp(nd2(i)*2);    % extract v displacement of node
               teller2 = teller2 + 2;
           end
       end
   end
end
%-------------------------------------------------------------------------
%             Numerical integration in the zeta = constant direction
%-------------------------------------------------------------------------
         for intx=x_path
            x=point2(intx,1);                                  % sampling point in x-axis

            if choose_x == 3
                x = -1.0;
            end

            if choose_x == 4
                x = 1;
            end

            wtx=weight2(intx,1);                               % weight in x-axis

            for inty=1:ngly
                y=point2(inty,2);                              % sampling point in y-axis
                wty=weight2(inty,2);                           % weight in y-axis

                [shape,dhdr,dhds]=feisoq4(x,y);                % compute shape functions and

                jacob2=fejacob2(nnel,dhdr,dhds,xcoord,ycoord); % compute Jacobian
                detjacob=det(jacob2);                          % determinant of Jacobian
                invjacob=inv(jacob2);                          % inverse of Jacobian matrix

                [dhdx,dhdy]=federiv2(nnel,dhdr,dhds,invjacob); % derivatives of shape functions w.r.t.
```

```
                                                % physical coordinate
dxdr = jacob2(1,1);                             % derivative of x with respect to r
dydr = jacob2(1,2);                             % derivative of y with respect to r
dxds = jacob2(2,1);                             % derivative of x with respect to s
dyds = jacob2(2,2);                             % derivative of y with respect to s

D = [dyds*(dyds*dxdr - dxds*dydr), dxds*(dxds*dydr-dyds*dxdr),0]';  % Vector product of A and C
                                                                    % Vector normal to the line
                                                                    % r = constant
kinmtx2=fekine2d(nnel,dhdx,dhdy);               % compute kinematic matrix
kinmtx2_omgekeer = fekine_J(nnel,dhdx,dhdy);
Stress = matmtx*dudx_dvdy;                      % compute stresses in integration point
dudy_dvdx = kinmtx2_omgekeer*eldisp;

dudx_dvdy=kinmtx2*eldisp;                       % compute strains in integration point

if Stress_eq == 3 % Adjacent element
    if choose_x == 4
        if Path_element(E,1) ~= Path_element(E,3)
           [shape2,dhdr2,dhds2]=feisoq4(-1,y);                 % compute shape functions and
           jacob3=fejacob2(nnel,dhdr2,dhds2,xcoord2,ycoord2);  % compute Jacobian
           detjacob2=det(jacob3);                              % determinant of Jacobian
           invjacob2=inv(jacob3);                              % inverse of Jacobian matrix
           [dhdx2,dhdy2]=federiv2(nnel,dhdr2,dhds2,invjacob2); % derivatives of shape functions w.r.t.
           kinmtx3=fekine2d(nnel,dhdx2,dhdy2);                 % compute kinematic matr
           dudx_dvdy2=kinmtx3*eldisp2;                         % compute strains in integration point
           Stress2 = matmtx*dudx_dvdy2;                        % compute stresses in integration point
           Stress3 = Stress;                                   % compute stresses in integration point
           % Calculate stress on element bound
           Stress4(1,1) = 0.5*(Stress2(1,1) + Stress3(1,1));
           Stress4(2,1) = 0.5*(Stress2(2,1) + Stress3(2,1));
           Stress4(3,1) = 0.5*(Stress2(3,1) + Stress3(3,1));
      end
   end
end

Stress = matmtx*dudx_dvdy;                      % compute stresses in integration point
dudy_dvdx = kinmtx2_omgekeer*eldisp;

dudx = dudx_dvdy(1,1);                          % Strain xx (dudx)
dvdy = dudx_dvdy(2,1);                          % Strain yy (dvdy)

dudy = dudy_dvdx(1,1);                          % dudy derivative of u with respect to y
dvdx = dudy_dvdx(2,1);                          % dvdx derivative of v wiht respect to x

estrain(1,1) = dudx_dvdy(1,1);                  % strain xx
estrain(3,1) = dudx_dvdy(3,1);                  % strain xy
estrain(2,1) = dudx_dvdy(2,1);                  % strain yy

if Stress_eq == 3
    if choose_x == 4
        if Path_element(E,1) ~= Path_element(E,3)
            Stress = Stress4;
        end
    end
end

estress(1,1) = Stress(1,1);                     % stress xx
estress(2,1) = Stress(2,1);                     % stress yy
estress(3,1) = Stress(3,1);                     % stress xy

% Strain energy density for plane problems
A = 0.5*((a11*estrain(1,1) + a12*estrain(2,1) + a13*estrain(3,1))*estrain(1,1) +...
(a21*estrain(1,1) + a22*estrain(2,1) + a23*estrain(3,1))*estrain(2,1) +...
(a31*estrain(1,1) + a32*estrain(2,1)+ a33*estrain(3,1))*estrain(3,1));

% Calculate J integral terms
U_dyds = A*(dyds);                              % To be able to integrate
```

```
                normal = sqrt(D(1,1)^2 + D(2,1)^2);             % Normal to zeta = constant line

                n = [(D(1,1)/normal),(D(2,1)/normal),0];        % Unit normal vector to line zeta = constant
                n1 = n(1,1);
                n2 = n(1,2);

                t_dddx = ((estress(1,1)*n1) + (estress(3,1)*n2))*dudx +((estress(3,1)*n1) + (estress(2,1)*n2))*dvdx;
                ds = sqrt(dxds^2 + dyds^2); % Path length in element
                Sy_lengte(E,1) = Sy_lengte(E,1) + ds;
                J(E,1) = J(E,1) + (U_dyds - t_dddx*ds)*wty;
            end
        end
end

L = length(J);
J_tot = 0;

for i = 1:L
    J_tot = J(i)+ J_tot;                                        % Sum of elements contribution to J
end

J_totaal = abs(2*J_tot)                                          % Jx2 for symmetry around crack tip
%-------------------------------------------------------------------------
%           Material properties
%-------------------------------------------------------------------------
if iopt == 1
     kappa = (3-poisson)/(1+poisson);
end
if iopt == 2
    kappa = (3 - 4*poisson);
end
shear_m = emodule/(2*(1+poisson));         % shear modules

%-------------------------------------------------------------------------
%    Calculate Stress intensity factor for J int value
%-------------------------------------------------------------------------
K1 = sqrt((8*shear_m*J_totaal)/(1+kappa));

if iopt == 2
    K = sqrt(J_totaal*(emodule/(1-poisson^2)));
end
if iopt == 1
    K = sqrt(J_totaal*emodule);                          % uit Dual analysis for path integrals...
end

if K1 ~= K
    disp('K calculations error');
end

end
```

C.2 Element routines: I^* integral (for a PS(α) element)

For the sake of brevity, only the implementation for PS(α) is shown

```
function [K1,I] = J_integral(nnel,matmtx,nodes,gcoord,disp,iopt,poisson,emodule,begin_Jnode,Type,t,Alpha)
if  Type ~= 0
%-------------------------------------------------------------------------
%           I* Integraal
%-------------------------------------------------------------------------
Cinv = inv(matmtx);
[Path_element] = path_element_def(Type)
[Junk1,Stress_eq] = size(Path_element);
```

```
Path_plot(disp,gcoord,nodes,begin_Jnode,Path_element);
%-------------------------------------------------------------------------
number_of_elm = length(Path_element);
I = zeros(number_of_elm,1);

choose_int=menu('Choose the integration scheme to be used',...
   '  1 Point quadrature rule  ','  2 Point quadrature rule  ',...
   ' 3 Point quadrature rule ','  4 Point quadrature rule  ',...
   ' 5 Point quadrature rule ');

 if (choose_int == 1)
     nglx=1; ngly=1;
     nglxy=nglx*ngly;
 end
 if (choose_int == 2)
     nglx=2; ngly=2;
     nglxy=nglx*ngly;
 end
 if (choose_int == 3)
     nglx=3; ngly=3;
     nglxy=nglx*ngly;
 end
 if (choose_int == 4)
     nglx=4; ngly=4;
     nglxy=nglx*ngly;
 end
 if (choose_int == 5)
     nglx=5; ngly=5;
     nglxy=nglx*ngly;
 end

[point2,weight2]=feglqd2(nglx,ngly);      % sampling points & weights
[point_b,weight_b]=feglqd2(4,4);          % sampling points & weights

choose_x = menu('Specify path in element','Positive integrasion points','Negative integration points',' -1 ',' 1 ');

if choose_x == 1
    x_path = nglx;
end
if choose_x == 2
    x_path = 1;
end
if choose_x == 3;
    x_path = 1;
end
if choose_x == 4
    x_path = 1;
end

S_matrix = inv(matmtx);

b11 = S_matrix(1,1);
b12 = S_matrix(1,2);
b16 = S_matrix(1,3);
b21 = S_matrix(2,1);
b22 = S_matrix(2,2);
b26 = S_matrix(2,3);
b61 = S_matrix(3,1);
b62 = S_matrix(3,2);
b66 = S_matrix(3,3);
%-------------------------------------------------------------------------
%               Loop over all the elements in path
%-------------------------------------------------------------------------
for E = 1:number_of_elm                        % Loop over all the elements in path
    teller = 1;
    geval = 0;
    Element = Path_element(E,1);
```

```
    for i=1:nnel
        nd(i)=nodes(Path_element(E,1),i);       % extract connected node for (iel)-th element
    end

    if Path_element(E,2) ==1                    % Change the node connectivity, for element on the left
        nd2(:,:) = nd(:,:);
        nd(1,1) = nd2(1,3);
        nd(1,2) = nd2(1,4);
        nd(1,3) = nd2(1,1);
        nd(1,4) = nd2(1,2);
    end

    if Path_element(E,2) ==3                    % Change the node connectivity, for elements on the top
        nd3(:,:) = nd(:,:);
        nd(1,1) = nd3(1,2);
        nd(1,2) = nd3(1,3);
        nd(1,3) = nd3(1,4);
        nd(1,4) = nd3(1,1);
    end

    for i=1:nnel
        xcoord(i)=gcoord(nd(i),1);              % extract x value of the node
        ycoord(i)=gcoord(nd(i),2);              % extract y value of the node
        eldisp(teller,1) = disp(nd(i)*2-1);     % extract u displacement of node
        eldisp(teller+ 1,1) = disp(nd(i)*2);    % extract v displacement of node
        teller = teller + 2;
    end
%-------------------------------------------------------------------------
%        Calculate H and G matrix for path element
%-------------------------------------------------------------------------
    H =sparse(5,5);
    Hp = sparse(5,5);
    G = sparse(5,8);

    for intx=1:4
        xb=point_b(intx,1);                                     % sampling point in x-axis
        wtxb=weight_b(intx,1);                                  % weight in x-axis

        for inty=1:4
            yb=point_b(inty,2);                                 % sampling point in y-axis
            wtyb=weight_b(inty,2) ;                             % weight in y-axis
            [shaped,dhdrd,dhdsd]=feisoq4(xb,yb);                % compute shape functions and x - zeta waarde
                                                                % derivatives at sampling
            jacob2d=fejacob2(nnel,dhdrd,dhdsd,xcoord,ycoord);   % compute Jacobian
            detjacobd=det(jacob2d);                             % determinant of Jacobian
            invjacobd=inv(jacob2d);                             % inverse of Jacobian matrix
            [dhdxd,dhdyd]=federiv2(nnel,dhdrd,dhdsd,invjacobd);% derivatives w.r.t.
            kinmtx2d=fekine2d(nnel,dhdxd,dhdyd);                % B -matrix, compute kinematic matrix
            [Pd,ab] =P_matr(xcoord,ycoord,xb,yb);

            H = H + Pd'*Cinv*Pd*wtxb*wtyb*detjacobd*t;
            G = G + Pd'*kinmtx2d*wtxb*wtyb*detjacobd*t;
         end
   end                                                  % end of numerical integration loop
%-------------- Penalty for PS($\alpha$) formulation ----------------------

    J0 = ab(1,1)*ab(3,2) - ab(3,1)*ab(1,2);
    J1 = ab(1,1)*ab(2,2) - ab(2,1)*ab(1,2);
    J2 = ab(2,1)*ab(3,2) - ab(3,1)*ab(2,2);

    A = (((ab(1,1))^2 + (ab(1,2))^2)*J1^2);
    B = (((ab(3,1))^2 + (ab(3,2))^2)*J2^2);
    C = ((ab(1,1))*(ab(3,1)) + (ab(1,2))*(ab(3,2)))*J1*J2;

    Hp = ((4*t)/(3*J0))*[0 0 0 0 0;
                         0 0 0 0 0;
                         0 0 0 0 0;
                         0 0 0 A C;
```

```
                        0 0 0 C B;];

    H= H + (Alpha/emodule)*Hp;
%-------------------------------------------------------------------------
%              aangrensende element
%-------------------------------------------------------------------------
   if Stress_eq ==3
       if choose_x == 4
           if Path_element(E,1) ~= Path_element(E,3)
           teller2 = 1;
           for i=1:nnel
               nd2(i)=nodes(Path_element(E,3),i);          % extract connected node for (iel)-th element
           end

           if Path_element(E,2) ==1                        % Change the node connectivity, for element on the left
              nd3(:,:) = nd2(:,:);
              nd2(1,1) = nd3(1,3);
              nd2(1,2) = nd3(1,4);
              nd2(1,3) = nd3(1,1);
              nd2(1,4) = nd3(1,2);
           end

           if Path_element(E,2) ==3                        % Change the node connectivity, for elements on the top
              nd3(:,:) = nd2(:,:);
              nd2(1,1) = nd3(1,2);
              nd2(1,2) = nd3(1,3);
              nd2(1,3) = nd3(1,4);
              nd2(1,4) = nd3(1,1);

           end

           for i=1:nnel
               xcoord2(i)=gcoord(nd2(i),1);                % extract x value of the node
               ycoord2(i)=gcoord(nd2(i),2);                % extract y value of the node
               eldisp2(teller2,1) = disp(nd2(i)*2-1);      % extract u displacement of node
               eldisp2(teller2+ 1,1) = disp(nd2(i)*2);     % extract v displacement of node
               teller2 = teller2 + 2;
           end
%-------------------------------------------------------------------------
%               Calculate H and G matrix
%-------------------------------------------------------------------------
           H2 =sparse(5,5);
           Hp2 = sparse(5,5);
           G2 = sparse(5,8);

           for intx=1:4
                xb2=point_b(intx,1);                                    % sampling point in x-axis
                wtxb2=weight_b(intx,1);                                 % weight in x-axis

                for inty=1:4
                    yb2=point_b(inty,2);                                 % sampling point in y-axis
                    wtyb2=weight_b(inty,2) ;                             % weight in y-axis
                    [shaped2,dhdrd2,dhdsd2]=feisoq4(xb2,yb2);            % compute shape functions and x - zeta waarde
                                                                         % derivatives at sampling
                    jacob2d2=fejacob2(nnel,dhdrd2,dhdsd2,xcoord2,ycoord2);  % compute Jacobian
                    detjacobd2=det(jacob2d2);                            % determinant of Jacobian
                    invjacobd2=inv(jacob2d2);                            % inverse of Jacobian matrix
                    [dhdxd2,dhdyd2]=federiv2(nnel,dhdrd2,dhdsd2,invjacobd2);% derivatives w.r.t.
                    kinmtx2d2=fekine2d(nnel,dhdxd2,dhdyd2);              % B -matrix, compute kinematic matrix
                    [Pd2,ab2] =P_matr(xcoord2,ycoord2,xb2,yb2);

                    H2 = H2 + Pd2'*Cinv*Pd2*wtxb2*wtyb2*detjacobd2*t;
                    G2 = G2 + Pd2'*kinmtx2d2*wtxb2*wtyb2*detjacobd2*t;
                end
          end                                                       % end of numerical integration loop
%------------- Penalty for PS($\alpha$) formulation -----------------------

          J02 = ab2(1,1)*ab2(3,2) - ab2(3,1)*ab2(1,2);
```

```
          J12 = ab2(1,1)*ab2(2,2) - ab2(2,1)*ab2(1,2);
          J22 = ab2(2,1)*ab2(3,2) - ab2(3,1)*ab2(2,2);

          A2 = (((ab2(1,1))^2 + (ab2(1,2))^2)*J12^2);
          B2 = (((ab2(3,1))^2 + (ab2(3,2))^2)*J22^2);
          C2 = ((ab2(1,1))*(ab2(3,1)) + (ab2(1,2))*(ab2(3,2)))*J12*J22;

          Hp2 = ((4*t)/(3*J02))*[0 0 0 0 0;
                                 0 0 0 0 0;
                                 0 0 0 0 0;
                                 0 0 0 A2 C2;
                                 0 0 0 C2 B2;];

          H2= H2 + (Alpha/emodule)*Hp2;

      end
   end
end
%-------------------------------------------------------------------------
%        Numerical integration for I
%-------------------------------------------------------------------------
        for intx=x_path
            x=point2(intx,1);                                  % sampling point in x-axis
            if choose_x == 3
                x = -1.0;
            end
            if choose_x == 4
                x = 1;
            end

            for inty=1:ngly
                y=point2(inty,2);                              % sampling point in y-axis
                wty=weight2(inty,2);                           % weight in y-axis
                [shape,dhdr,dhds]=feisoq4(x,y);                % compute shape functions and
                jacob2=fejacob2(nnel,dhdr,dhds,xcoord,ycoord); % compute Jacobian
                detjacob=det(jacob2);                          % determinant of Jacobian
                invjacob=inv(jacob2);                          % inverse of Jacobian matrix
                [dhdx,dhdy]=federiv2(nnel,dhdr,dhds,invjacob); % derivatives of shape functions w.r.t.
                                                               % physical coordinate
                dxdr = jacob2(1,1);                            % derivative of x with respect to r
                dydr = jacob2(1,2);                            % derivative of y with respect to r
                dxds = jacob2(2,1);                            % derivative of x with respect to s
                dyds = jacob2(2,2);                            % derivative of y with respect to s

                kinmtx2 = fekine2d(nnel,dhdx,dhdy);            % compute kinematic matrix
                kinmtx2_omgekeer = fekine_J(nnel,dhdx,dhdy);

                dudx_dvdy=kinmtx2*eldisp;                      % compute strains in integration point

                [P,ab] =P_matr(xcoord,ycoord,x,y);             % compute P matrix for path element
                Beta = inv(H)*G*eldisp;                        % determin Beta for path element
                Stress = P*Beta;                               % calculate stress for path element

                if Stress_eq == 3
                    if choose_x == 4
                        if Path_element(E,1) ~= Path_element(E,3)
                           Stress2 = Stress;                                % calculate stress for path element
                           [P2,ab2] = P_matr(xcoord2,ycoord2,-1,y);         % compute P matrix for adjacent element
                           Beta2 = inv(H2)*G2*eldisp2;                      % determin Beta for adjacent element
                           Stress3 = P2*Beta2;                              % calculate stress for adjacent element

                           % Calculate average stress on element bound
                           Stress4(1,1) = 0.5*(Stress2(1,1) + Stress3(1,1));
                           Stress4(2,1) = 0.5*(Stress2(2,1) + Stress3(2,1));
                           Stress4(3,1) = 0.5*(Stress2(3,1) + Stress3(3,1));
                        end
                    end
                end
```

```
                dudy_dvdx = kinmtx2_omgekeer*eldisp;

                dudx = dudx_dvdy(1,1);                          % Strain xx (dudx)
                dvdy = dudx_dvdy(2,1);                          % Strain yy (dvdy)

                dudy = dudy_dvdx(1,1);                          % dudy derivative of u with respect to y
                dvdx = dudy_dvdx(2,1);                          % dvdx derivative of v wiht respect to x

                estrain(1,1) = dudx_dvdy(1,1);                  % strain xx
                estrain(3,1) = dudx_dvdy(3,1);                  % strain xy
                estrain(2,1) = dudx_dvdy(2,1);                  % strain yy

                if Stress_eq == 3
                    if choose_x == 4
                        if Path_element(E,1) ~= Path_element(E,3)
                            Stress = Stress4(1:3,1);
                        end
                    end
                end

                estress(1,1) = Stress(1,1);                     % stress xx
                estress(2,1) = Stress(2,1);                     % stress yy
                estress(3,1) = Stress(3,1);                     % stress xy

                % Complementary strain energy
                B = (1/2)*((b11*estress(1,1) + (b12)*estress(2,1) + b16*estress(3,1))*estress(1,1) + ...
                ((b21)*estress(1,1) + (b22)*estress(2,1) + b26*estress(3,1))*estress(2,1) + ...
                ((b61)*estress(1,1) + b62*estress(2,1) + b66*estress(3,1))*estress(3,1));

                % Calculate terms in I ingtegral
                Term2 = (dudy*estress(3,1) + dvdy*estress(2,1));
                Term3 = (dudx*estress(3,1) + dvdx*estress(2,1));

                Bdy = B*dyds;
                Term2dy = Term2*dyds;
                Term3dx = Term3*dxds;

                I(E,1) = I(E,1) + (-Bdy + Term2dy + Term3dx)*wty;

            end
        end
end

L = length(I);
I_tot = 0;

for i = 1:L
    I_tot = I(i)+ I_tot;
end
I_totaal = abs(2*I_tot); % Calculate total I integral

K1 = sqrt(I_totaal*(emodule/(1-poisson^2))); % Calculate stress intensity factor

end
```

C.3 Element: Element with drilling degrees of freedom (8$\beta\alpha$) for composite material

C.3.1 Element routines: Main program

```
function Drilling_element_8BA
```

```
clear all;
[props,joints,loads,nnode,restraints,nd_d4d,begin_Jnode,Type] = choose;
iopt2 = menu('Choose the amount of integration points for the penalty','Displacement model','mixed formulation');
path(path,'./functions')
%-------------------------------------------------------------------------
%           Material type
%-------------------------------------------------------------------------
thick = 0;
matmtx = zeros(3,3);
[layer,junk] = size(props);
for i = 1:layer
    emodule1(i) = props(i,1);
    emodule2(i) = props(i,2);
    poisson12(i) = props(i,4);
    G12(i) = props(i,3);
    t(i) = props(i,5);
    theta(i) = (pi/180)*(props(i,6));
    thick = thick + t(i);
end

for laag = 1:layer
    matmtx = matmtx + Compfematiso(props(laag,1),props(laag,2),props(laag,4),theta(laag),props(laag,5),props(laag,3));
end

Cinv = inv(matmtx);
%-------------------------------------------------------------------------
% initialize
%-------------------------------------------------------------------------
kkuu=sparse(nnode*6,nnode*6);
ff=sparse(nnode*6,1);
qq=sparse(nnode,1);
uu=sparse(nnode*6,1);
[Total_elm,junk] = size(nd_d4d);

BBGG = zeros(3,12,props(1,7),Total_elm);
PP = zeros(3,8,props(1,7),Total_elm);
H_M = zeros(8,8,Total_elm);
G_M = zeros(8,12,Total_elm);
HP_M = zeros(8,8,Total_elm);
bbgg = zeros(1,12,Total_elm);
Po_M = zeros(3,8,Total_elm);
he_el = zeros(12,1,Total_elm);
area_el = zeros(1,Total_elm);
gamma_el = zeros(1,Total_elm);

%-------------------------------------------------------------------------
% process boundary conditions
%-------------------------------------------------------------------------
[bcdofval]  = essboundy(restraints);
[ff] = natboundary(1,loads,ff);
%-------------------------------------------------------------------------
% process drilling dof elements
%-------------------------------------------------------------------------
fprintf('Processing D4d elements ...\n')
[nel_d4d,temp] = size(nd_d4d);

if nel_d4d~=0;
    h = waitbar(0,'Processing D4d elements. Please wait...');

    for id4d = 1:nel_d4d
        waitbar(id4d/nel_d4d,h);
        elno = id4d;                    % [elno] extract element number
        nodes = nd_d4d(id4d,1:4);       % [nodes] extract nodes
        for j=1:length(nodes)           % [gcoord] extract nodal coordinates
            inode = nodes(j);
            gcoord(j,1:3) = joints(inode,1:3);
        end
```

```
        [kkuu,bcdofval,BG,Hmatr,Gmatr,HPmatr,P_int,he,area,gamma] =
                  d4d(nodes,props,gcoord,kkuu,bcdofval,id4d,iopt2,matmtx,thick);
        BBGG(:,:,:,id4d) = BG;
        PP(:,:,:,id4d) = P_int;
        H_M(:,:,id4d) = Hmatr;
        G_M(:,:,id4d)= Gmatr;
        HP_M(:,:,id4d) = HPmatr;
        he_el(:,:,id4d) = he;
        area_el(1,id4d) = area;
        gamma_el(1,id4d) = gamma;

    end
close(h)
end

matmtx=fematiso(iopt,props(1,2),props(1,3));
fprintf('Processing D4d elements COMPLETE.\n')
%-----------------------------------------------------------------
% solve system of equations
%-----------------------------------------------------------------
fprintf('Solving ...\n')
[uu] = solvefem(kkuu,ff,bcdofval,nnode);
fprintf('Solving COMPLETE.\n')
%-----------------------------------------------------------------
% solve system stress
%-----------------------------------------------------------------
[nel d]=size(nd_d4d);     % number of elements
nnel=4;
for element_nom = 1:nel
    nodes = nd_d4d(element_nom,1:4);

    for i = 1:4
        displacement((i*3)-2,1) = disp((nodes(1,i))*6 - 5);
        displacement((i*3)-1,1) = disp((nodes(1,i))*6 - 4);
        displacement((i*3)  ,1) = disp((nodes(1,i))*6);
    end

    Beta = inv(H_M(:,:,element_nom))*G_M(:,:,element_nom)*displacement;

    for teller = 1:ninpt
        Stress(teller,:,element_nom) = PP(:,:,teller,element_nom)*Beta;
        [s1,s2,VonM] = Stress_funk(Stress(teller,:,element_nom));
    end
    if iopt2 ==2
        tau_o(1,element_nom) = (
           gamma_el(1,element_nom)/(area_el(1,element_nom)*elprop(1,1)))*he_el(:,:,element_nom)'*displacement;
    end
end

%-------------------------------------------------------------------------
%           Material properties
%-------------------------------------------------------------------------
props = elprop;
poisson = props(1,3);
emodule = props(1,2);
if iopt == 1
     kappa = (3-poisson)/(1+poisson);
end
if iopt == 2
    kappa = (3 - 4*poisson);
end
shear_m = emodule/(2*(1+poisson));         % shear modules
%=========================================================================
%       Post Processing
%=========================================================================
choose12=menu('POST PROCESSING','K1 evaluation (Disp extra)','Plot displacement','Plot stresses',
              'Jplot','J integral','I integral','Exit');
```

```
while choose12 ~= 7
  if (choose12 == 1)
        %-------------------------------------------------------------------------
        %   K1 evaluasie deur displacement extrapolation
        %-------------------------------------------------------------------------
        [K1] = K1_dis_extra(nel,nnel,props(1,3),props(1,2),joints,nd_d4d,iopt,uu)
  end
  if (choose12 == 2)
        %-------------------------------------------------------------------------
        %  Plot the displacement of nodes
        %-------------------------------------------------------------------------
        displot_drill(uu,joints,nd_d4d);
  end
  if (choose12 == 3)
        %-------------------------------------------------------------------------
        %  Plot a countour map of the stresses
        %-------------------------------------------------------------------------
        CONPLOT4_br(Counter,Sigma,StressXY,gcoord,nodes);
  end
  if (choose12 == 4)
        %-------------------------------------------------------------------------
        %  Help to select path for J integral
        %-------------------------------------------------------------------------
     [Path_element] = Jplot4(displace,gcoord,nodes,begin_Jnode)
  end
  if (choose12 == 5)
        %-------------------------------------------------------------------------
        %  J integral to determine Stress intensity
        %-------------------------------------------------------------------------
        [K1,J] = J_integral2_Drill(4,matmtx,nd_d4d,joints,uu,iopt,poisson,emodule,begin_Jnode,Type);
  end
  if choose12 == 6
        %-------------------------------------------------------------------
        %  I integral to determine Stress intensity
        %-------------------------------------------------------------------
        [K1,I] = I_integral_8BA(4,matmtx,nd_d4d,joints,uu,iopt,poisson,emodule,begin_Jnode,Type,elprop(1,4),elprop(1,1));
  end
 close all;
 choose12=menu('POST PROCESSING','K1 evaluation (Disp extra)','Plot displacement','Plot stresses',
               'Jplot','J integral','I integral','Exit');
end
close all;
```

C.3.2 Element routines: Stiffness matrix

```
function [kk,bcdofval,BG_T,Hmatr,Gmatr,HPmatr,P_int,he,area,gamma] =
d4d(nodes,props,gcoord,kk,bcdofval,element_nom,iopt2,matmtx,thick);

nintpts = props(1,7); % integration scheme for main part of k
G12 = props(1,3);
gamma = G12;
%-------------------------------------------------------------
% additional inputs <defaults>
%-------------------------------------------------------------
nintpts_pen = 1;          % integration scheme for penalty
nintpts_tay = 4;          % integration scheme for locking correction
%-------------------------------------------------------------
% input data for control parameters
%-------------------------------------------------------------
nnel=4;                  % number of nodes per element
ndof=3;                  % number of dofs per node
edof=nnel*ndof;          % degrees of freedom per element
%-------------------------------------------------------------
% initialization of matrices and vectors
```

```
%-------------------------------------------------------------
index=zeros(edof,1);     % index vector
kinmtx2=zeros(3,edof);   % kinematic matrix
matmtx=zeros(3,3);       % constitutive matrix
k=zeros(edof,edof);      % initialization of element matrix to zero
ke=zeros(edof,edof);     % initialization of element matrix to zero
he = zeros(12,1);        % initialization of element matrix to zero
kp=zeros(edof,edof);     % initialization of element matrix to zero
taycorr=zeros(3,4);      % initialization of element matrix to zero
H = zeros(8,8);          % initialization of element matrix to zero
HP = zeros(8,8);         % initialization of element matrix to zero
G = zeros(8,12);         % initialization of element matrix to zero
%-------------------------------------------------------------
% computation of element matrices and vectors and their assembly
%-------------------------------------------------------------
[rsk,wtk]=intsch(nintpts);            % integration points and weights
[rspen,wtpen]=intsch(nintpts_pen);    % integration points and weights
[rstay,wttay]=intsch(nintpts_tay);    % integration points and weights

Cinv = inv(matmtx);                   % material constitutive matrix

for i=1:nnel
    xcoord(i)=gcoord(i,1);            % extract x value of the node
    ycoord(i)=gcoord(i,2);            % extract y value of the node
end
[l_cos_sin]=alpha_l(xcoord,ycoord);   % side lengths, cos(alpha) and sin(alpha)
[area] = quad_area(xcoord,ycoord);    % element area
%-------------------------------------------------------------
%  numerical integration (locking correction)
%-------------------------------------------------------------
[nintp,junk]=size(rstay);
for intp=1:4
    r=rstay(intp,1);
    s=rstay(intp,2);
    wtr=wttay(intp,1);
    wts=wttay(intp,2);

    [shape,dhdr,dhds]=feisoq4(r,s);      % compute shape functions and derivatives at sampling point (NI)
    [shape8,dhdr8,dhds8]=feisonsi8(r,s); % compute shape functions and derivatives at sampling point (NSI)

    jacob2=fejacob2(nnel,dhdr,dhds,xcoord,ycoord);     % compute Jacobian
    detjacob=det(jacob2);                              % determinant of Jacobian
    invjacob=inv(jacob2);                              % inverse of Jacobian matrix

    [dhdx8,dhdy8]=federiv2(nnel,dhdr8,dhds8,invjacob); % derivatives w.r.t. physical coordinate
    GI = fekinegi(nnel,dhdx8,dhdy8,l_cos_sin);         % compute kinematic matrix [GI]
    %-----------------------------------------------------------
    %  compute element matrix
    %-----------------------------------------------------------
    taycorr = taycorr + GI*wtr*wts*detjacob;
end                                                    % end of numerical integration loop

taycorr=taycorr/area;
%-------------------------------------------------------------
%  numerical integration (ke)
%-------------------------------------------------------------
[nintp,junk]=size(rsk);

BG_T = zeros(3,12,nintp);
P_int = zeros(3,8,nintp);
Hmatr = zeros(8,8);
HPmatr = zeros(8,8);
Gmatr = zeros(8,12);

for intp=1:nintp
    r=rsk(intp,1);
    s=rsk(intp,2);
    wtr=wtk(intp,1);
```

```
    wts=wtk(intp,2);

    [shape,dhdr,dhds]=feisoq4(r,s);      % compute shape functions and derivatives at sampling point (NI)
    [shape8,dhdr8,dhds8]=feisonsi8(r,s); % compute shape functions and derivatives at sampling point (NSI)

    jacob2=fejacob2(nnel,dhdr,dhds,xcoord,ycoord);     % compute Jacobian
    detjacob=det(jacob2);                              % determinant of Jacobian
    invjacob=inv(jacob2);                              % inverse of Jacobian matrix

    [dhdx,dhdy]=federiv2(nnel,dhdr,dhds,invjacob);     % derivatives w.r.t. physical coordinate
    [dhdx8,dhdy8]=federiv2(nnel,dhdr8,dhds8,invjacob); % derivatives w.r.t. physical coordinate

    BI = fekine2d(nnel,dhdx,dhdy);                     % compute kinematic matrix [BI]
    GI = fekinegi(nnel,dhdx8,dhdy8,l_cos_sin);         % compute kinematic matrix [GI]

    GI = GI-(taycorr);
    BG=[BI(:,1:2) GI(:,1) BI(:,3:4) GI(:,2) BI(:,5:6) GI(:,3) BI(:,7:8) GI(:,4)];
    BG_T(:,:,intp) = BG;

    [P] = Pmatrix(r,s,xcoord,ycoord);
    P_int(:,:,intp) = P;
    [Po] = Pmatrix(0,0,xcoord,ycoord);

    H = H + P'*Cinv*P*wtr*wts*detjacob*thick;
    G = G + P'*BG*wtr*wts*detjacob*thick;

end                                                    % end of numerical integration loop

for intp=1:nintp
    r=rsk(intp,1);
    s=rsk(intp,2);
    wtr=wtk(intp,1);
    wts=wtk(intp,2);

    [shape,dhdr,dhds]=feisoq4(r,s);      % compute shape functions and derivatives at sampling point (NI)
    [shape8,dhdr8,dhds8]=feisonsi8(r,s); % compute shape functions and derivatives at sampling point (NSI)

    jacob2=fejacob2(nnel,dhdr,dhds,xcoord,ycoord);     % compute Jacobian
    detjacob=det(jacob2);                              % determinant of Jacobian
    invjacob=inv(jacob2);                              % inverse of Jacobian matrix

    [dhdx,dhdy]=federiv2(nnel,dhdr,dhds,invjacob);     % derivatives w.r.t. physical coordinate
    [dhdx8,dhdy8]=federiv2(nnel,dhdr8,dhds8,invjacob); % derivatives w.r.t. physical coordinate

    [PD] = PDmatrix(r,s,xcoord,ycoord,jacob2(1,1),jacob2(2,2),jacob2(1,2),jacob2(2,1),detjacob);
    HP = HP + PD'*PD*wtr*wts*detjacob*thick;

end                                                    % end of numerical integration loop

alpha = 1000;
H = H + alpha*HP;
Hmatr(:,:) = H;
Gmatr(:,:) = G;
HPmatr(:,:) = HP;
ke = G'*inv(H)*G;

if iopt2 == 1
    %=========================================================================
    %                   Penelty met 1 punt
    %=========================================================================
    %-----------------------------------------------------------
    %  numerical integration (kp)
    %-----------------------------------------------------------
    [nintp,junk]=size(rspen);

for intp=1:1
    r=rspen(intp,1);
    s=rspen(intp,2);
```

```
    wtr=wtpen(intp,1);
    wts=wtpen(intp,2);

    [shape,dhdr,dhds]=feisoq4(r,s);      % compute shape functions and derivatives at sampling point (NI)
    [shape8,dhdr8,dhds8]=feisonsi8(r,s); % compute shape functions and derivatives at sampling point (NSI)

    jacob2=fejacob2(nnel,dhdr,dhds,xcoord,ycoord);        % compute Jacobian
    detjacob=det(jacob2);                                 % determinant of Jacobian
    invjacob=inv(jacob2);                                 % inverse of Jacobian matrix

    [dhdx,dhdy]=federiv2(nnel,dhdr,dhds,invjacob);        % derivatives w.r.t. physical coordinate
    [dhdx8,dhdy8]=federiv2(nnel,dhdr8,dhds8,invjacob);    % derivatives w.r.t. physical coordinate
    bi = fekine2dpenal(nnel,dhdx,dhdy);                   % compute kinematic matrix [bi]
    gi = fekinegipenal(nnel,dhdx8,dhdy8,l_cos_sin,shape); % compute kinematic matrix [gi]
    bg= [bi(:,1:2) gi(:,1) bi(:,3:4) gi(:,2) bi(:,5:6) gi(:,3) bi(:,7:8) gi(:,4)];

    %-------------------------------------------------------------
    %  compute element matrix
    %-------------------------------------------------------------
    kp = kp + gamma*bg'*bg*wtr*wts*detjacob*thick;
end                                                    % end of numerical integration loop
end

if iopt2 == 2
%=========================================================================
%           Penelty met 4 punt
%=========================================================================

%-------------------------------------------------------------
%  numerical integration (kp)
%-------------------------------------------------------------
[nintp,junk]=size(rspen);

for intp=1:4
    r=rstay(intp,1);
    s=rstay(intp,2);
    wtr=wttay(intp,1);
    wts=wttay(intp,2);

    [shape,dhdr,dhds]=feisoq4(r,s);      % compute shape functions and derivatives at sampling point (NI)
    [shape8,dhdr8,dhds8]=feisonsi8(r,s); % compute shape functions and derivatives at sampling point (NSI)

    jacob2=fejacob2(nnel,dhdr,dhds,xcoord,ycoord);        % compute Jacobian
    detjacob=det(jacob2);                                 % determinant of Jacobian
    invjacob=inv(jacob2);                                 % inverse of Jacobian matrix

    [dhdx,dhdy]=federiv2(nnel,dhdr,dhds,invjacob);        % derivatives w.r.t. physical coordinate
    [dhdx8,dhdy8]=federiv2(nnel,dhdr8,dhds8,invjacob);    % derivatives w.r.t. physical coordinate
    bi = fekine2dpenal(nnel,dhdx,dhdy);                   % compute kinematic matrix [bi]
    gi = fekinegipenal(nnel,dhdx8,dhdy8,l_cos_sin,shape); % compute kinematic matrix [gi]
    bg= [bi(:,1:2) gi(:,1) bi(:,3:4) gi(:,2) bi(:,5:6) gi(:,3) bi(:,7:8) gi(:,4)];

    %-----------------------------------------------------------
    %  compute element matrix
    %-----------------------------------------------------------
    he = he + bg'*wtr*wts*detjacob*thick;

end % end of numerical integration loop
kp= (gamma/(area*thick))*he*he';
end
k = ke + kp;
%-------------------------------------------------------------
% expand local stiffness matrix
%-------------------------------------------------------------
sparsek = sparse(k);
clear k
index_red = [1 2 3 4  5  6  7  8 9 10 11 12];% entries in reduced local stiffness matrix with 2 dof per node
index_ful = [1 2 6 7 8 12 13 14 18 19 20 24];% entries in full local stiffness matrix with 6 dof per node
```

```
k = sparse(6*nnel, 6*nnel);
k(index_ful,index_ful) = k(index_ful,index_ful) + sparsek(index_red,index_red);
%------------------------------------------------------------
% assemble global stiffness matrix
%------------------------------------------------------------
index=feeldof(nodes,nnel,6); % extract system dofs associated with element
kk=feasmbl1(kk,k,index);     % assemble element matrices
%------------------------------------------------------------
% append the boundary condition matrix
%------------------------------------------------------------
for j=1:nnel
    nd = nodes(j);
    addbc = [((nd-1)*6 + 3) 0
        ((nd-1)*6 + 4) 0
        ((nd-1)*6 + 5) 0];
    bcdofval = union(bcdofval,addbc,'rows');
end
% ******************************************************* %
```

C.3.3 Element routines: P matrix for 8β

```
function [P] = Pmatrix(R,S,xcoord,ycoord);
%-------------------------------------------------------
%   P matrix for 8$\beta \alpha$
%-------------------------------------------------------
P = zeros(3,8);
Phigh = zeros(3,5);

P(1,1) = 1;
P(2,2) = 1;
P(3,3) = 1;

Phigh = [S 0 R 0 S^2;
         0 R 0 S -R^2;
         0 0 -S -R 0;];

A1 = (- xcoord(1) + xcoord(2) + xcoord(3) - xcoord(4))/4;
A2 = (- xcoord(1) - xcoord(2) + xcoord(3) + xcoord(4))/4;
B1 = (- ycoord(1) + ycoord(2) + ycoord(3) - ycoord(4))/4;
B2 = (- ycoord(1) - ycoord(2) + ycoord(3) + ycoord(4))/4;

To(1,1)=A1*A1;
To(1,2)=A2*A2;
To(1,3)=A1*A2*2;
To(2,1)=B1*B1;
To(2,2)=B2*B2;
To(2,3)=B1*B2*2;
To(3,1)=A1*B1;
To(3,2)=A2*B2;
To(3,3)=A1*B2+A2*B1;

P_2 = To*Phigh;

P(1,4) = P_2(1,1);
P(1,5) = P_2(1,2);
P(1,6) = P_2(1,3);
P(1,7) = P_2(1,4);
P(1,8) = P_2(1,5);

P(2,4) = P_2(2,1);
P(2,5) = P_2(2,2);
P(2,6) = P_2(2,3);
P(2,7) = P_2(2,4);
P(2,8) = P_2(2,5);
```

```
P(3,4) = P_2(3,1);
P(3,5) = P_2(3,2);
P(3,6) = P_2(3,3);
P(3,7) = P_2(3,4);
P(3,8) = P_2(3,5);
```

C.3.4 Element routines: P matrix for 9β

```
function [P] = Pmatrix(R,S,xcoord,ycoord)
%-------------------------------------------------------
%   P matrix for 8$\beta \alpha$
%-------------------------------------------------------
P = zeros(3,9);

P(1,1) = 1;
P(2,2) = 1;
P(3,3) = 1;

Phigh = [S 0  R   0  S^2   0;
         0 R  0   S   0  -R^2;
         0 0 -S  -R   0    0;];

A1 = (- xcoord(1) + xcoord(2) + xcoord(3) - xcoord(4))/4;
A2 = (- xcoord(1) - xcoord(2) + xcoord(3) + xcoord(4))/4;
B1 = (- ycoord(1) + ycoord(2) + ycoord(3) - ycoord(4))/4;
B2 = (- ycoord(1) - ycoord(2) + ycoord(3) + ycoord(4))/4;

To(1,1)=A1*A1;
To(1,2)=A2*A2;
To(1,3)=A1*A2*2;
To(2,1)=B1*B1;
To(2,2)=B2*B2;
To(2,3)=B1*B2*2;
To(3,1)=A1*B1;
To(3,2)=A2*B2;
To(3,3)=A1*B2+A2*B1;

P_2 = To*Phigh;

P(1,4) = P_2(1,1);
P(1,5) = P_2(1,2);
P(1,6) = P_2(1,3);
P(1,7) = P_2(1,4);
P(1,8) = P_2(1,5);
P(1,9) = P_2(1,6);

P(2,4) = P_2(2,1);
P(2,5) = P_2(2,2);
P(2,6) = P_2(2,3);
P(2,7) = P_2(2,4);
P(2,8) = P_2(2,5);
P(2,9) = P_2(2,6);

P(3,4) = P_2(3,1);
P(3,5) = P_2(3,2);
P(3,6) = P_2(3,3);
P(3,7) = P_2(3,4);
P(3,8) = P_2(3,5);
P(3,9) = P_2(3,6);
```

C.3.5 Element routines: Material matrix for composite material

```
function  [matmtx] = Compfematiso(E1,E2,v12,theta,t,G12);

v21 = v12*E2/E1;
Q11 = E1/(1-v12*v21);
Q22 = E2/(1-v12*v21);
Q12_2 = (v21*E1)/(1-v21*v12);
Q12 = (v12*E2)/(1-v12*v21);
Q66 = G12;

Q = [Q11 Q12 0;
     Q12 Q22 0;
     0 0 Q66;];

T = [(cos(theta))^2 (sin(theta))^2  2*(cos(theta))*sin(theta);
     (sin(theta))^2 (cos(theta))^2  (-2*(cos(theta))*(sin(theta)));
     (-1*(cos(theta))*sin(theta)) (cos(theta))*sin(theta) (cos(theta))^2 - (sin(theta)^2)];

T_inv = [(cos(theta))^2 (sin(theta))^2 (-2*(sin(theta))*cos(theta));
         (sin(theta))^2 (cos(theta))^2 2*(cos(theta))*(sin(theta));
         (cos(theta))*sin(theta) (-1*(cos(theta))*sin(theta)) (cos(theta))^2 - (sin(theta)^2)];

R = [ 1 0 0;
    0 1 0;
    0 0 2;];

R_inv = [ 1 0 0;
        0 1 0;
        0 0 0.5];

matmtx = T_inv*Q*R*T*R_inv;
matmtx = [matmtx(1,1)*t matmtx(1,2)*t matmtx(1,3)*t;
          matmtx(2,1)*t matmtx(2,2)*t matmtx(2,3)*t;
          matmtx(3,1)*t matmtx(3,2)*t matmtx(3,3)*t;];
```

C.4 Element: Q4 with penalized equilibrium

C.4.1 Element routines: Main program

```
%=====================================================================%
%             Patchtest for Q4 with penelty                           %
%=====================================================================%
% Variable descriptions : Same as Q4
%---------------------------------------------------------------------
clear all;
%---------------------------------------------------------------------
% Load Mesh and define integration scheme
%---------------------------------------------------------------------
[gcoord,nodes,bcdof,bcval,ff,emodule,poisson,t,choose3,Type,begin_Jnode] = kieslys;
[nglx,ngly,nglxy] = integration_points;
%-----------------------------------
%  input data for control parameters
%-----------------------------------
nel=5;                    % number of elements
nnel=4;                   % number of nodes per element
ndof=2;                   % number of dofs per node
nnode=8;                  % total number of nodes in system
sdof=nnode*ndof;          % total system dofs
edof=nnel*ndof;           % degrees of freedom per element
emodule=1;                % elastic modulus
poisson=0.25;             % Poisson's ratio
nglx=3; ngly=3;           % 3x3 Gauss-Legendre quadrature
```

```
nglxy=nglx*ngly;         % number of sampling points per element
%----------------------------------------
%  initialization of matrices and vectors
%----------------------------------------
ff=zeros(sdof,1);       % system force vector
kk=zeros(sdof,sdof);    % system matrix
kke=zeros(sdof,sdof);
disp=zeros(sdof,1);     % system displacement vector
eldisp=zeros(edof,1);   % element displacement vector
stress=zeros(nglxy,3);  % matrix containing stress components
strain=zeros(nglxy,3);  % matrix containing strain components
index=zeros(edof,1);    % index vector
kinmtx2=zeros(3,edof);  % kinematic matrix
matmtx=zeros(3,3);      % constitutive matrix
dispcoord=zeros(sdof,2);% coordinates position with force aplied
% ---------------------------------------------------------
% MENU DISPLAY (SELECTION OF PLANE STRESS OR PLANE STRAIN)
% ---------------------------------------------------------
iopt = menu('Choose the method of solving','Plane strain','Plane Stress');
if iopt == 1
   Plane=1;
end
if iopt == 2
   Plane=2;
end
%-----------------------------------------------------------------
%  computation of element matrices and vectors and their assembly
%-----------------------------------------------------------------
[point2,weight2]=feglqd2(nglx,ngly);       % sampling points & weights
matmtx=fematiso(iopt,emodule,poisson);     % compute constitutive matrix

for iel=1:nel           % loop for the total number of elements
 xcoord = zeros(1,4);
 ycoord = zeros(1,4);
    for i=1:4
        nd(i)=nodes(iel,i);         % extract connected node for (iel)-th element
        xcoord(i)=gcoord(nd(i),1);  % extract x value of the node
        ycoord(i)=gcoord(nd(i),2);  % extract y value of the node
    end

    k=zeros(edof,edof);         % initialization of element matrix to zero
    ke = zeros(edof,edof);
%--------------------------------
%  numerical integration
%--------------------------------
   for intx=1:nglx
        x=point2(intx,1);                  % sampling point in x-axis
        wtx=weight2(intx,1);               % weight in x-axis

   for inty=1:ngly
        y=point2(inty,2);                  % sampling point in y-axis
        wty=weight2(inty,2) ;              % weight in y-axis

    [shape,dhdr,dhds]=feisoq4(x,y);               % compute shape functions and
                                                  % derivatives at sampling point
    jacob2=fejacob2(nnel,dhdr,dhds,xcoord,ycoord); % compute Jacobian
    detjacob=det(jacob2);                         % determinant of Jacobian
    invjacob=inv(jacob2);                         % inverse of Jacobian matrix
    [dhdx,dhdy]=federiv2(nnel,dhdr,dhds,invjacob); % derivatives w.r.t.
                                                  % physical coordinate
    kinmtx2=fekine2d(nnel,dhdx,dhdy);             % compute kinematic matrix
%------------------------------
%  compute element matrix
%------------------------------
    k=k+kinmtx2'*matmtx*kinmtx2*wtx*wty*detjacob;  % element matrix
    ke =ke + Penelty_db(xcoord',ycoord',x,y,poisson,emodule);
    end
    end                                  % end of numerical integration loop
```

```
    index=feeldof(nd,nnel,ndof);          % extract system dofs associated with element
    kk=feasmbl1(kk,k,index);              % assemble element matrices
    kke = feasmbl1(kke,ke,index);
end
Alfa = 0.1;
Pen =(kk - (Alfa/emodule)* kke)
%----------------------------
%   apply boundary conditions
%----------------------------
[Pen,ff]=feaplyc2(Pen,ff,bcdof,bcval);
%----------------------------
%  solve the matrix equation
%----------------------------
disp=Pen\ff;
num=1:1:sdof;
displace=[num' disp]                  % print nodal displacements
%--------------------------------------
%  element stress computation
%--------------------------------------
for ielp=1:nel             % loop for the total number of elements

    for i=1:nnel
        nd(i)=nodes(ielp,i);        % extract connected node for (iel)-th element
        xcoord(i)=gcoord(nd(i),1);  % extract x value of the node
        ycoord(i)=gcoord(nd(i),2);  % extract y value of the node
    en
%--------------------------------
%  numerical integration
%--------------------------------
    intp=0;

    for intx=1:nglx
        x=point2(intx,1);                  % sampling point in x-axis
        wtx=weight2(intx,1);               % weight in x-axis

   for inty=1:ngly
        y=point2(inty,2);                  % sampling point in y-axis
        wty=weight2(inty,2) ;              % weight in y-axis
        intp=intp+1;

    [shape,dhdr,dhds]=feisoq4(x,y);               % compute shape functions and
                                                  % derivatives at sampling point
    jacob2=fejacob2(nnel,dhdr,dhds,xcoord,ycoord); % compute Jacobian
    detjacob=det(jacob2);                         % determinant of Jacobian
    invjacob=inv(jacob2);                         % inverse of Jacobian matrix
    [dhdx,dhdy]=federiv2(nnel,dhdr,dhds,invjacob); % derivatives w.r.t.
                                                  % physical coordinate
    kinmtx2=fekine2d(nnel,dhdx,dhdy);             % kinematic matrix
    index=feeldof(nd,nnel,ndof);                  % extract system dofs for the element
%-------------------------------------------------------
%  extract element displacement vector
%-------------------------------------------------------
    for i=1:edof
        eldisp(i)=disp(index(i));
    end
    kinmtx2=fekine2d(nnel,dhdx,dhdy);  % compute kinematic matrix
    estrain=kinmtx2*eldisp             % compute strains
    estress=matmtx*estrain             % compute stresses

    for i=1:3
        strain(intp,i)=estrain(i);          % store for each element
        stress(intp,i)=estress(i);          % store for each element
    end

    location=[ielp,intx,inty];         % print location for stress
    stress(intp,:) ;                   % print stress values

    Sm(ielp,1) =ielp;
```

```
    Sm(ielp,2) =stress(intp,1);
    Sm(ielp,3) =stress(intp,2);
    Sm(ielp,4) =stress(intp,3);
    end
    end                                % end of integration loop
end
%-----------------------------------------------------
%  Plot the displacement of nodes
%-----------------------------------------------------

% Plot the relative diplacement
[dispcoord]=displot(displace,gcoord,nodes);
%-------------------------------------------------------------
```

C.4.2 Element routines: Calculate penalized stiffness matrix

```
function [kPe] = Penelty_db(xn,yn,x,y,v,E);

syms r s L P real;

kPe = zeros(8,8);
[h,hr,hs,hrs] = Q4vorm;
[hxx,hyy,hxy,hx,hy,detJ] = Afgeleidevormfunk(h,hr,hs,hrs,xn,yn);

 h1xx = subs(hxx(1),{s,r},{x,y});
 h2xx = subs(hxx(2),{s,r},{x,y});
 h3xx = subs(hxx(3),{s,r},{x,y});
 h4xx = subs(hxx(4),{s,r},{x,y});

 h1yy = subs(hyy(1),{s,r},{x,y});
 h2yy = subs(hyy(2),{s,r},{x,y});
 h3yy = subs(hyy(3),{s,r},{x,y});
 h4yy = subs(hyy(4),{s,r},{x,y});

 h1xy = subs(hxy(1),{s,r},{x,y});
 h2xy = subs(hxy(2),{s,r},{x,y});
 h3xy = subs(hxy(3),{s,r},{x,y});
 h4xy = subs(hxy(4),{s,r},{x,y});

 h1x = subs(hx(1),{s,r},{x,y});
 h2x = subs(hx(2),{s,r},{x,y});
 h3x = subs(hx(3),{s,r},{x,y});
 h4x = subs(hx(4),{s,r},{x,y});

 h1y = subs(hy(1),{s,r},{x,y});
 h2y = subs(hy(2),{s,r},{x,y});
 h3y = subs(hy(3),{s,r},{x,y});
 h4y = subs(hy(4),{s,r},{x,y});

% ----------------B matriks-----------------
B = [h1x 0 h2x 0 h3x 0 h4x 0
       0 h1y 0 h2y 0 h3y 0 h4y
     h1y h1x h2y h2x h3y h3x h4y h4x];

Btrans = transpose(B);

% ----------------dB = d(CB)---------------
dB =((E/(1-v^2))*[ (v*h1xx+((1-v)/2)*h1yy)  (v*h1xy + ((1-v)/2)*h1xy)   (v*h2xx+((1-v)/2)*h2yy) ...
     (v*h2xy + ((1-v)/2)*h2xy) (v*h3xx+((1-v)/2)*h3yy)  (v*h3xy + ((1-v)/2)*h3xy) (v*h4xx+((1-v)/2)*h4yy)...
     (v*h4xy + ((1-v)/2)*h4xy) (v*h1xy + ((1-v)/2)*h1xy) (((1-v)/2)*h1xx+h1yy)  (v*h2xy + ((1-v)/2)*h2xy)...
     (((1-v)/2)*h2xx+h2yy)  (v*h3xy + ((1-v)/2)*h3xy) (((1-v)/2)*h3xx+h3yy) (v*h4xy + ((1-v)/2)*h4xy)...
     (((1-v)/2)*h4xx+h4yy) ]);

dBtrans =(transpose(dB));
```

```
detj =subs(detJ,{s,r},{x,y});
kPe = kPe + dBtrans*dB*detj;
```

C.4.3 Element routines: Derivatives of form functions

```
function[hxx,hyy,hxy,hx,hy,detJ] = Afgeleidevormfunk(h,hr,hs,hrs,xn,yn);

syms x y r s E v A real;

y=h*yn;
x=h*xn;

% Bepaal die Jacobiaan
syms J11 J12 J21 J22
J11 = diff(x,r);
J12 = diff(y,r);
J21 = diff(x,s);
J22 = diff(y,s);

J = [J11 J12
     J21 J22];

% Bepaal die determinant van die Jacobiaan
detJ = det(J);

%Bepaal die inverse van die Jacobiaan
invJ = (1/detJ)*[ J22 -J12
                 -J21  J11];

%============================================================
% Bepaal die afgeleides van die vorm funksies
%============================================================

%----------- Afgeleide van vormfunksie 1 metode 1---------------
hx(1) = hr(1) *(1/detJ)*J22 + hs(1)*(1/detJ)*(-J12);

h1xr = diff(hx(1),r); % Afgeleide van H1,x na r
h1xs = diff(hx(1),s); % Afgeleide van H1,x na s

hxx(1) = h1xr*(1/detJ)*J22 + h1xs*(1/detJ)*(-J12); % H1,xx = H1x,r * r,x + H1x,s *s,x

hy(1) = hr(1) *(1/detJ)*(-J21) + hs(1)*(1/detJ)*(J11);
h1yr = diff(hy(1),r); % Afgeleide van H1,y na r
h1ys = diff(hy(1),s); % Afgeleide van H1,y na s

hyy(1) = h1yr*(1/detJ)*(-J21) + h1ys*(1/detJ)*J11; % H1,yy = H1y,r * r,y + H1y,s *s,y

hxy(1) = h1xr*(1/detJ)*(-J21) + h1xs*(1/detJ)*(J11); % H1,xy = H1x,r * r,y + H1x,s *s,y
                              % h1xy = h1yx


%---------- Afgeleide van vormfunksie 2 metode 1-----------------
hx(2) = hr(2) *(1/detJ)*J22 + hs(2)*(1/detJ)*(-J12);

h2xr = diff(hx(2),r); % Afgeleide van H1,x na r
h2xs = diff(hx(2),s); % Afgeleide van H1,x na s

hxx(2) = h2xr*(1/detJ)*J22 + h2xs*(1/detJ)*(-J12); % H1,xx = H1x,r * r,x + H1x,s *s,x

hy(2) = hr(2) *(1/detJ)*(-J21) + hs(2)*(1/detJ)*(J11);
h2yr = diff(hy(2),r); % Afgeleide van H1,y na r
h2ys = diff(hy(2),s); % Afgeleide van H1,y na s

hyy(2) = h2yr*(1/detJ)*(-J21) + h2ys*(1/detJ)*J11; % H1,yy = H1y,r * r,y + H1y,s *s,y
```

```
hxy(2) = h2xr*(1/detJ)*(-J21) + h2xs*(1/detJ)*(J11); % H1,xy = H1x,r * r,y + H1x,s *s,y
                              % h1xy = h1yx

%----------- Afgeleide van vormfunksie 3 metode 1-----------------------
hx(3) = hr(3) *(1/detJ)*J22 + hs(3)*(1/detJ)*(-J12);

h3xr = diff(hx(3),r); % Afgeleide van H1,x na r
h3xs = diff(hx(3),s); % Afgeleide van H1,x na s

hxx(3) = h3xr*(1/detJ)*J22 + h3xs*(1/detJ)*(-J12); % H1,xx = H1x,r * r,x + H1x,s *s,x

hy(3) = hr(3)*(1/detJ)*(-J21) + hs(3)*(1/detJ)*(J11);

h3yr = diff(hy(3),r); % Afgeleide van H1,y na r
h3ys = diff(hy(3),s); % Afgeleide van H1,y na s

hyy(3) = h3yr*(1/detJ)*(-J21) + h3ys*(1/detJ)*J11; % H1,yy = H1y,r * r,y + H1y,s *s,y

hxy(3) = h3xr*(1/detJ)*(-J21) + h3xs*(1/detJ)*(J11);% H1,xy = H1x,r * r,y + H1x,s *s,y
                              % h1xy = h1yx

% -----------------Afgeleide van vormfunksie 4 metode 1-----------------------
hx(4) = hr(4) *(1/detJ)*J22 + hs(4)*(1/detJ)*(-J12);

h4xr = diff(hx(4),r); % Afgeleide van H1,x na r
h4xs = diff(hx(4),s); % Afgeleide van H1,x na s

hxx(4) = h4xr*(1/detJ)*J22 + h4xs*(1/detJ)*(-J12); % H1,xx = H1x,r * r,x + H1x,s *s,x

hy(4) = hr(4) *(1/detJ)*(-J21) + hs(4)*(1/detJ)*(J11);

h4yr = diff(hy(4),r); % Afgeleide van H1,y na r
h4ys = diff(hy(4),s); % Afgeleide van H1,y na s

hyy(4) = h4yr*(1/detJ)*(-J21) + h4ys*(1/detJ)*J11; % H1,yy = H1y,r * r,y + H1y,s *s,y

hxy(4) = h4xr*(1/detJ)*(-J21) + h4xs*(1/detJ)*(J11); % H1,xy = H1x,r * r,y + H1x,s *s,y
                              % h1xy = h1yx
```